

**SYNTHESIS, CHARACTERIZATION AND
ELECTROCHEMICAL STUDIES OF Cu(II), Fe(II), Fe(III) AND
Ni(II) COMPLEXES OF SOME
o-PHENYLENEDIAMINE SCHIFF BASES**

ABDULAZIZ ALI ALOMARI

**DEPARTMENT OF CHEMISTRY
FACULTY OF SCIENCE
UNIVERSITY OF MALAYA
KUALA LUMPUR**

2010

**SYNTHESIS, CHARACTERIZATION AND
ELECTROCHEMICAL STUDIES OF Cu(II), Fe(II), Fe(III) AND
Ni(II) COMPLEXES OF SOME
o-PHENYLENEDIAMINE SCHIFF BASES**

ABDULAZIZ ALI ALOMARI

**A DISSERTATION SUBMITTED IN FULFILMENT OF THE
REQUIREMENTS FOR THE DEGREE OF MASTER OF
SCIENCE**

**DEPARTMENT OF CHEMISTRY
FACULTY OF SCIENCE
UNIVERSITY OF MALAYA
KUALA LUMPUR**

2010

**UNIVERSITI MALAYA
ORIGINAL LITERARY WORK DECLARATION**

Name of Candidate: Alomary, Abdulaziz Ali (I.C/Passport No: H163267)
Registration/Matric No: SGR080173
Name of Degree: MSc
Title of Project Paper/Research Report/Dissertation/Thesis ("this Work"):

Synthesis, characterization and electrochemical studies of Cu(II), Fe(II), Fe(III) and Ni(II) complexes of some o-phenylenediamine Schiff bases.

Field of Study: Inorganic chemistry

I do solemnly and sincerely declare that:

- (1) I am the sole author/writer of this Work;
- (2) This Work is original;
- (3) Any use of any work in which copyright exists was done by way of fair dealing and for permitted purposes and any excerpt or extract from, or reference to or reproduction of any copyright work has been disclosed expressly and sufficiently and the title of the work and its authorship have been acknowledged in this Work;
- (4) I do not have any actual knowledge nor do I ought reasonably to know that the making of this work constitutes an infringement of any copyright work;
- (5) I hereby assign all and every rights in the copyright to this Work to the University of Malaya ("UM"), who henceforth shall be owner of the copyright in this work and that any reproduction or use in any form or by any means whatsoever is prohibited without the written consent of UM having been first had and obtained;
- (6) I am fully aware that if in the course of making this Work I have infringed any copyright whether intentionally or otherwise, I may be subject to legal action or any other action as may be determined by UM.

Candidate's Signature

Date: 20.05.2010

Subscribed and solemnly declared before,

Witness's Signature

Dr. Norbani Abdullah
Prof. Madya
Jabatan Kimia, Universiti Malaya
50603 Kuala Lumpur

Date: 20.05.2010

Name: Norbani Abdullah
Designation: Assoc. Prof./supervisor

TABLE OF CONTENTS

	Page
Acknowledgement	i
Abstract	ii
Abstrak	iv
List of Figures	iv
List of Tables	vii
CHAPTER 1: INTRODUCTION	1
CHAPTER 2: LITERATURE REVIEW	
2.1 Schiff bases and their metal complexes	4
2.2 Catalytic properties	10
2.3 FTIR spectroscopy	12
2.4 NMR spectroscopy	13
2.5 Ultraviolet-visible spectroscopy	16
2.6 Elemental analysis	18
2.7 Cyclic voltammetry	18
CHAPTER 3: EXPERIMENTAL	
3.1 Materials	21
3.2 Preparation of H ₂ L1 and its metal complexes	21
3.2.1 Preparation of H ₂ L1	21
3.2.2 Preparation of CuL1	21
3.2.3 Preparation of FeL1	22

3.2.4 Preparation of NiL1	22
3.3 Preparation of H ₂ L2 and its metal complexes	22
3.3.1 Preparation of H ₂ L2	22
3.3.2 Preparation of CuL2	23
3.3.3 Preparation of FeL2	23
3.3.4 Preparation of NiL2	23
3.4 Preparation of H ₂ L3 and its metal complexes	24
3.4.1 Preparation of H ₂ L3	24
3.4.2 Preparation of CuL3	24
3.4.3 Preparation of FeL3	24
3.4.4 Preparation of NiL3	25
3.5 Preparation of H ₂ L4 and its metal complexes	25
3.5.1 Preparation of H ₂ L4	25
3.5.2 Preparation of CuL4	25
3.5.3 Preparation of FeL4	25
3.5.4 Preparation of NiL4	26
3.6 Analysis	26
3.6.1 FTIR spectroscopy	26
3.6.2 Elemental analyses	26
3.6.3 ¹ H-NMR spectroscopy	26
3.6.4 UV-Vis spectroscopy	27
3.6.5 Cyclic Voltammetry	27
3.6.6 X-ray Crystallography	27

CHAPTER 4: RESULTS AND DISCUSSION

4.1	Introduction	28
4.2	N,N'-1,2-benzene-1,2-diyl-bis(5-chlorosalicylideneimine) (H ₂ L1)	29
	and its copper(II), iron(II) and nickel(II) complexes	
4.2.1	Copper(II) complex, CuL1	32
4.2.2	Iron(II) complex, FeL1	36
4.2.3	Nickel(II) complex, NiL1	37
4.3	N,N'-1,2-benzene-1,2-diyl-bis(5-bromosalicylideneimine) (H ₂ L2)	42
	and its copper(II), iron(II) and nickel(II) complexes	
4.3.1	Copper(II) complex, CuL2	45
4.3.2	Iron(II) complex, FeL2	49
4.3.3	Nickel(II) complex, NiL2	53
4.4	N,N'-1,2-benzene-1,2-diyl-bis(4-hydroxysalicylideneimine) (H ₂ L3)	56
	and its copper(II), iron(II) and nickel(II) complexes	
4.4.1	Copper(II) complex, CuL3	59
4.4.2	Iron(II) complex, FeL3	63
4.4.3	Nickel(II) complex, NiL3	66
4.5	N,N'-1,2-benzene-1,2-diyl-bis(3-bromo-5-chlorosalicylideneimine)	69
	(H ₂ L4) and its copper(II), iron(II) and nickel(II) complexes	
4.5.1	Copper(II) complex, CuL4	72
4.5.2	Iron(II) complex, FeL4	76
4.5.3	Nickel(II) complex, NiL4	79

CHAPTER 5: CONCLUSION AND SUGGESTIONS FOR FUTURE WORK

5.1 Conclusion	84
5.2 Suggestions for future work	85
APPENDIX	87
REFERENCES	92

ACKNOWLEDGEMENT

I would like to express my sincere gratitude to my supervisors Assoc.Prof. Dr. Norbani Abdullah and Prof. Dato' Dr. Mohd. Jamil Maah for their dedicated guidance and considerate supports throughout my MSc program.

Moreover, my keen appreciation was conveyed to Assoc. Prof. Dr. Kong Mun Lo, for his help in X-ray crystallography.

Also sincere thanks go to all inorganic research lab's students, department of chemistry staff, instruments technicians, for their help in both academic and technical affairs that enable me to successfully complete my study, and to all those who contribute directly or indirectly.

Finally, I would like to record my deepest gratitude to Saudi Arabian Government for offering me a scholarship to complete this research and University Malaya support through PPP research grant (PS340/2009C) as well as my family for moral and never-ending assistance.

ABSTRACT

Four Schiff base ligands, N,N'-1,2-benzene-1,2-diyl-bis(5-chlorosalicylideneimine) (H₂L1), N,N'-1,2-benzene-1,2-diyl-bis(4-bromosalicylideneimine) (H₂L2), N,N'-1,2-benzene-1,2-diyl-bis(4-hydroxysalicylideneimine) (H₂L3), and N,N'-1,2-benzene-1,2-diyl-bis(3-bromo-5-chlorosalicylideneimine) (H₂L4) were obtained in good yields from the condensation reaction of *o*-phenylenediamine with 5-chlorosalicylaldehyde, 5-bromosalicylaldehyde, 4-hydroxysalicylaldehyde and 3-bromo-5-chlorosalicylaldehyde respectively.

These Schiff bases formed complexes with copper(II), iron(II) and nickel(II) ions in good yields. The structures of these complexes are mainly square planar, which is confirmed by the crystal structure of nickel(II) complex of bis-N,N'-3-chloro-5-bromosalicylideneamine-1,2-diaminobenzene. Attempts to prepare the corresponding iron(III) complexes were unsuccessful.

The ligands were characterized by Fourier transform infrared spectroscopy, elemental analysis, ¹H-Nuclear magnetic resonance spectroscopy and UV-vis spectroscopy, while the complexes were characterized by Fourier transform infrared spectroscopy, elemental analysis, UV-vis spectroscopy and cyclic voltammetry. H₂L4 nickel(II) complex has been subjected to X-ray crystal structure analysis which reveals that the nickel atom is coordinated to two phenoxy oxygen atoms and two imino nitrogen atoms in the *cis* configuration. The local coordination geometry around the nickel atom is a square planar configuration, with a rms deviation of 0.034 (1) Å from a least-squares

plane defined by the two nitrogen, two oxygen and the nickel atoms in the molecule. The nickel atom is situated 0.003(1)Å away from this plane.

The cyclic voltammetry studies showed that CuL1, CuL2, FeL2, and NiL3 may be suitable to be used as redox catalysts.

ABSTRAK

Empat ligand bes Schiff, N,N'-1,2-benzena-1,2-diyl-bis(5-klorosalisilidenaimina) (H₂L1), N,N'-1,2-benzena-1,2-diyl-bis(4-bromosalisilidenaimina) (H₂L2), N,N'-1,2-benzena-1,2-diyl-bis(4-hidroksalisilidenaimina) (H₂L3), dan N,N'-1,2-benzena-1,2-diyl-bis(3-bromo-5-klorosalisilidenaimina) (H₂L4) diperoleh dengan hasilan yang baik daripada tindak balas kondensasi *o*-fenilenadamina dengan 5-klorosalisilaldehid, 5-bromosalisilaldehid, 4-hidroksalisilaldehid dan 3-bromo-5-klorosalisilaldehid masing-masing.

Kesemua bes Schiff tersebut membentuk kompleks dengan ion-ion kuprum(II), ferum(II) dan nikel(II) dalam hasilan yang baik. Struktur utama kompleks ini adalah satah empat segi sama, yang disahkan melalui struktur hablur kompleks nikel(II) dengan N,N'-1,2-benzena-1,2-diyl-bis(3-bromo-5-klorosalisilidenaimina). Cubaan untuk menyediakan kompleks ferum(III) yang sepadan adalah tidak berjaya.

Ligand-ligand ini dicirikan secara spektroskopi transformasi inframerah Fourier, analisis unsur, spektroskopi resonans ¹H-nukleus magnetic dan spektroskopi UV-nampak, manakala kompleks dicirikan secara spektroskopi transformasi inframerah Fourier, analisis unsur, spektroskopi UV-nampak dan voltametri siklik. Struktur kompleks nikel(II) bagi H₂L4 dianalisis secara hablur sinar-X yang menunjukkan bahawa atom nikel terkoordinat kepada dua atom oksigen fenoksil dan dua atom nitrogen imino dalam konfigurasi *cis*. Geometri setempat pada atom nikel ialah satah segi empat sama, dengan sisihan rms 0.034 (1) Å daripada satah “least-squares” yang ditakrifkan oleh dua atom

nitrogen, dua atom oksigen dan satu atom nikel dalam molekul. Atom nikel terletak sejauh 0.003(1)Å dari satah ini.

Voltametri siklik menunjukkan bahawa CuL1, CuL2, FeL2, dan NiL3 mungkin sesuaikan digunakan sebagai mangkin redoks.

LIST OF FIGURES

Figure 2.1 The structural formula of (a) salenH ₂ ; (b) salphenH ₂	5
Figure 2.2 SalenH ₂ complexes of (a) Cr(0) and (b) Mo(IV+)	7
Figure 2.3 The structural formula of shaH ₂	7
Figure 2.4 ShaH ₂ complexes of (a) Cr; and (b) W, formed under reduced pressure	8
Figure 2.5 ShaH ₂ complexes of Mo formed in air	8
Figure 2.6 A simple cyclic voltammogram	19
Figure 3.1 Structural formula of Schiff bases: (a) H ₂ L1; (b) H ₂ L2; (c) H ₂ L3; and (d) H ₂ L4	20
Figure 4.1 FTIR of H ₂ L1	29
Figure 4.2 ¹ H-NMR spectrum of H ₂ L1	30
Figure 4.3 ¹ H-NMR assignment of H ₂ L1	31
Figure 4.4 UV-vis spectrum of H ₂ L1 in DMSO	31
Figure 4.5 FTIR spectrum of CuL1	32
Figure 4.6 UV-vis spectrum of CuL1 in DMSO	33
Figure 4.7 Visible spectrum of CuL1 in DMSO	34
Figure 4.8 Proposed structural formula for CuL1 ([Cu(C ₂₀ H ₁₂ O ₂ N ₂ Cl ₂)])	34
Figure 4.9 CV of CuL1 in DMSO	35
Figure 4.10 FTIR spectrum of FeL1	36
Figure 4.11 UV-vis spectrum of FeL1 in DMSO	37
Figure 4.12 CV of FeL1 in DMSO	38
Figure 4.13 FTIR spectrum of NiL1	39
Figure 4.14 UV-vis spectrum of NiL1 in DMSO	40

Figure 4.15 CV of NiL1 in DMSO	41
Figure 4.16 FTIR spectrum of H ₂ L2	42
Figure 4.17 ¹ H-NMR spectrum of H ₂ L2	43
Figure 4.18 Proposed structural formula of H ₂ L2	44
Figure 4.19 UV-vis spectrum of H ₂ L2 in DMSO	44
Figure 4.20 FTIR spectrum of CuL2	45
Figure 4.21 UV-vis spectrum of CuL2 in DMSO	46
Figure 4.22 Proposed structural formula for CuL2, ([Cu(C ₂₀ H ₁₂ O ₂ N ₂ Br ₂)])	47
Figure 4.23 CV of CuL2 in DMSO	48
Figure 4.24 FTIR spectrum of FeL2	49
Figure 4.25 UV-vis spectrum of FeL2 in DMSO	51
Figure 4.26 CV of FeL2 in DMSO	52
Figure 4.27 FTIR spectrum of NiL2	53
Figure 4.28 UV-vis spectrum of NiL2 in DMSO	55
Figure 4.29 CV of NiL2 in DMSO	56
Figure 4.30 FTIR spectrum of H ₂ L3	57
Figure 4.31 ¹ H-NMR spectrum of H ₂ L3	58
Figure 4.32 UV-vis spectrum of H ₂ L3 in DMSO	59
Figure 4.33 FTIR spectrum of CuL3	60
Figure 4.34 UV-vis spectrum of CuL3 in DMSO	62
Figure 4.35 Proposed structural formula for CuL3, [Cu(C ₂₀ H ₁₂ O ₂ N ₂ (OH) ₂)]	62
Figure 4.36 CV of CuL3 in DMSO	63
Figure 4.37 FTIR spectrum of FeL3	64

Figure 4.38 UV-vis spectrum of FeL3 in DMSO	65
Figure 4.39 CV of FeL3 in DMSO	66
Figure 4.40 FTIR spectrum of NiL3	67
Figure 4.41 UV-vis spectrum of NiL3 in DMSO	68
Figure 4.42 CV of NiL3 in DMSO	69
Figure 4.43 FTIR spectrum of H ₂ L4	70
Figure 4.44 ¹ H-NMR spectrum of H ₂ L4 in DMSO-d ₆	71
Figure 4.45 Proposed structural formula of H ₂ L4	72
Figure 4.46 UV-vis spectrum of H ₂ L4 in DMSO	72
Figure 4.47 FTIR spectrum of CuL4	73
Figure 4.48 UV-vis spectrum of CuL4 in DMSO	74
Figure 4.49 Proposed structural formula for CuL4, ([Cu(C ₂₀ H ₁₀ O ₂ N ₂ Br ₂ Cl ₂)])	75
Figure 4.50 CV of CuL4 in DMSO	76
Figure 4.51 FTIR spectrum of FeL4	77
Figure 4.52 UV-vis spectrum of FeL4 in DMSO	78
Figure 4.53 CV of FeL4 in DMSO	79
Figure 4.54 Molecular structure of NiL4	80
Figure 4.55 FTIR spectrum of NiL4	81
Figure 4.56 UV-vis spectrum of NiL4 in DMSO	82
Figure 4.57 CV of NiL4 in DMSO	83

CHAPTER 1

INTRODUCTION

CHAPTER 2: LITERATURE REVIEW

2.1 Schiff bases and their metal complexes

Schiff Bases are organic compounds which contain the azomethine group ($-C=N-$). These compounds are synthesized by the reaction of a primary amine and an active carbonyl compound (aldehyde or ketone) [4-6]. The wide applications of Schiff bases have generated a great deal of interest in metal complexes.

Schiff bases are widely employed as ligands in coordination chemistry [7, 8]. This is because they are readily available, versatile and have tunable properties which depend on the starting materials (primary amine and carbonyl precursors). They exhibit various reactivities and functionalities. Moreover, the number, the nature and the relative position of the donor atoms of a Schiff base ligand allow a good control over stereochemistry of the metallic centres, as well as the number of the metal ions within homo- and hetero-polynuclear complexes. All these advantages make Schiff bases very good ligands to form metal complexes that are of interest in bioinorganic chemistry, catalysis, encapsulation, transport and separation process [1, 9, and 10].

Salicylaldehyde and its derivatives are useful carbonyl precursors for the synthesis of a large variety of Schiff bases. Examples are their reaction with monoamines, diamines with two primary amino groups, or diamines with one primary and one tertiary amino group. In the last case, the condensation reaction leads to tridentate (NNO) Schiff bases [11-13]. Additional coordinating groups attached to salicylaldehyde increase not only the denticity of the resulting Schiff bases, but also their versatility and ability to generate polynuclear complexes. An example of such

salicylaldehyde derivative is 3-methoxysalicylaldehyde (*o*-vanilin), which was largely employed for the synthesis of compartmental ligands [14, 15].

Another very important Schiff bases are those of tetradentate ligands having N_2O_2 or N_4 donor sets, such as bis(salicylaldehyde)ethylenediimine, salenH₂ and bis(salicylaldehyde)phenylenediimine, salphenH₂ (Figure 2.1). Their metal complexes were found to have catalytic activity for epoxidation reactions [16-18].

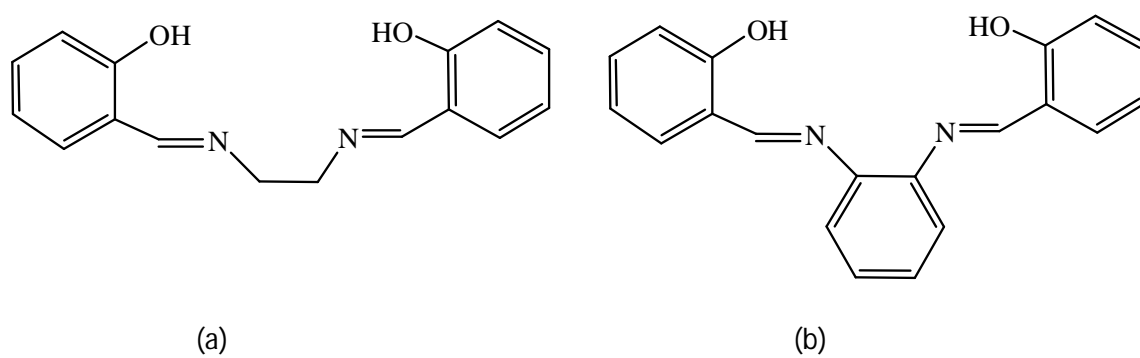


Figure 2.1 The structural formula of (a) salenH₂; (b) salphenH₂

During the past two decades, metal complexes with Schiff bases as ligands have been amongst the most widely studied coordination compounds. Schiff base complexes have been studied extensively due to various reasons like manifestation of novel structural features, up-normal magnetic properties and relevance to biological processes. Considerable attention had been paid to the chemistry of the metal complexes of Schiff bases containing nitrogen and other donors. This may be attributed to their stability, biological activity and potential applications in many fields such as oxidation catalysis, electrochemistry etc. [19, 20]. Schiff base complexes have also applications in clinical [21] and analytical fields [22]. Some Schiff bases are used as model molecules for

biological oxygen carrier systems [23]. Tetradentate Schiff bases complexes are well known to form stable complexes, where the coordination takes place through the N_2O_2 donor set [24-26]. Complexes of transition metal ions with polydentate Schiff bases containing nitrogen and oxygen donor atoms play an important role in biological systems and represent interesting models for metalloenzymes that catalyze the reduction of dinitrogen and dioxygen [27, 28]

Metal complexes of tetradentate ligands having N_2O_2 or N_4 donor sets were studied [16]. Electrochemical and spectrochemical studies of Co(salen) and Co(salphen) showed that both compounds formed adducts with oxygen and exhibited catalytic activities for oxygen reduction. Furthermore, complexes of chromium, manganese, nickel and ruthenium with Schiff bases having N_2O_2 and N_4 donor atoms were found to be catalytic for epoxidation reactions [29]. These complexes bound reversibly to molecular oxygen with a change in the oxidation state of the metal [16, 17, 30, and 31].

Reactions of those Schiff bases with group 6 and 8 metal carbonyls have been studied recently [32-34]. Reactions of $M(CO)_6$ ($M = Cr, Mo$) with the Schiff base bis(2-hydroxyacetophenone)ethylenediimine (happenH₂) in air gave the oxo derivative $M(O)(happen)$ with the metal in the +4 formal oxidation state. The dihydride complex $MoH_2(CO)(happen)$ was also isolated under reduced pressure [32]. On the other hand, reaction of happenH₂ with $Ru_3(CO)_{12}$ resulted in the formation of the dicarbonyl derivative $Ru(CO)_2(happenH_2)$ [34]. Reaction of bis(salicylaldehyde)ethylenediimine (salenH₂) with $Cr(CO)_6$ under reduced pressure yielded the dicarbonyl derivative $Cr(CO)_2(salenH_2)$ with the chromium atom in the zero oxidation state, while its reaction with $Mo(CO)_6$ in air

gave the paramagnetic oxo metal complexes Mo(CO)(O)(salen) with a +IV metal oxidation state and a high-spin d^2 configuration [32] ((Figure 2.2).

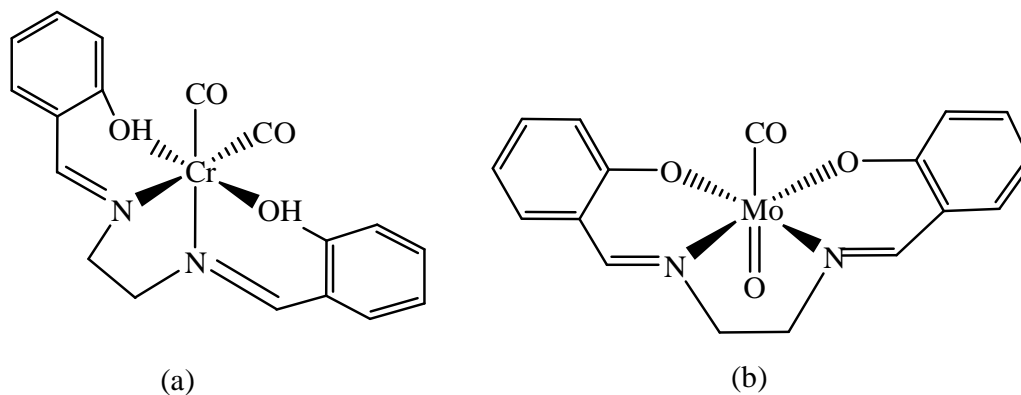


Figure 2.2 SalenH₂ complexes of (a) Cr(0) and (b) Mo(IV+)

Recently, reactions of M(CO)_6 ($\text{M} = \text{Cr}, \text{Mo}$ and W) with N-salicylidene-2-hydroxyaniline (shaH₂) (Figure 2.3) were reported.

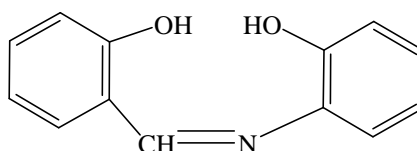


Figure 2.3 The structural formula of shaH₂

Under reduced pressure, the reaction yielded $\text{CrO}_2(\text{CO})_2(\text{shaH}_2)$ and $\text{W(CO)}_2(\text{shaH})_2$ (Figure 2.4), while in air the reaction yielded $\text{MoO}(\text{sha})$ and $\text{Mo}_2\text{O}_4(\text{sha})_2$ (Figure 2.5) [2]. Structural studies of the complexes revealed that shaH₂ binds to the metal through the oxygen atoms of the hydroxyl groups and the nitrogen atom of the imine group. Thus, the type of ligand and the reaction conditions play a vital role in determining the type of products isolated.

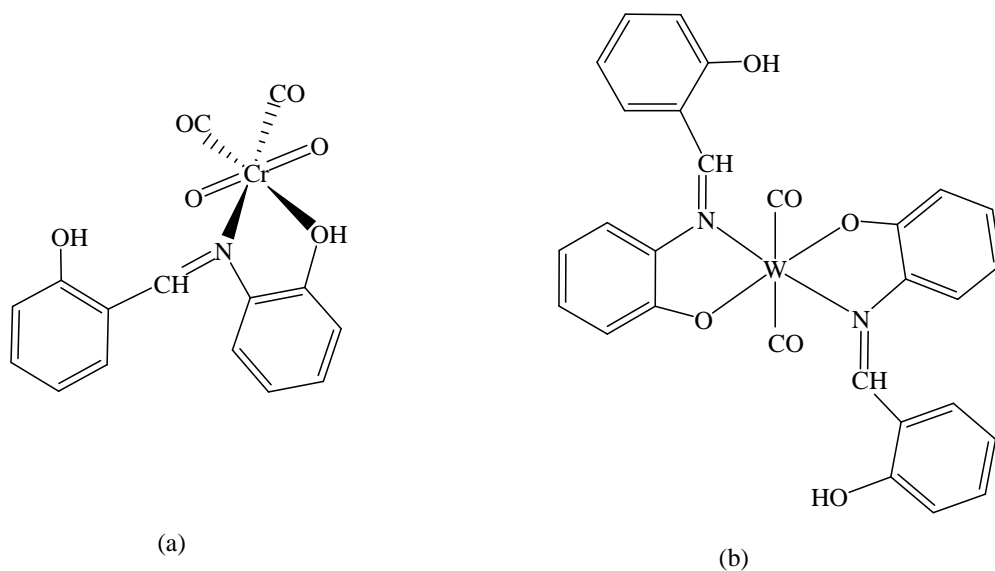


Figure 2.4 ShaH₂ complexes of (a) Cr; and (b) W, formed under reduced pressure

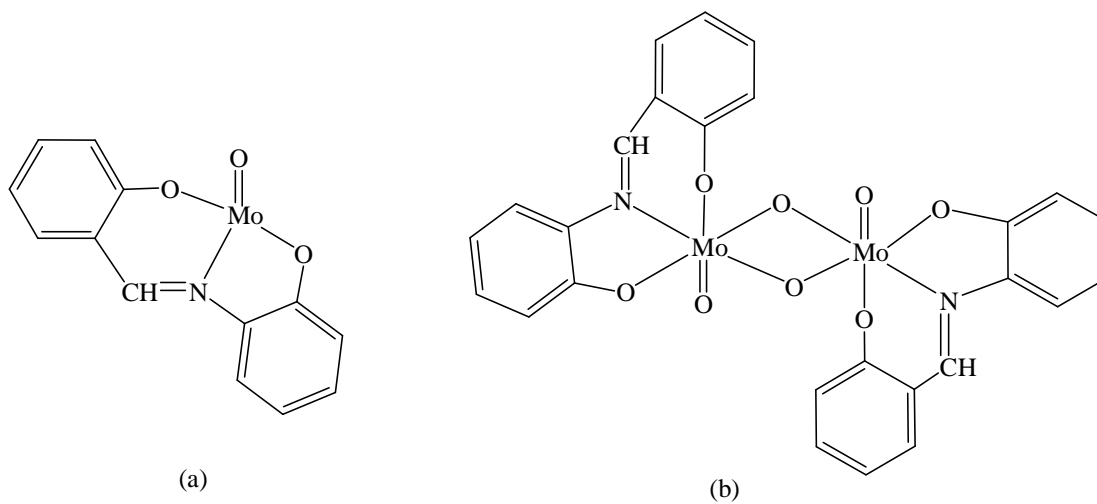


Figure 2.5 ShaH₂ complexes of Mo formed in air

Interaction of metal carbonyls $M(CO)_6$ ($M = Cr, Mo$ and W) with the tetradentate Schiff base, bis(salicylaldehyde)phenylenediimine (salphenH₂) was studied in THF [3]. Under reduced pressure, the reaction with $Cr(CO)_6$ and $Mo(CO)_6$ yielded $Cr(CO)_2(salphen)$ and $MoO(CO)(salphen)$ respectively, while in air the reaction yielded

$\text{MoO}_2(\text{salphenH})_2$ and $\text{W}_2\text{O}_6(\text{salphenH}_2)$. All complexes were characterized by elemental analysis, mass spectrometry and IR and ^1H -NMR spectroscopies. Spectroscopic studies supported the proposed structures. The UV-vis spectra of the complexes in different solvents showed bands due to either metal-to-ligand or ligand-to-metal charge transfer transition.

Several Schiff base complexes contain two or more metal ions [35, 36]. There is increasing evidence that binuclear transition metal complexes have played important roles in the development of coordination chemistry. Examples are models for more complex systems of polymetallic or cluster catalyzed reactions, and applications of mixed metal systems in organic synthesis [20]. In addition, they act as models in bioinorganic chemistry [37]. The development of a large number and varieties of binucleating ligands has led to the successful synthesis of a variety of homo and hetero-binuclear metal complexes [38]. An evolution started few decades ago toward hetero-bimetallic complexes, but still limited number of these complexes are known and fully structurally characterized. The literature survey reported that Schiff base and their complexes possess good luminescence and pigmentation properties. A number of Schiff base metal complexes were also reported to be a great utility in pharmacological and biological aspects. These properties depend on the structure of ligand and the nature of metal ion [35-38].

2.2 Catalytic properties

M.J Alcon et. al studied the catalytic properties of phenylenediamine complexes of the type $[\text{Cu}(\text{L})]\text{ClO}_4$ and $[\text{Mn}(\text{L})\text{Cl}(\text{H}_2\text{O})]\text{PF}_6$, ($\text{L} = N,N'$ -bis(*S*-prolyl)phenylenediamine, *N,N'*-bis(*S-N*-benzylprolyl)phenylenediamine, *N,N'*-bis[(*S*-pyrrolidin-2-yl)methyl]phenylenediamine, and *N,N'*-bis-[(*S-N*-benzyl-pyrrolidin-2-yl)methyl]phenylenediamine, in which the ligands were coordinated to the metal ion in tetradentate manner. The complexes were found to catalyze the cyclopropanation of styrene with ethyl and *t*-butyl diazoacetate to afford *cis/trans* 2-phenylcyclopropan-1-carboxylates with good yields and selectivity against dimerisation and low ee (<10%). On the other hand, the manganese and copper complexes also catalyse the oxidation of organic sulfides to sulfoxides with high selectivity, and moderate to low enantioselectivity. If an excess of oxidant were used the reaction yields sulfone as only product with excellent yield [39].

The oxidative mechanism of isatin Schiff base Cu(II) complexes have been studied towards the oxidation of common carbohydrates such as glucose, fructose and galactose by molecular oxygen. The imine ligands are capable of modifying selectively the environment of the copper(II) ion in a pH controlled process, through keto–enolic equilibria similar to those occurring with carbohydrates. Kinetic studies revealed that the reaction follows pseudo-first order behavior depending both on the catalyst and substrate concentrations, followed by a saturation effect, for all the compounds studied. Further, the pH profile indicated that reaction occurs significantly only in very alkaline medium ($\text{pH} \geq 10$), and some influence of ionic strength (controlled by carbonate buffer) was also verified [40].

Polydentate Schiff base ligands derived from the reaction of 2-(2-aminoethyliminomethyl)phenol with phthaldialdehyde, 4-methyl-2,6-diformylphenol and 4-*t*-butyl-2,6-diformylphenol in ethanol solution were prepared and the complexes of Cd(II), Cu(II), Co(II), Ni(II), Zn(II) and Sn(II) have been investigated [41]. The catalytic properties of Cu(II) and Co(II) complexes were studied on 3,5-di-*tert*-butylcatechol and ascorbic acid as a substrate. The oxidative C–C coupling properties of the Co(II) and Cu(II) complexes have been investigated on the sterically hindered 2,6-di-*tert*-butylphenol.

In 2008, Kefeng et. al prepared a series of tridentate N,N,N iron(II) and cobalt(II) complexes containing *N*-((pyridin-2-yl)methylene)-quinolin-8-amine derivatives [42]. On treatment with modified methylaluminoxane, these metal complexes exhibited good catalytic activities up to $2.8 \times 10^6 \text{ g mol}^{-1}(\text{Fe}) \text{ h}^{-1}$ for ethylene oligomerization, and butenes were the major products with nice selectivity for 1-C₄. The steric and electronic effects on catalytic activities of metal complexes were carefully investigated as well as the influence of various reaction parameters. In the catalytic system, Fe(II) complexes performed better catalytic activities than their Co(II) analogues. With ligands having bulky substituents, the better catalytic activity was observed in catalytic system of Fe(II) complex, however, the lower catalytic activity was obtained in catalytic system of Co(II) complexes.

Further more, catalytic ethylene polymerization properties of iron(II) and cobalt(II) complexes of 2,6-bis(4-nitro-2,6-R₂-phenylimino)pyridines, LMCl₂, R = Me, M = Fe; R = *i*Pr, M = Fe; R = Me, M = Co; R = *i*Pr, M = Co, have been investigated. Among these complexes, the iron(II) pre-catalyst bearing the *ortho*-isopropyl groups

exhibited higher activities and produced higher molecular weight polymers than the other complexes in the presence of methylaluminoxane (MAO). A comparison of this complex with the reference catalyst, (2,6-bis(2,6 diisopropylphenylimino)pyridyl)FeCl₂, revealed a modest increase of the catalytic activity and longer lifetime upon substitution of the *para*-positions with nitro groups, converting ethylene to highly linear polyethylenes with a unimodal molecular weight distribution around 456.4 kg mol⁻¹. However, the iron(II) pre-catalyst on changing from *ortho*-isopropyl to methyl groups displayed much lower activities (over an order of magnitude) than the iron(II) pre-catalyst under mild conditions. As expected, the cobalt analogues showed relatively low polymerization activities [43].

2.3 FTIR spectroscopy

The infrared portion of the electromagnetic spectrum is divided into three regions: near-, mid- and far- infrared, named for their relation to the visible spectrum. The far-infrared, approximately 400-10 cm⁻¹ (1000–30 μm), lying adjacent to the microwave region, has low energy and may be used for rotational spectroscopy. The mid-infrared, approximately 4000-400 cm⁻¹ (30–2.5 μm) may be used to study the fundamental vibrations and associated rotational-vibrational structure. The higher energy near-IR, approximately 14000-4000 cm⁻¹ (2.5–0.8 μm) can excite overtone or harmonic vibrations. The names and classifications of these subregions are merely conventions. They are neither strict division nor based on exact molecular or electromagnetic properties.

Infrared spectroscopy exploits the fact that molecules have specific frequencies at which they rotate or vibrate corresponding to discrete energy levels (vibrational modes).

These resonant frequencies are determined by the shape of the molecular potential energy surfaces, the masses of the atoms and, by the associated vibronic coupling. In order for a vibrational mode in a molecule to be IR active, it must be associated with changes in the permanent dipole. In particular, in the Born-Oppenheimer and harmonic approximations, i.e. when the molecular Hamiltonian corresponding to the electronic ground state can be approximated by a harmonic oscillator in the neighborhood of the equilibrium molecular geometry, the resonant frequencies are determined by the normal modes corresponding to the molecular electronic ground state potential energy surface. Nevertheless, the resonant frequencies can be in a first approach related to the strength of the bond, and the mass of the atoms at either end of it. Thus, the frequency of the vibrations can be associated with a particular bond type.

Simple diatomic molecules have only one bond, which may stretch. More complex molecules have many bonds, and vibrations can be conjugated, leading to infrared absorptions at characteristic frequencies that may be related to chemical groups. For example, the atoms in a CH₂ group, commonly found in organic compounds can vibrate in six different ways: symmetrical and antisymmetrical stretching, and 4 different bending modes: scissoring, wagging, rocking and twisting [44-48].

2.4 NMR spectroscopy

Nuclear magnetic resonance spectroscopy (NMR) is a technique which exploits the magnetic properties of certain nuclei. The most important applications for the organic chemist are proton NMR and carbon-13 NMR spectroscopy. In principle, NMR is applicable to any nucleus possessing spin.

Many information can be obtained from an NMR spectrum. Much like using infrared spectroscopy to identify functional groups, analysis of a 1D NMR spectrum provides information on the number and type of chemical entities in a molecule. However, NMR provides much more information than IR.

The impact of NMR spectroscopy on the natural sciences has been substantial. It can, among other things, be used to study mixtures of analytes, to understand dynamic effects such as change in temperature and reaction mechanisms, and is an invaluable tool in understanding protein and nucleic acid structure and function. It can be applied to a wide variety of samples, both in the solution and the solid state.

When placed in a magnetic field, NMR active nuclei (such as ^1H or ^{13}C) absorb at a frequency characteristic of the isotope. The resonant frequency, energy of the absorption and the intensity of the signal are proportional to the strength of the magnetic field. For example, in a 21 tesla magnetic field, protons resonate at 900 MHz. It is common to refer to a 21 T magnet as a 900 MHz magnet, although different nuclei resonate at a different frequency at this field strength.

Depending on the local chemical environment, different protons in a molecule resonate at slightly different frequencies. Since both this frequency shift and the fundamental resonant frequency are directly proportional to the strength of the magnetic field, the shift is converted into a field-independent dimensionless value known as the chemical shift. The chemical shift is reported as a relative measure from some reference resonance frequency. For the nuclei ^1H , ^{13}C , and ^{29}Si , TMS (tetramethylsilane) is commonly used as a reference. This difference between the frequency of the signal and

the frequency of the reference is divided by frequency of the reference signal to give the chemical shift. The frequency shifts are extremely small in comparison to the fundamental NMR frequency. A typical frequency shift might be 100 Hz, compared to a fundamental NMR frequency of 100 MHz, so the chemical shift is generally expressed in parts per million (ppm) [49].

By understanding different chemical environments, the chemical shift can be used to obtain some structural information about the molecule in a sample. The conversion of the raw data to this information is called assigning the spectrum. For example, for the ^1H -NMR spectrum for ethanol ($\text{CH}_3\text{CH}_2\text{OH}$), one would expect three specific signals at three specific chemical shifts: one for the CH_3 group, one for the CH_2 group and one for the OH group. A typical CH_3 group has a shift around 1 ppm, a CH_2 attached to an OH has a shift of around 4 ppm and an OH has a shift around 2–3 ppm depending on the solvent used.

Because of molecular motion at room temperature, the three methyl protons *average* out during the course of the NMR experiment (which typically requires a few ms). These protons become degenerate and form a peak at the same chemical shift which is difficult to interpret in more complicated NMR experiments. The shape and size of peaks are indicators of chemical structure too. In the example above—the proton spectrum of ethanol—the CH_3 peak would be three times as large as the OH. Similarly the CH_2 peak would be twice the size of the OH peak but only $2/3$ the size of the CH_3 peak.

Modern analysis software allows analysis of the size of peaks to understand how many protons give rise to the peak. This is known as integration—a mathematical process which calculates the area under a graph (essentially what a spectrum is). The analyst must integrate the peak and not measure its height because the peaks also have *width*—and thus its size is dependent on its area not its height. However, it should be mentioned that the number of protons, or any other observed nucleus, is only proportional to the intensity, or the integral, of the NMR signal, in the very simplest one-dimensional NMR experiments. In more elaborate experiments, for instance, experiments typically used to obtain carbon-13 NMR spectra, the integral of the signals depends on the relaxation rate of the nucleus, and its scalar and dipolar coupling constants. Very often these factors are poorly understood - therefore, the integral of the NMR signal is very difficult to interpret in more complicated NMR experiments [50].

2.5 Ultraviolet-visible spectroscopy

Ultraviolet-visible spectroscopy or ultraviolet-visible spectrophotometry (UV-Vis or UV/Vis) involves the spectroscopy of photons in the UV-visible region. This means it uses light in the visible and adjacent (near ultraviolet (UV) and near infrared (NIR)) ranges. The absorption in the visible ranges directly affects the color of the chemicals involved. In this region of the electromagnetic spectrum, molecules undergo electronic transitions. This technique is complementary to fluorescence spectroscopy, in that fluorescence deals with transitions from the excited state to the ground state, while absorption measures transitions from the ground state to the excited state.

UV/Vis spectroscopy is routinely used in the quantitative determination of solutions of transition metal ions and highly conjugated organic compounds.

- Solutions of transition metal ions can be coloured (i.e., absorb visible light) because d electrons within the metal atoms can be excited from one electronic state to another. The colour of metal ion solutions is strongly affected by the presence of other species, such as certain anions or ligands. For instance, the colour of a dilute solution of copper sulfate is a very light blue; adding ammonia intensifies the colour and changes the wavelength of maximum absorption (λ_{max}).
- Organic compounds, especially those with a high degree of conjugation, also absorb light in the UV or visible regions of the electromagnetic spectrum. The solvents for these determinations are often water for water soluble compounds, or ethanol for organic-soluble compounds. (Organic solvents may have significant UV absorption; not all solvents are suitable for use in UV spectroscopy. Ethanol absorbs very weakly at most wavelengths.) Solvent polarity and pH can affect the absorption spectrum of an organic compound. Tyrosine, for example, increases in absorption maxima and molar extinction coefficient when pH increases from 6 to 13 or when solvent polarity decreases.
- While charge transfer complexes also give rise to colours, the colours are often too intense to be used for quantitative measurement.

The Beer-Lambert law states that the absorbance of a solution is directly proportional to the concentration of the absorbing species in the solution and the path length. Thus, for a fixed path length, UV/VIS spectroscopy can be used to determine the

concentration of the absorber in a solution. It is necessary to know how quickly the absorbance changes with concentration. This can be taken from references (tables of molar extinction coefficients), or more accurately, determined from a calibration curve [51].

2.6 Elemental analysis

To determine the precise amounts of elements (carbon, hydrogen, nitrogen, sulphur) present in an unknown substance, a quantitative analysis is required. Commercially available elemental analyzers are capable of determining simultaneously the percentages of carbon, hydrogen and nitrogen in a compound. In these instruments the sample is burned in a stream of oxygen. The gaseous products are converted to carbon dioxide, water, and nitrogen, which can be detected via gas chromatography, using thermal conductivity detectors. The precise amount of each gas produced in the combustion is determined by integration of the corresponding gas chromatography peaks [52].

2.7 Cyclic voltammetry

Electrolysis, cyclic voltammetry, amperometry and several other techniques might be described as “active” electrochemical methods because the experimenter drives an electrochemical reaction by incorporating the chemistry into a circuit and then controlling the reaction by circuit parameters such as voltage. In typical cyclic voltammetry, a solution component is electrolyzed (oxidized or reduced) by placing it in contact with an electrode surface, and then making that surface sufficiently positive or negative in voltage to force electron transfer.

In simple cases, the electrode surface is initially at a particular voltage with respect to a reference half-cell, such as calomel or Ag/AgCl, the electrode voltage is changed to a higher or lower voltage at a linear rate, and finally, the voltage is changed back to the original value at the same linear rate. When the surface becomes sufficiently negative or positive, a solution species may gain electrons from the surface or transfer electrons to the surface. This results in a measurable current in the electrode circuitry. However, if the solution is not mixed, the concentration of transferring species near the surface drops, and the electrolysis current then falls off. When the voltage cycle is reversed, it is often the case that electron transfer between electrode and chemical species will also be reversed, leading to an “inverse” current peak. These features are illustrated in Figure 2.6 [53].

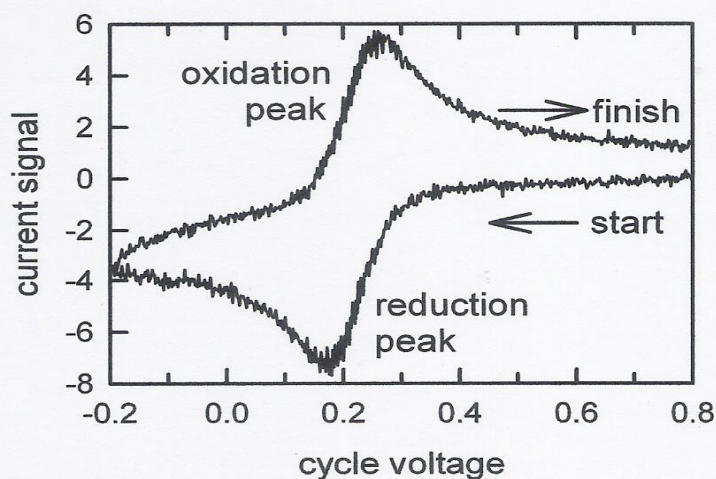


Figure 2.6 A simple cyclic voltammogram

CHAPTER 1: INTRODUCTION

Schiff bases may be formed by the condensation of a primary amine with an active carbonyl compound. These compounds have been used extensively as ligands in coordination chemistry, and have found applications in different fields [2-4]. The focus of research is now directed to the bioactivities and catalytic properties of these metal complexes.

Our current research focused on phenylenediamine Schiff bases substituted with Cl, Br and OH, and their copper(II), iron(II) and nickel(II) complexes. Previous works of these ligands reported the synthesis and characterization of platinum(II) complexes, which showed promising antimicrobial activities [5]. Other studies evaluated the thermal properties of chromium(III), molybdenum(VI), and tungsten(II) [6]. Catalytic activities of other complexes of these Schiff bases for epoxidation reaction have also been studied [7-11].

Thus, it is of interest to further study other metal complexes of these ligands, especially their potential use as redox catalysts. The main aim of this study is to compare the effect of monosubstituted Cl, Br and OH, and disubstituted halogens (Cl and Br), on the structure and redox properties of the metal complexes. The Schiff bases were synthesized from the condensation reaction of *o*-phenylenediamine with 5-chlorosalicylaldehyde, 5-bromosalicylaldehyde, 4-hydroxysalicylaldehyde and 3-bromo-5-chlorosalicylaldehyde. The ligands were then complexed with Cu(II), Fe(II) and Ni(II).

The structures of the Schiff bases and the metal complexes were elucidated by elemental analyses, Fourier transform infrared spectroscopy, ¹H-NMR spectroscopy, UV-

visible spectroscopy, and for crystals, X-ray crystallography. The electrochemical properties of the complexes were studied by cyclic voltammetry.

Preliminary results of this work were communicated as a poster presentation in an international conference [Appendix 1], and a paper on the crystal structure of the novel nickel(II) complexes of the ligand substituted with Br and Cl at the 3- and 5- positions respectively is published in an international journal [Appendix 2].

This thesis contains five chapters. Chapter 2 discusses the literature review on Schiff bases and their metal complexes, their potential uses and their catalytic properties. This chapter also contains general theoretical and physical aspects of the methods used to characterize Schiff bases and complexes, namely elemental analysis, Fourier transform infrared spectroscopy, ^1H -NMR spectroscopy, UV-visible spectroscopy, and cyclic voltammetry. Chapter 3 presents the experimental methods to synthesize the ligands and their metal complexes, and techniques to characterize them. Chapter 4 presents the results and discussion of the findings of the research, and Chapter 5 presents the conclusions and suggestions for future work. A list of references and two appendixes were included at the end of the thesis.

CHAPTER 2

LITERATURE REVIEW

CHAPTER 2: LITERATURE REVIEW

2.1 Schiff bases and their metal complexes

Schiff Bases are organic compounds which contain the azomethine group ($-C=N-$). These compounds are synthesized by the reaction of a primary amine and an active carbonyl compound (aldehyde or ketone) [4-6]. The wide applications of Schiff bases have generated a great deal of interest in metal complexes.

Schiff bases are widely employed as ligands in coordination chemistry [7, 8]. This is because they are readily available, versatile and have tunable properties which depend on the starting materials (primary amine and carbonyl precursors). They exhibit various reactivities and functionalities. Moreover, the number, the nature and the relative position of the donor atoms of a Schiff base ligand allow a good control over stereochemistry of the metallic centres, as well as the number of the metal ions within homo- and hetero-polynuclear complexes. All these advantages make Schiff bases very good ligands to form metal complexes that are of interest in bioinorganic chemistry, catalysis, encapsulation, transport and separation process [1, 9, and 10].

Salicylaldehyde and its derivatives are useful carbonyl precursors for the synthesis of a large variety of Schiff bases. Examples are their reaction with monoamines, diamines with two primary amino groups, or diamines with one primary and one tertiary amino group. In the last case, the condensation reaction leads to tridentate (NNO) Schiff bases [11-13]. Additional coordinating groups attached to salicylaldehyde increase not only the denticity of the resulting Schiff bases, but also their versatility and ability to generate polynuclear complexes. An example of such

salicylaldehyde derivative is 3-methoxysalicylaldehyde (*o*-vanilin), which was largely employed for the synthesis of compartmental ligands [14, 15].

Another very important Schiff bases are those of tetradentate ligands having N_2O_2 or N_4 donor sets, such as bis(salicylaldehyde)ethylenediimine, salenH₂ and bis(salicylaldehyde)phenylenediimine, salphenH₂ (Figure 2.1). Their metal complexes were found to have catalytic activity for epoxidation reactions [16-18].

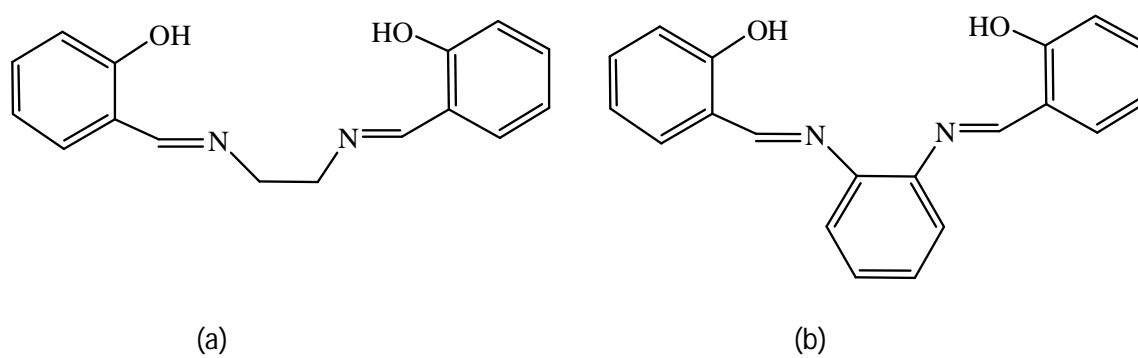


Figure 2.1 The structural formula of (a) salenH₂; (b) salphenH₂

During the past two decades, metal complexes with Schiff bases as ligands have been amongst the most widely studied coordination compounds. Schiff base complexes have been studied extensively due to various reasons like manifestation of novel structural features, up-normal magnetic properties and relevance to biological processes. Considerable attention had been paid to the chemistry of the metal complexes of Schiff bases containing nitrogen and other donors. This may be attributed to their stability, biological activity and potential applications in many fields such as oxidation catalysis, electrochemistry etc. [19, 20]. Schiff base complexes have also applications in clinical [21] and analytical fields [22]. Some Schiff bases are used as model molecules for

biological oxygen carrier systems [23]. Tetradentate Schiff bases complexes are well known to form stable complexes, where the coordination takes place through the N_2O_2 donor set [24-26]. Complexes of transition metal ions with polydentate Schiff bases containing nitrogen and oxygen donor atoms play an important role in biological systems and represent interesting models for metalloenzymes that catalyze the reduction of dinitrogen and dioxygen [27, 28]

Metal complexes of tetradentate ligands having N_2O_2 or N_4 donor sets were studied [16]. Electrochemical and spectrochemical studies of Co(salen) and Co(salphen) showed that both compounds formed adducts with oxygen and exhibited catalytic activities for oxygen reduction. Furthermore, complexes of chromium, manganese, nickel and ruthenium with Schiff bases having N_2O_2 and N_4 donor atoms were found to be catalytic for epoxidation reactions [29]. These complexes bound reversibly to molecular oxygen with a change in the oxidation state of the metal [16, 17, 30, and 31].

Reactions of those Schiff bases with group 6 and 8 metal carbonyls have been studied recently [32-34]. Reactions of $M(CO)_6$ ($M = Cr, Mo$) with the Schiff base bis(2-hydroxyacetophenone)ethylenediimine (happenH₂) in air gave the oxo derivative $M(O)(happen)$ with the metal in the +4 formal oxidation state. The dihydride complex $MoH_2(CO)(happen)$ was also isolated under reduced pressure [32]. On the other hand, reaction of happenH₂ with $Ru_3(CO)_{12}$ resulted in the formation of the dicarbonyl derivative $Ru(CO)_2(happenH_2)$ [34]. Reaction of bis(salicylaldehyde)ethylenediimine (salenH₂) with $Cr(CO)_6$ under reduced pressure yielded the dicarbonyl derivative $Cr(CO)_2(salenH_2)$ with the chromium atom in the zero oxidation state, while its reaction with $Mo(CO)_6$ in air

gave the paramagnetic oxo metal complexes Mo(CO)(O)(salen) with a +IV metal oxidation state and a high-spin d^2 configuration [32] ((Figure 2.2).

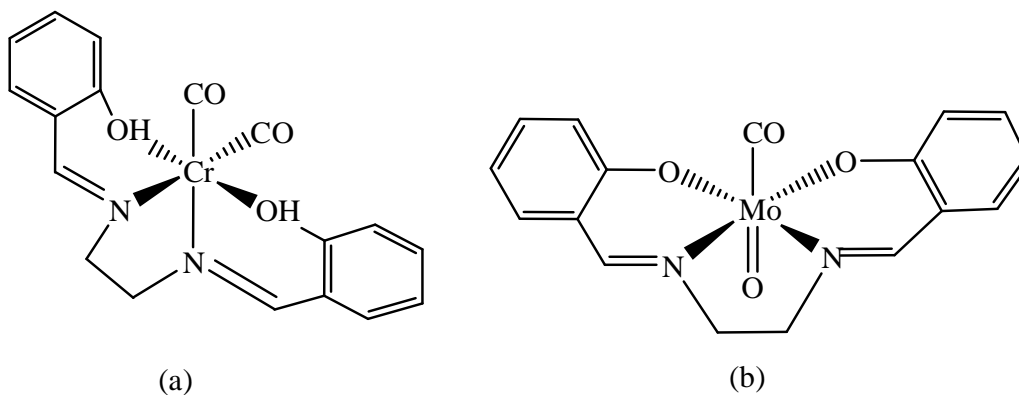


Figure 2.2 SalenH₂ complexes of (a) Cr(0) and (b) Mo(IV+)

Recently, reactions of M(CO)_6 ($\text{M} = \text{Cr, Mo and W}$) with N-salicylidene-2-hydroxyaniline (shaH₂) (Figure 2.3) were reported.

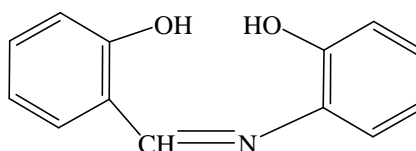


Figure 2.3 The structural formula of shaH₂

Under reduced pressure, the reaction yielded $\text{CrO}_2(\text{CO})_2(\text{shaH}_2)$ and $\text{W(CO)}_2(\text{shaH})_2$ (Figure 2.4), while in air the reaction yielded $\text{MoO}(\text{sha})$ and $\text{Mo}_2\text{O}_4(\text{sha})_2$ (Figure 2.5) [2]. Structural studies of the complexes revealed that shaH₂ binds to the metal through the oxygen atoms of the hydroxyl groups and the nitrogen atom of the imine group. Thus, the type of ligand and the reaction conditions play a vital role in determining the type of products isolated.

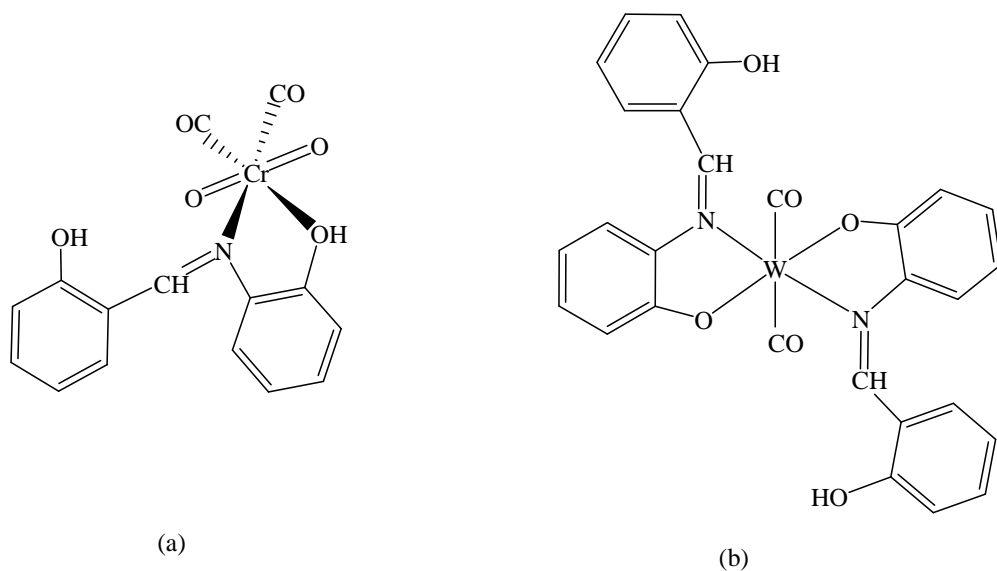


Figure 2.4 ShaH₂ complexes of (a) Cr; and (b) W, formed under reduced pressure

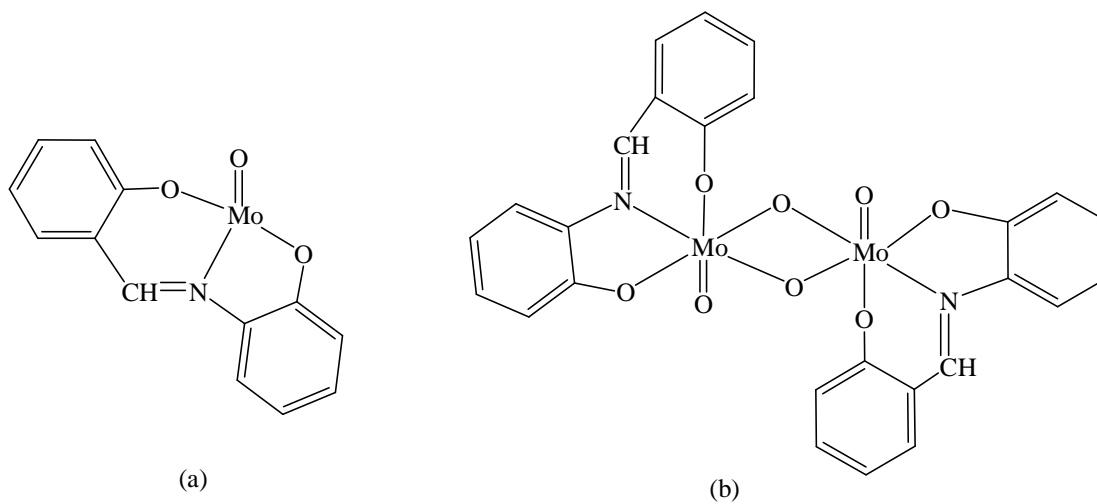


Figure 2.5 ShaH₂ complexes of Mo formed in air

Interaction of metal carbonyls $M(CO)_6$ ($M = Cr, Mo$ and W) with the tetradentate Schiff base, bis(salicylaldehyde)phenylenediimine (salphenH₂) was studied in THF [3]. Under reduced pressure, the reaction with $Cr(CO)_6$ and $Mo(CO)_6$ yielded $Cr(CO)_2(salphen)$ and $MoO(CO)(salphen)$ respectively, while in air the reaction yielded

$\text{MoO}_2(\text{salphenH})_2$ and $\text{W}_2\text{O}_6(\text{salphenH}_2)$. All complexes were characterized by elemental analysis, mass spectrometry and IR and ^1H -NMR spectroscopies. Spectroscopic studies supported the proposed structures. The UV-vis spectra of the complexes in different solvents showed bands due to either metal-to-ligand or ligand-to-metal charge transfer transition.

Several Schiff base complexes contain two or more metal ions [35, 36]. There is increasing evidence that binuclear transition metal complexes have played important roles in the development of coordination chemistry. Examples are models for more complex systems of polymetallic or cluster catalyzed reactions, and applications of mixed metal systems in organic synthesis [20]. In addition, they act as models in bioinorganic chemistry [37]. The development of a large number and varieties of binucleating ligands has led to the successful synthesis of a variety of homo and hetero-binuclear metal complexes [38]. An evolution started few decades ago toward hetero-bimetallic complexes, but still limited number of these complexes are known and fully structurally characterized. The literature survey reported that Schiff base and their complexes possess good luminescence and pigmentation properties. A number of Schiff base metal complexes were also reported to be a great utility in pharmacological and biological aspects. These properties depend on the structure of ligand and the nature of metal ion [35-38].

2.2 Catalytic properties

M.J Alcon et. al studied the catalytic properties of phenylenediamine complexes of the type $[\text{Cu}(\text{L})]\text{ClO}_4$ and $[\text{Mn}(\text{L})\text{Cl}(\text{H}_2\text{O})]\text{PF}_6$, ($\text{L} = N,N'$ -bis(*S*-prolyl)phenylenediamine, *N,N'*-bis(*S-N*-benzylprolyl)phenylenediamine, *N,N'*-bis[(*S*-pyrrolidin-2-yl)methyl]phenylenediamine, and *N,N'*-bis-[(*S-N*-benzyl-pyrrolidin-2-yl)methyl]phenylenediamine, in which the ligands were coordinated to the metal ion in tetradentate manner. The complexes were found to catalyze the cyclopropanation of styrene with ethyl and *t*-butyl diazoacetate to afford *cis/trans* 2-phenylcyclopropan-1-carboxylates with good yields and selectivity against dimerisation and low ee (<10%). On the other hand, the manganese and copper complexes also catalyse the oxidation of organic sulfides to sulfoxides with high selectivity, and moderate to low enantioselectivity. If an excess of oxidant were used the reaction yields sulfone as only product with excellent yield [39].

The oxidative mechanism of isatin Schiff base Cu(II) complexes have been studied towards the oxidation of common carbohydrates such as glucose, fructose and galactose by molecular oxygen. The imine ligands are capable of modifying selectively the environment of the copper(II) ion in a pH controlled process, through keto–enolic equilibria similar to those occurring with carbohydrates. Kinetic studies revealed that the reaction follows pseudo-first order behavior depending both on the catalyst and substrate concentrations, followed by a saturation effect, for all the compounds studied. Further, the pH profile indicated that reaction occurs significantly only in very alkaline medium ($\text{pH} \geq 10$), and some influence of ionic strength (controlled by carbonate buffer) was also verified [40].

Polydentate Schiff base ligands derived from the reaction of 2-(2-aminoethyliminomethyl)phenol with phthaldialdehyde, 4-methyl-2,6-diformylphenol and 4-*t*-butyl-2,6-diformylphenol in ethanol solution were prepared and the complexes of Cd(II), Cu(II), Co(II), Ni(II), Zn(II) and Sn(II) have been investigated [41]. The catalytic properties of Cu(II) and Co(II) complexes were studied on 3,5-di-*tert*-butylcatechol and ascorbic acid as a substrate. The oxidative C–C coupling properties of the Co(II) and Cu(II) complexes have been investigated on the sterically hindered 2,6-di-*tert*-butylphenol.

In 2008, Kefeng et. al prepared a series of tridentate N,N,N iron(II) and cobalt(II) complexes containing *N*-((pyridin-2-yl)methylene)-quinolin-8-amine derivatives [42]. On treatment with modified methylaluminoxane, these metal complexes exhibited good catalytic activities up to $2.8 \times 10^6 \text{ g mol}^{-1}(\text{Fe}) \text{ h}^{-1}$ for ethylene oligomerization, and butenes were the major products with nice selectivity for 1-C₄. The steric and electronic effects on catalytic activities of metal complexes were carefully investigated as well as the influence of various reaction parameters. In the catalytic system, Fe(II) complexes performed better catalytic activities than their Co(II) analogues. With ligands having bulky substituents, the better catalytic activity was observed in catalytic system of Fe(II) complex, however, the lower catalytic activity was obtained in catalytic system of Co(II) complexes.

Further more, catalytic ethylene polymerization properties of iron(II) and cobalt(II) complexes of 2,6-bis(4-nitro-2,6-R₂-phenylimino)pyridines, LMCl₂, R = Me, M = Fe; R = *i*Pr, M = Fe; R = Me, M = Co; R = *i*Pr, M = Co, have been investigated. Among these complexes, the iron(II) pre-catalyst bearing the *ortho*-isopropyl groups

exhibited higher activities and produced higher molecular weight polymers than the other complexes in the presence of methylaluminoxane (MAO). A comparison of this complex with the reference catalyst, (2,6-bis(2,6 diisopropylphenylimino)pyridyl)FeCl₂, revealed a modest increase of the catalytic activity and longer lifetime upon substitution of the *para*-positions with nitro groups, converting ethylene to highly linear polyethylenes with a unimodal molecular weight distribution around 456.4 kg mol⁻¹. However, the iron(II) pre-catalyst on changing from *ortho*-isopropyl to methyl groups displayed much lower activities (over an order of magnitude) than the iron(II) pre-catalyst under mild conditions. As expected, the cobalt analogues showed relatively low polymerization activities [43].

2.3 FTIR spectroscopy

The infrared portion of the electromagnetic spectrum is divided into three regions: near-, mid- and far- infrared, named for their relation to the visible spectrum. The far-infrared, approximately 400-10 cm⁻¹ (1000–30 μm), lying adjacent to the microwave region, has low energy and may be used for rotational spectroscopy. The mid-infrared, approximately 4000-400 cm⁻¹ (30–2.5 μm) may be used to study the fundamental vibrations and associated rotational-vibrational structure. The higher energy near-IR, approximately 14000-4000 cm⁻¹ (2.5–0.8 μm) can excite overtone or harmonic vibrations. The names and classifications of these subregions are merely conventions. They are neither strict division nor based on exact molecular or electromagnetic properties.

Infrared spectroscopy exploits the fact that molecules have specific frequencies at which they rotate or vibrate corresponding to discrete energy levels (vibrational modes).

These resonant frequencies are determined by the shape of the molecular potential energy surfaces, the masses of the atoms and, by the associated vibronic coupling. In order for a vibrational mode in a molecule to be IR active, it must be associated with changes in the permanent dipole. In particular, in the Born-Oppenheimer and harmonic approximations, i.e. when the molecular Hamiltonian corresponding to the electronic ground state can be approximated by a harmonic oscillator in the neighborhood of the equilibrium molecular geometry, the resonant frequencies are determined by the normal modes corresponding to the molecular electronic ground state potential energy surface. Nevertheless, the resonant frequencies can be in a first approach related to the strength of the bond, and the mass of the atoms at either end of it. Thus, the frequency of the vibrations can be associated with a particular bond type.

Simple diatomic molecules have only one bond, which may stretch. More complex molecules have many bonds, and vibrations can be conjugated, leading to infrared absorptions at characteristic frequencies that may be related to chemical groups. For example, the atoms in a CH₂ group, commonly found in organic compounds can vibrate in six different ways: symmetrical and antisymmetrical stretching, and 4 different bending modes: scissoring, wagging, rocking and twisting [44-48].

2.4 NMR spectroscopy

Nuclear magnetic resonance spectroscopy (NMR) is a technique which exploits the magnetic properties of certain nuclei. The most important applications for the organic chemist are proton NMR and carbon-13 NMR spectroscopy. In principle, NMR is applicable to any nucleus possessing spin.

Many information can be obtained from an NMR spectrum. Much like using infrared spectroscopy to identify functional groups, analysis of a 1D NMR spectrum provides information on the number and type of chemical entities in a molecule. However, NMR provides much more information than IR.

The impact of NMR spectroscopy on the natural sciences has been substantial. It can, among other things, be used to study mixtures of analytes, to understand dynamic effects such as change in temperature and reaction mechanisms, and is an invaluable tool in understanding protein and nucleic acid structure and function. It can be applied to a wide variety of samples, both in the solution and the solid state.

When placed in a magnetic field, NMR active nuclei (such as ^1H or ^{13}C) absorb at a frequency characteristic of the isotope. The resonant frequency, energy of the absorption and the intensity of the signal are proportional to the strength of the magnetic field. For example, in a 21 tesla magnetic field, protons resonate at 900 MHz. It is common to refer to a 21 T magnet as a 900 MHz magnet, although different nuclei resonate at a different frequency at this field strength.

Depending on the local chemical environment, different protons in a molecule resonate at slightly different frequencies. Since both this frequency shift and the fundamental resonant frequency are directly proportional to the strength of the magnetic field, the shift is converted into a field-independent dimensionless value known as the chemical shift. The chemical shift is reported as a relative measure from some reference resonance frequency. For the nuclei ^1H , ^{13}C , and ^{29}Si , TMS (tetramethylsilane) is commonly used as a reference. This difference between the frequency of the signal and

the frequency of the reference is divided by frequency of the reference signal to give the chemical shift. The frequency shifts are extremely small in comparison to the fundamental NMR frequency. A typical frequency shift might be 100 Hz, compared to a fundamental NMR frequency of 100 MHz, so the chemical shift is generally expressed in parts per million (ppm) [49].

By understanding different chemical environments, the chemical shift can be used to obtain some structural information about the molecule in a sample. The conversion of the raw data to this information is called assigning the spectrum. For example, for the ^1H -NMR spectrum for ethanol ($\text{CH}_3\text{CH}_2\text{OH}$), one would expect three specific signals at three specific chemical shifts: one for the CH_3 group, one for the CH_2 group and one for the OH group. A typical CH_3 group has a shift around 1 ppm, a CH_2 attached to an OH has a shift of around 4 ppm and an OH has a shift around 2–3 ppm depending on the solvent used.

Because of molecular motion at room temperature, the three methyl protons *average* out during the course of the NMR experiment (which typically requires a few ms). These protons become degenerate and form a peak at the same chemical shift which is difficult to interpret in more complicated NMR experiments. The shape and size of peaks are indicators of chemical structure too. In the example above—the proton spectrum of ethanol—the CH_3 peak would be three times as large as the OH. Similarly the CH_2 peak would be twice the size of the OH peak but only $2/3$ the size of the CH_3 peak.

Modern analysis software allows analysis of the size of peaks to understand how many protons give rise to the peak. This is known as integration—a mathematical process which calculates the area under a graph (essentially what a spectrum is). The analyst must integrate the peak and not measure its height because the peaks also have *width*—and thus its size is dependent on its area not its height. However, it should be mentioned that the number of protons, or any other observed nucleus, is only proportional to the intensity, or the integral, of the NMR signal, in the very simplest one-dimensional NMR experiments. In more elaborate experiments, for instance, experiments typically used to obtain carbon-13 NMR spectra, the integral of the signals depends on the relaxation rate of the nucleus, and its scalar and dipolar coupling constants. Very often these factors are poorly understood - therefore, the integral of the NMR signal is very difficult to interpret in more complicated NMR experiments [50].

2.5 Ultraviolet-visible spectroscopy

Ultraviolet-visible spectroscopy or ultraviolet-visible spectrophotometry (UV-Vis or UV/Vis) involves the spectroscopy of photons in the UV-visible region. This means it uses light in the visible and adjacent (near ultraviolet (UV) and near infrared (NIR)) ranges. The absorption in the visible ranges directly affects the color of the chemicals involved. In this region of the electromagnetic spectrum, molecules undergo electronic transitions. This technique is complementary to fluorescence spectroscopy, in that fluorescence deals with transitions from the excited state to the ground state, while absorption measures transitions from the ground state to the excited state.

UV/Vis spectroscopy is routinely used in the quantitative determination of solutions of transition metal ions and highly conjugated organic compounds.

- Solutions of transition metal ions can be coloured (i.e., absorb visible light) because d electrons within the metal atoms can be excited from one electronic state to another. The colour of metal ion solutions is strongly affected by the presence of other species, such as certain anions or ligands. For instance, the colour of a dilute solution of copper sulfate is a very light blue; adding ammonia intensifies the colour and changes the wavelength of maximum absorption (λ_{max}).
- Organic compounds, especially those with a high degree of conjugation, also absorb light in the UV or visible regions of the electromagnetic spectrum. The solvents for these determinations are often water for water soluble compounds, or ethanol for organic-soluble compounds. (Organic solvents may have significant UV absorption; not all solvents are suitable for use in UV spectroscopy. Ethanol absorbs very weakly at most wavelengths.) Solvent polarity and pH can affect the absorption spectrum of an organic compound. Tyrosine, for example, increases in absorption maxima and molar extinction coefficient when pH increases from 6 to 13 or when solvent polarity decreases.
- While charge transfer complexes also give rise to colours, the colours are often too intense to be used for quantitative measurement.

The Beer-Lambert law states that the absorbance of a solution is directly proportional to the concentration of the absorbing species in the solution and the path length. Thus, for a fixed path length, UV/VIS spectroscopy can be used to determine the

concentration of the absorber in a solution. It is necessary to know how quickly the absorbance changes with concentration. This can be taken from references (tables of molar extinction coefficients), or more accurately, determined from a calibration curve [51].

2.6 Elemental analysis

To determine the precise amounts of elements (carbon, hydrogen, nitrogen, sulphur) present in an unknown substance, a quantitative analysis is required. Commercially available elemental analyzers are capable of determining simultaneously the percentages of carbon, hydrogen and nitrogen in a compound. In these instruments the sample is burned in a stream of oxygen. The gaseous products are converted to carbon dioxide, water, and nitrogen, which can be detected via gas chromatography, using thermal conductivity detectors. The precise amount of each gas produced in the combustion is determined by integration of the corresponding gas chromatography peaks [52].

2.7 Cyclic voltammetry

Electrolysis, cyclic voltammetry, amperometry and several other techniques might be described as “active” electrochemical methods because the experimenter drives an electrochemical reaction by incorporating the chemistry into a circuit and then controlling the reaction by circuit parameters such as voltage. In typical cyclic voltammetry, a solution component is electrolyzed (oxidized or reduced) by placing it in contact with an electrode surface, and then making that surface sufficiently positive or negative in voltage to force electron transfer.

In simple cases, the electrode surface is initially at a particular voltage with respect to a reference half-cell, such as calomel or Ag/AgCl, the electrode voltage is changed to a higher or lower voltage at a linear rate, and finally, the voltage is changed back to the original value at the same linear rate. When the surface becomes sufficiently negative or positive, a solution species may gain electrons from the surface or transfer electrons to the surface. This results in a measurable current in the electrode circuitry. However, if the solution is not mixed, the concentration of transferring species near the surface drops, and the electrolysis current then falls off. When the voltage cycle is reversed, it is often the case that electron transfer between electrode and chemical species will also be reversed, leading to an “inverse” current peak. These features are illustrated in Figure 2.6 [53].

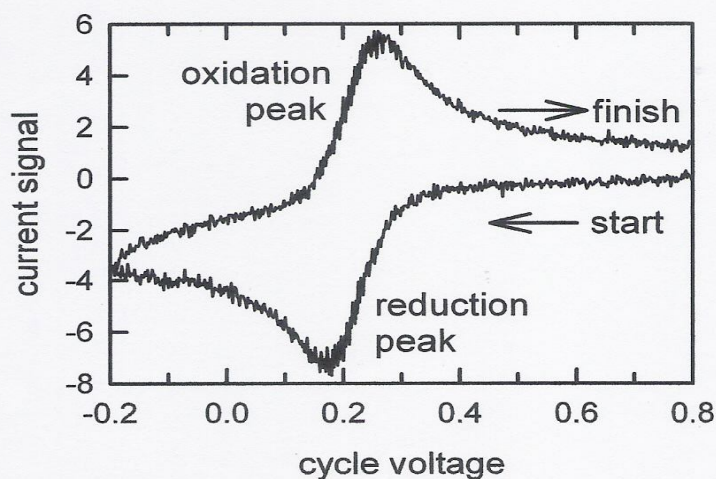


Figure 2.6 A simple cyclic voltammogram

CHAPTER 3

EXPERIMENTAL

CHAPTER 3: EXPERIMENTAL

Four Schiff base ligands, N,N'-1,2-benzene-1,2-diyl-bis(5-chlorosalicylideneimine) (H_2L1), N,N'-1,2-benzene-1,2-diyl-bis(4-bromosalicylideneimine) (H_2L2), N,N'-1,2-benzene-1,2-diyl-bis(4-hydroxysalicylideneimine) (H_2L3), and N,N'-1,2-benzene-1,2-diyl-bis(3-bromo-5-chlorosalicylideneimine) (H_2L4) (Figure 3.1) and their copper(II), iron(II) and nickel(II) complexes (a total of twelve complexes) were prepared according to published methods [54,55].

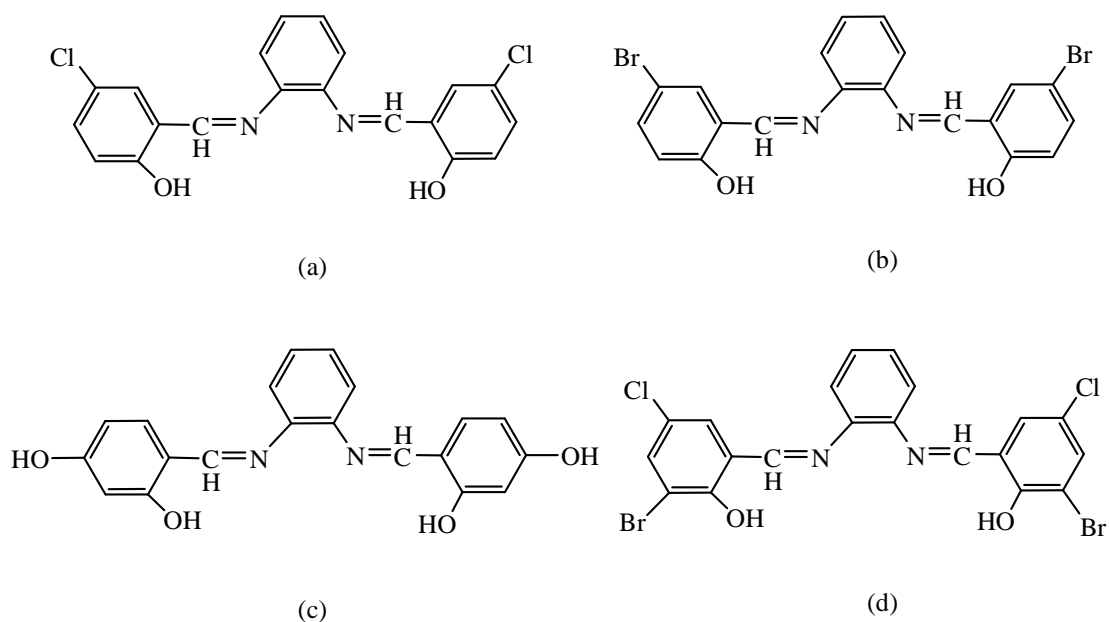


Figure 3.1 Structural formula of Schiff bases: (a) H_2L1 ; (b) H_2L2 ; (c) H_2L3 ; and (d) H_2L4

The ligands were characterized by Fourier transform infrared spectroscopy, elemental analysis, 1H -nuclear magnetic resonance spectroscopy and UV-vis spectroscopy, while the complexes were characterized by Fourier transform infrared spectroscopy, elemental analysis, UV-vis spectroscopy and cyclic voltammetry.

3.1 Materials

The chemicals used in the synthesis were 1,2-diaminobenzene (*o*-C₆H₄(NH₂)₂; FW 108.14), 5-chlorosalicylaldehyde (5-ClC₆H₃(OH)CHO; FW 156.57), 5-bromosalicylaldehyde (5-BrC₆H₃(OH)CHO; FW 210.02), 2,4-dihydroxybenzaldehyde (2,4-C₆H₃(OH)₂CHO; FW 138.12), 3-bromo-5-chlorosalicylaldehyde (BrC₆H₂(Cl)-2-(OH)CHO; FW 235.47), triethylamine, copper(II) acetate monohydrate (CuC₄H₆O₄.H₂O; FW 199.65), iron(II) sulphate heptahydrate (FeSO₄.7H₂O; FW 278.02), and nickel(II) acetate tetrahydrate (NiC₄H₆O₄.4H₂O; FW 248.86). These chemicals and common organic solvents were commercially available and used as received.

3.2 Preparation of H₂L1 and its metal complexes

3.2.1 Preparation of H₂L1

A solution of 5-chlorosalicylaldehyde (0.60 g, 3.83 mmol) in ethanol (40 cm³) was mixed with a solution of 1,2-diaminobenzene (0.21 g, 1.94 mmol) in ethanol (40 cm³). The mixture was stirred under reflux for 2 hours. The orange powder formed was filtered and recrystallized from ethanol. It was dried in an oven (80°C) for 30 min. The yield was 0.58 g (78%). Selected FTIR data (KBr, cm⁻¹): 3329 (m, -OH), 2923 (m, C-H), 1612 (s, C=N), 1273 (s, C-O). Anal. Calc. for [C₂₀H₁₄O₂N₂Cl₂; FW 385.25]: C, 62.29; H, 3.63; N, 7.26. Found: C, 62.53; H, 3.29; N, 7.43%.

3.2.2 Preparation of CuL1

A solution of H₂L1 (0.10 g, 0.26 mmol) in ethanol (40 cm³) was added to a solution of copper(II) acetate monohydrate (0.05 g, 0.25 mmol) in ethanol (30 cm³). A few drops of triethylamine were then added to the mixture. The mixture was magnetically

stirred and refluxed for 3 hours. The brown powder formed was filtered and recrystallized from DMSO. The yield was 0.06 g (54%). Selected FTIR data (KBr, cm^{-1}): 3432 (m, OH), 1580 (s, C=N), 1168 (s, C-O), 552 (w, Cu-O). Anal. Calc. for $[\text{CuC}_{20}\text{H}_{12}\text{O}_2\text{N}_2\text{Cl}_2]$; FW 446.79]: C, 53.71; H, 2.68; N, 6.26. Found: C, 53.42; H, 2.47; N, 6.51%.

3.2.3 Preparation of FeL1

The method is the same as for CuL1, using H₂L1 (0.10 g, 0.26 mmol) and iron(II) sulphate heptahydrate (0.07 g, 0.25 mmol). The product was a reddish brown powder, and the yield was 0.07 g (64%). Selected FTIR data (KBr, cm^{-1}): 3422 (m, -OH), 1608 (s, C=N), 1312 (s, C-O), 548 (w, Fe-O). Anal. Calc. for $[\text{FeC}_{20}\text{H}_{12}\text{O}_2\text{N}_2\text{Cl}_2]$; FW 439.09]: C, 54.65; H, 2.73; N, 6.37. Found: C, 54.35; H, 2.57; N, 6.34%.

Trials were done to prepare the Fe(III) complex but in vain.

3.2.5 Preparation of NiL1

The method is the same as for CuL1, using H₂L1 (0.10 g, 0.26 mmol) and nickel(II) acetate tetrahydrate (0.06 g, 0.24 mmol). The product was a red powder, and the yield was 0.22 g (75%). Selected FTIR data (KBr, cm^{-1}): 3056 (m, -OH), 1608 (s, C=N), 1190 (s, C-O), 537 (w, Ni-O). Anal. Calc. for $[\text{NiC}_{20}\text{H}_{12}\text{O}_2\text{N}_2\text{Cl}_2]$; FW 441.94]: C, 54.30; H, 2.71; N, 6.33. Found: C, 54.10; H, 2.60; N, 6.55%.

3.3 Preparation of H₂L2 and its metal complexes

3.3.1 Preparation of H₂L2

The method is the same as for H₂L1, using 5-bromosalicylaldehyde (0.60 g, 2.98 mmol) and 1,2-diaminobenzene (0.16 g, 1.49 mmol). The product was an orange

powder, and the yield was 0.53 g (75%). Selected FTIR data (KBr, cm^{-1}): 3423 (m, -OH), 2925 (m, C-H), 1612 (s, C=N), 1273 (s, C-O). Anal. Calc. for $[\text{C}_{20}\text{H}_{14}\text{O}_2\text{N}_2\text{Br}_2]$; FW 474]: C, 50.60; H, 2.95; N, 5.90. Found: C, 50.90; H, 2.75; N, 6.12%.

3.3.2 Preparation of CuL2

The method is the same as for CuL1, using H_2L_2 (0.10 g, 0.21 mmol) and copper(II) acetate monohydrate (0.05 g, 0.25 mmol). The product was a brown powder, and the yield was 0.15 g (71%). Selected FTIR data (KBr, cm^{-1}): 3401 (m, -OH), 1606 (s, C=N), 1177 (s, C-O), 550 (w, Cu-O). Anal. Calc. for $[\text{CuC}_{20}\text{H}_{12}\text{O}_2\text{N}_2\text{Br}_2]$; FW 535.54]: C, 44.81; H, 2.24 N, 5.22. Found: C, 45.00; H, 2.24; N, 5.44 %.

3.3.3 Preparation of FeL2

The method is the same as for CuL1, using H_2L_2 (0.10 g, 0.21 mmol) and iron(II) sulphate heptahydrate (0.07 g, 0.25 mmol). The product was a reddish brown powder and the yield was 0.16 g (67%). Selected FTIR data (KBr, cm^{-1}): 3400 (m, OH), 1605 (s, C=N), 1170 (s, C-O), 546 (w, Fe-O). Anal. Calc. for $[\text{FeC}_{20}\text{H}_{12}\text{O}_2\text{N}_2\text{Br}_2]$; FW 427.84]: C, 45.46; H, 2.27; N, 5.30 Found: C, 45.28; H, 2.12; N, 5.12%.

Synthesis of Fe(III) complex gave no results.

3.3.4 Preparation of NiL2

The method is the same as for CuL1, using H_2L_2 (0.10 g, 0.21 mmol) and nickel(II) acetate tetrahydrate (0.06 g, 0.24 mmol). The product was a red powder and the yield was 0.08 g (72%). Selected FTIR data (KBr, cm^{-1}): 3398 (m, OH), 1606 (s, C=N), 1188 (s, C-O), 536 (w, Ni-O). Anal. Calc. for $[\text{NiC}_{20}\text{H}_{12}\text{O}_2\text{N}_2\text{Br}_2]$; FW 530.69]: C, 45.22; H, 2.26; N, 5.27. Found: C, 45.07; H, 2.17; N, 5.20%.

3.4 Preparation of H₂L3 and its metal complexes

3.4.1 Preparation of H₂L3

The method is the same as for H₂L1, using 2,4-dihydroxybenzaldehyde (0.60 g, 4.34 mmol) and 1,2-diaminobenzene (0.23 g, 2.17 mmol). The product was a yellow powder and the yield was 0.57 g (75%). Selected FTIR data (KBr, cm⁻¹): 3064 (m, -OH), 1610 (s, C=N), 1249 (s, C-O). Anal. Calc. for [C₂₀H₁₆O₄N₂; FW 348]: C, 68.90; H, 4.59; N, 8.04. Found: C, 68.73; H, 4.98; N, 7.95%.

3.4.2 Preparation of CuL3

The method is the same as for CuL1, using H₂L3 (0.10 g, 0.28 mmol) and copper(II) acetate monohydrate (0.05 g, 0.25 mmol). The product was a brown powder and the yield was 0.08 g (78%). Selected FTIR data (KBr, cm⁻¹): 3172 (m, OH), 1603 (s, C=N), 1237 (s, C-O), 533 (w, Cu-O). Anal. Calc. for [CuC₂₀H₁₄O₄N₂; FW 409.54]: C, 58.60; H, 3.41; N, 6.83. Found: C, 58.27; H, 3.65; N, 6.46%.

3.4.3 Preparation of FeL3

The method is the same as for CuL1, using H₂L3 (0.10 g, 0.28 mmol) and iron(II) sulphate heptahydrate (0.07 g, 0.25 mmol). The product was a deep brown powder and the yield was 0.07 g (70%). Selected FTIR data (KBr, cm⁻¹): 3385 (m, OH), 1597 (s, C=N), 1203 (s, C-O), 559 (w, Fe-O). Anal. Calc. for [FeC₂₀H₁₄O₄N₂; FW 401.84]: C, 59.72; H, 3.48; N, 6.96. Found: C, 59.43; H, 3.67; N, 6.55%.

Fe(III) complex couldn't be synthesized.

3.4.4 Preparation of NiL3

The method is the same as for CuL1, using H₂L3 (0.10 g, 0.21 mmol) and nickel(II) acetate tetrahydrate (0.06 g, 0.24 mmol). The product was a red powder and the yield was 0.07 g (82%). Selected FTIR data (KBr, cm⁻¹): 3331 (m, OH), 1604 (s, C=N), 1208 (s, C-O), 542 (Ni-O). Anal. Calc. for [NiC₂₀H₁₄O₄N₂; FW 404.69]: C, 59.30; H, 3.45; N, 6.91. Found: C, 59.14; H, 3.60; N, 6.67%.

3.5 Preparation of H₂L4 and its metal complexes

3.5.1 Preparation of H₂L4

The method is the same as for H₂L1, using 3-bromo-5-chlorosalicylaldehyde (0.60 g, 2.54 mmol) and 1,2-diaminobenzene (0.14 g, 1.27 mmol). The product was an orange powder and the yield was 0.49 g (71%). Selected FTIR data (KBr, cm⁻¹): 3078 (m, -OH), 1612 (s, C=N), 1165 (s, C-O). Anal. Calc. for [C₂₀H₁₂O₂N₂Cl₂Br₂; FW 543.04]: C, 44.24; H, 2.23; N, 5.16. Found: C, 44.31; H, 2.24; N, 5.22%.

3.5.2 Preparation of CuL4

The method is the same as for CuL1, using H₂L4 (0.10 g, 0.21 mmol) and nickel(II) acetate tetrahydrate (0.06 g, 0.24 mmol). The product was an orange powder, and the yield was 0.08 g (63%). Selected FTIR data (KBr, cm⁻¹): 3422 (m, OH), 1608 (s, C=N), 1157 (s, C-O), 571 (w, Cu-O). Anal. Calc. for [CuC₂₀H₁₀O₂N₂Cl₂Br₂; FW 604.58]: C, 39.73; H, 1.67; N, 4.63. Found: C, 39.33; H, 1.75; N, 4.67%.

3.5.3 Preparation of FeL4

The method is the same as for CuL1, using H₂L4 (0.10 g, 0.21 mmol) and iron(II) sulphate heptahydrate (0.04 g, 0.18 mmol). The product was a light brown powder,

and the yield was 0.075 g (70%). Selected FTIR data (KBr, cm^{-1}): 3402 (m, OH), 1604 (s, C=N), 1162 (s, C-O), 516 (w, Fe-O). Anal. Calc. for $[\text{FeC}_{20}\text{H}_{12}\text{O}_2\text{N}_2\text{Cl}_2\text{Br}_2]$; FW 596.88]: C, 40.25; H, 1.69; N, 4.69. Found: C, 40.00; H, 1.70; N, 4.59%.

Similar method was performed to synthesize Fe(III) complex but in vain.

3.5.4 Preparation of NiL4

The method is the same as for CuL1, using $\text{H}_2\text{L4}$ (0.10 g, 0.21 mmol) and nickel(II) acetate tetrahydrate (0.05 g, 0.18 mmol). The product was a red powder, and the yield was 0.08 g (74%). Selected FTIR data (KBr, cm^{-1}): 3423 (m, OH), 1606 (s, C=N), 1173 (s, C-O), 542 (w, Ni-O). Anal. Calc. for $[\text{NiC}_{20}\text{H}_{12}\text{O}_2\text{N}_2\text{Cl}_2\text{Br}_2]$; FW 599.73]: C, 40.05; H, 1.68; N, 4.67. Found: C, 39.79; H, 1.68; N, 4.55%.

3.6 Analysis

3.6.1 FTIR spectroscopy

FTIR spectra were recorded as KBr pellets in the range 4000-370 cm^{-1} on a Perkin-Elmer Spectrum 2000 FT-IR spectrophotometer.

3.6.2 Elemental analyses:

CHN analysis was carried out in PerkinElmer (Series II) CHNS/O analyzer 2400.

3.6.3 ^1H -NMR spectroscopy

The sample (about 20 mg) was dissolved in DMSO- d_6 (total volume about 1 cm^3). The spectrum was recorded at room temperature on a JEOL ECA-400 spectrometer, operating with a frequency of 400 MHz.

3.6.4 UV-Vis spectroscopy

The UV-vis spectra were recorded for samples dissolved in DMSO (about 0.02 M) in 1-cm quartz cuvettes on a Varian 50 UV-visible spectrophotometer in the wavelength range 200-800 nm.

3.6.5 Cyclic Voltammetry

Cyclic voltammetric measurement was performed on a Gambry Potentiostat/Galvanostat 600 instrument in DMSO at 25°C with tetrabutylammonium tetrafluoroborate (0.5 M) as supporting electrolyte. The mass of the complex was about 6.5 mg in 10 ml DMSO. A standard three-electrode assembly was employed: glassy carbon as working electrode, Ag/AgCl as reference electrode, and platinum wire as counter electrode. The scan rate was 100 mV s⁻¹, and the quoted E values are versus Ag/AgCl.

3.6.6 X-ray Crystallography

The crystal structures were recorded using ω -scan technique on an APEX-2 area detector diffractometer.

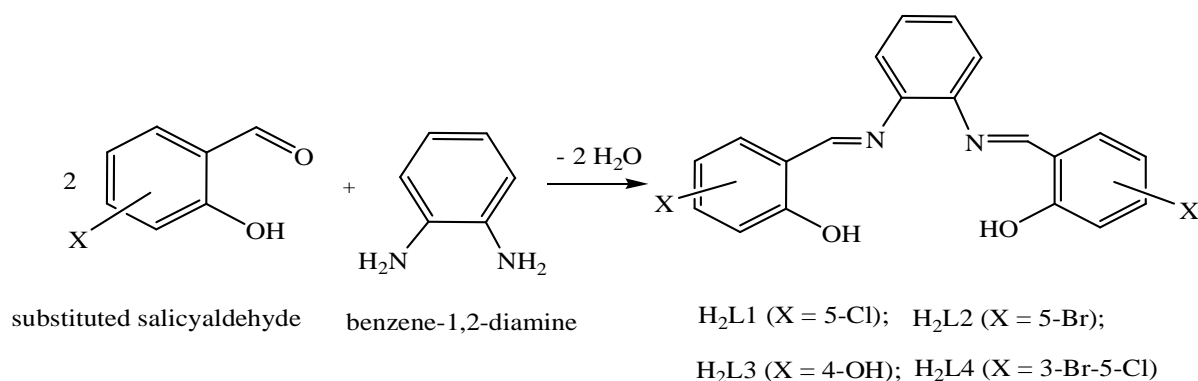
CHAPTER 4

RESULTS AND DISCUSSION

CHAPTER 4: RESULTS AND DISCUSSION

4.1 Introduction

Four Schiff bases were prepared from the reaction of mono- and disubstituted salicylaldehydes with 1,2-diaminobenzene in a 2:1 mole ratio. These ligands have substituents with different electronic effects, which may modify its physical and chemical properties. The method used was as published in the literature [54]. The general equation for the reaction is shown in **Scheme 4.1**.



Scheme 4.1 Reaction equation for the preparation of $\text{H}_2\text{L1}$, $\text{H}_2\text{L2}$, $\text{H}_2\text{L3}$, and $\text{H}_2\text{L4}$

Researches on $\text{H}_2\text{L1}$, $\text{H}_2\text{L2}$, and $\text{H}_2\text{L3}$ have been previously reported [55], while $\text{H}_2\text{L4}$ is a new Schiff base. The chemical and structural formulas of these ligands were confirmed by FTIR, elemental analyses and $^1\text{H-NMR}$, and its electronic properties by UV-vis spectroscopy.

Each of these Schiff bases were then reacted with Cu(II) , Fe(II) and Ni(II) salts according to the literature method [56]. These metal ions were chosen because they have been shown to be catalysts for several organic syntheses [57]. The chemical and structural formulas of these complexes were proposed from FTIR and elemental analyses. Additionally, the crystal structure of novel NiL4 was determined by single-crystal X-ray crystallography. Finally, the

electronic and electrochemical properties of these complexes were respectively probed by UV-vis spectroscopy and cyclic voltammetry.

The initial finding of this work was presented as a poster entitled “*Spectroscopic Studies of o-Phenylenediamine Schiff Bases and Their Metal Complexes*” at Malaysian Polymer International Conference (MPIC 2009) [Appendix 1].

4.2 *N,N'*-1,2-Benzene-1,2-diyl-bis(5-chlorosalicylideneimine) (H_2L1) and its copper(II), iron(II) and nickel(II) complexes

N,N'-1,2-Benzene-1,2-diyl-bis(5-chlorosalicylideneimine) (H_2L1) was obtained as an orange powder in good yield (78%) from the reaction shown in Scheme 4.1 ($X = 5\text{-Cl}$). The results from the C,H,N elemental analyses are in excellent agreement with the expected chemical formula, $C_{20}H_{14}O_2N_2Cl_2$.

The FTIR spectrum of H_2L1 , recorded as a KBr pellet, is shown in Figure 4.1.

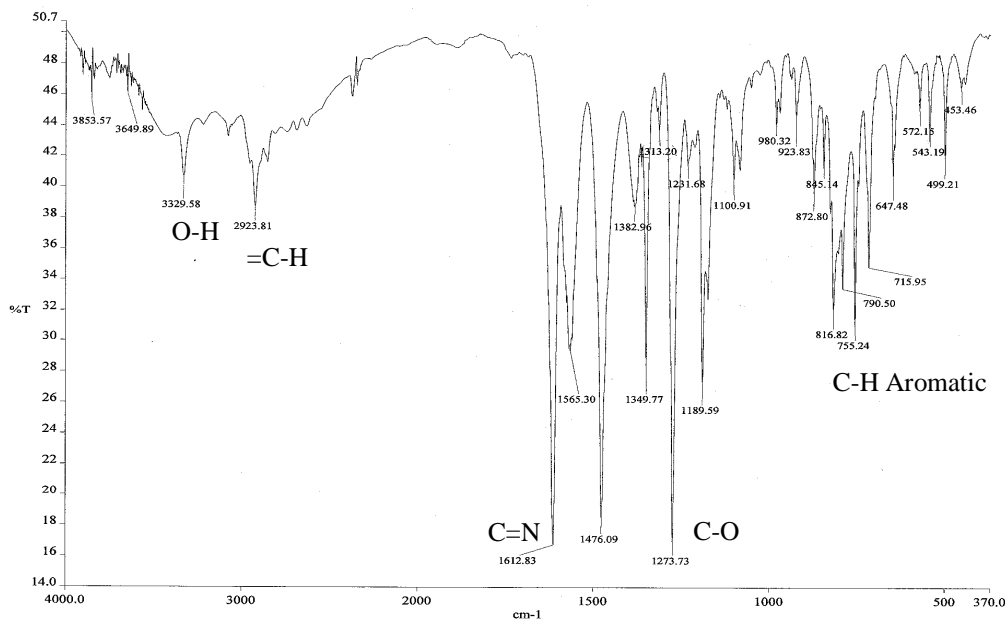


Figure 4.1 FTIR of H_2L1

The spectrum shows the characteristic strong peak due to C=N stretching at 1612 cm^{-1} , indicating the formation of the Schiff base. Another strong peak at 1273 cm^{-1} is assigned to C-O phenolic stretching, while a sharp weak peak at 3329 cm^{-1} is characteristic of free -OH group [1]. Other peaks bands in the region $1000 - 1500\text{ cm}^{-1}$ arise from benzene ring skeletal vibrations.

The ^1H -NMR spectrum of $\text{H}_2\text{L1}$, recorded as a solution in DMSO-d_6 , is shown in Figure 4.2.

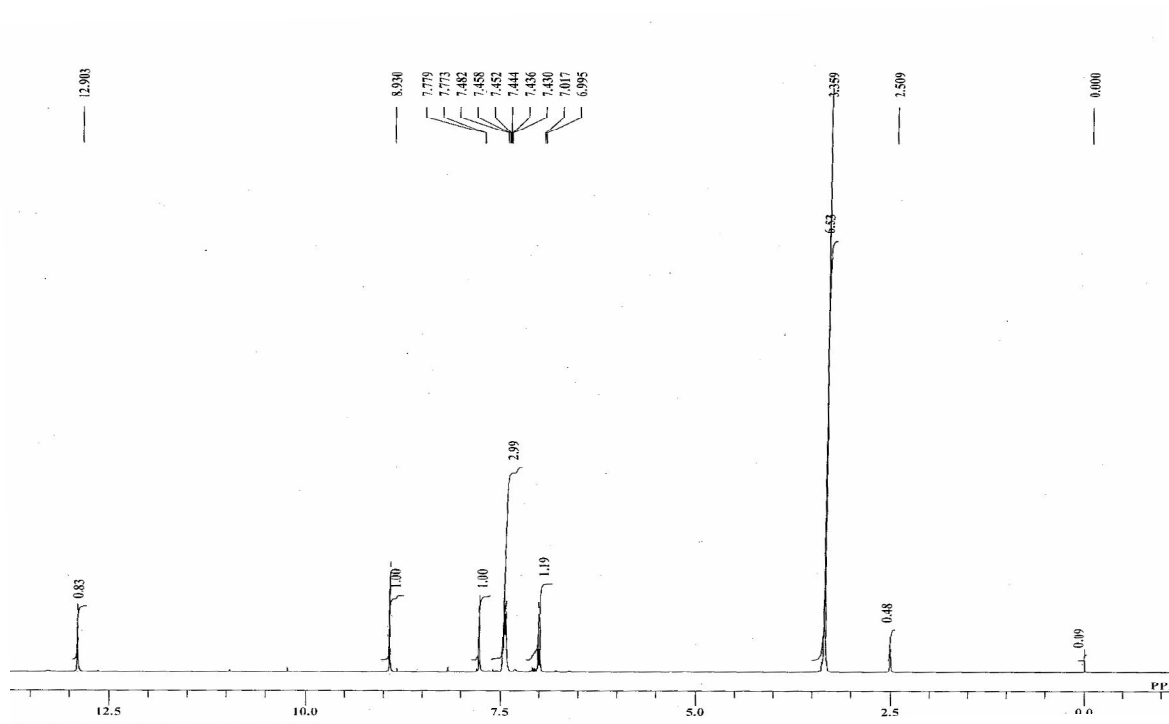


Figure 4.2 ^1H -NMR spectrum of $\text{H}_2\text{L1}$

The assignments of the above spectrum are consistent with the expected structural formula of $\text{H}_2\text{L1}$: a singlet at 12.9 ppm is due to phenolic hydrogen (H_a); a singlet at 8.9 ppm is due to imino hydrogen (H_b); and a multiplet in the range 6.9 - 7.7 ppm is due to the aromatic hydrogens (Figure 4.3). The integration ratio for these hydrogens is 1:1:5 respectively, and supports the molecular symmetry for the ligand (point group C_{2v}) [55].

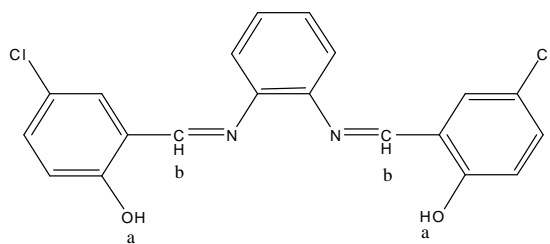


Figure 4.3 ^1H -NMR assignment of $\text{H}_2\text{L1}$

The electronic spectrum of a solution of $\text{H}_2\text{L1}$ in DMSO (Figure 4.4) shows two moderately intense absorption bands at 270 nm ($\epsilon = 350 \text{ M}^{-1}\text{cm}^{-1}$) and 343 nm ($\epsilon = 288 \text{ M}^{-1}\text{cm}^{-1}$). The bands are assigned to $\pi - \pi^*$ transition of the aromatic ring and $n - \pi^*$ transition of the azomethine chromophores, respectively. These values are in agreement with other Schiff bases reported in the literatures [58]. The weak shoulder at about 450 nm is probably due to $n - \pi^*$ transition of Cl chromophore on the ligand.

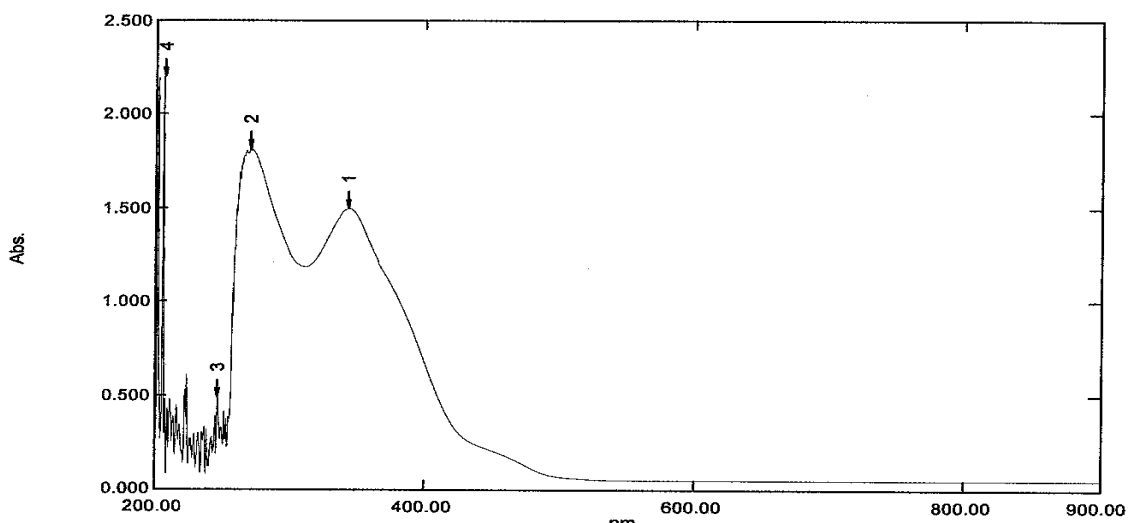


Figure 4.4 UV-vis spectrum of $\text{H}_2\text{L1}$ in DMSO

4.2.1 Copper(II) complex, CuL1

The copper (II) complex, CuL1, was obtained as a brown powder in good yield (54%) in the reaction between H₂L1 and copper(II) acetate monohydrate in the presence of triethylamine. The C,H,N elemental analyses are in excellent agreement with the expected chemical formula, [Cu(C₂₀H₁₂O₂N₂Cl₂)].

The FTIR spectrum of CuL1 (Figure 4.5) is compared with that of H₂L1 (Figure 4.1).

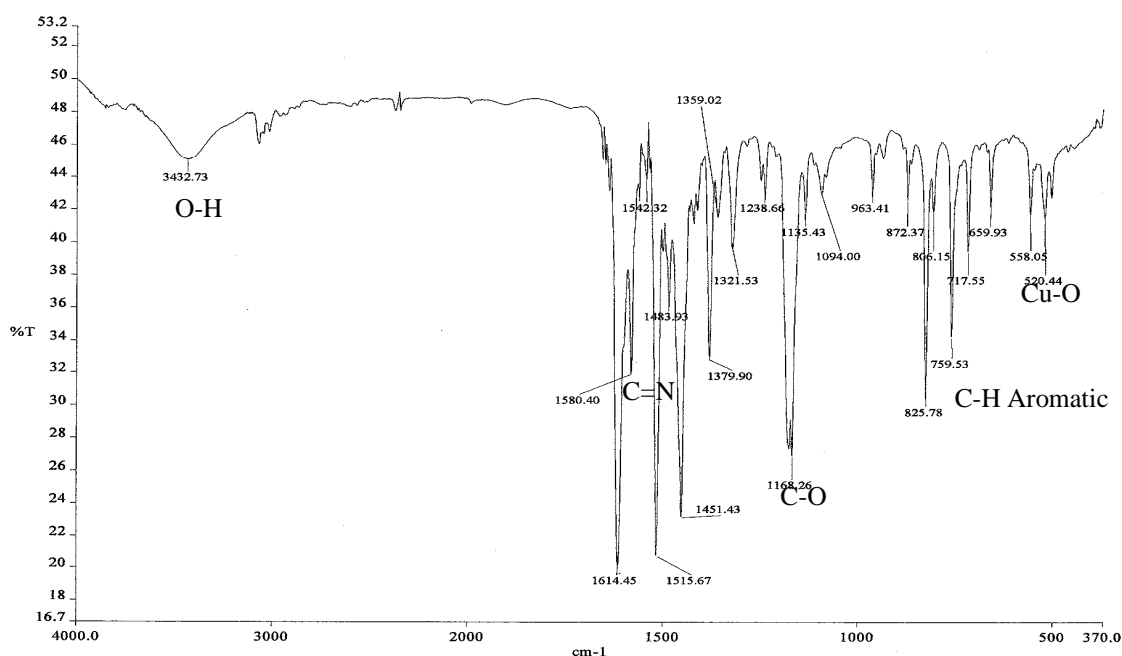


Figure 4.5 FTIR spectrum of CuL1

It is noted that the -OH peak of the ligand at 3329 cm⁻¹ has disappeared, indicating deprotonation of the phenolic group [56]. The peaks for C=N at 1612 cm⁻¹ and C-O at 1273 cm⁻¹ observed for H₂L1 have shifted to lower energy at 1580 cm⁻¹ and 1168 cm⁻¹ respectively in CuL1. These suggest that the phenolic oxygens and imino nitrogens are coordinated to Cu(II).

Additionally, a new peak observed at 572 cm^{-1} may be assigned to Cu-O bond [60]. Also observed in the spectrum is a new weak broad peak at 3432 cm^{-1} , assigned to H_2O molecule.

The UV-vis spectrum of CuL1 (Figure 4.6) is compared with that of $\text{H}_2\text{L1}$ (Figure 4.4). It is noted that the bands previously assigned to $\pi - \pi^*$ and $n - \pi^*$ transitions of the $\text{H}_2\text{L1}$ appears as overlapping peaks at 270 nm and 390 nm in the complex. Thus, the band assigned to $\pi - \pi^*$ of the aromatic ring and Cl chromophores remain almost unshifted. However, the $n - \pi^*$ transition is red shifted from 343 nm to 390 nm as a result of ligand-to-metal charge transfer (LMCT). These are in agreement with literature results [56, 58, 61] indicating the formation of the complex.

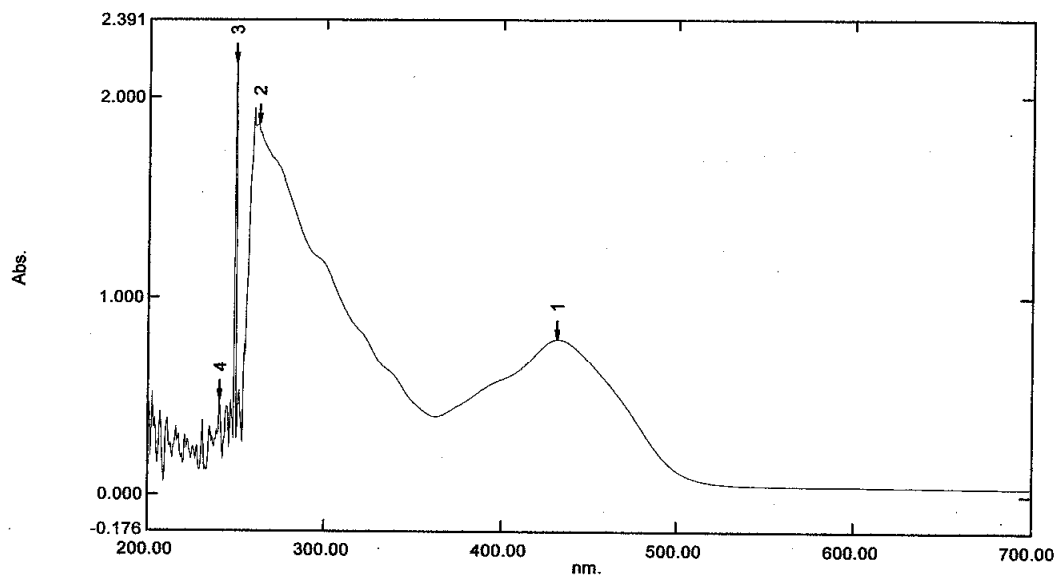


Figure 4.6 UV-vis spectrum of CuL1 in DMSO

In a separate run, the visible spectrum of CuL1 (Figure 4.7) shows a weak and broad band at 588 nm ($\epsilon = 12\text{ M}^{-1}\text{cm}^{-1}$), ascribed to the $d-d$ transition of Cu(II) in a square planar geometry under the influence of very strong ligand field effect of N_2O_2 chromophores. The band is very weak, consistent with the Laporte selection rule for a highly symmetrical complex.

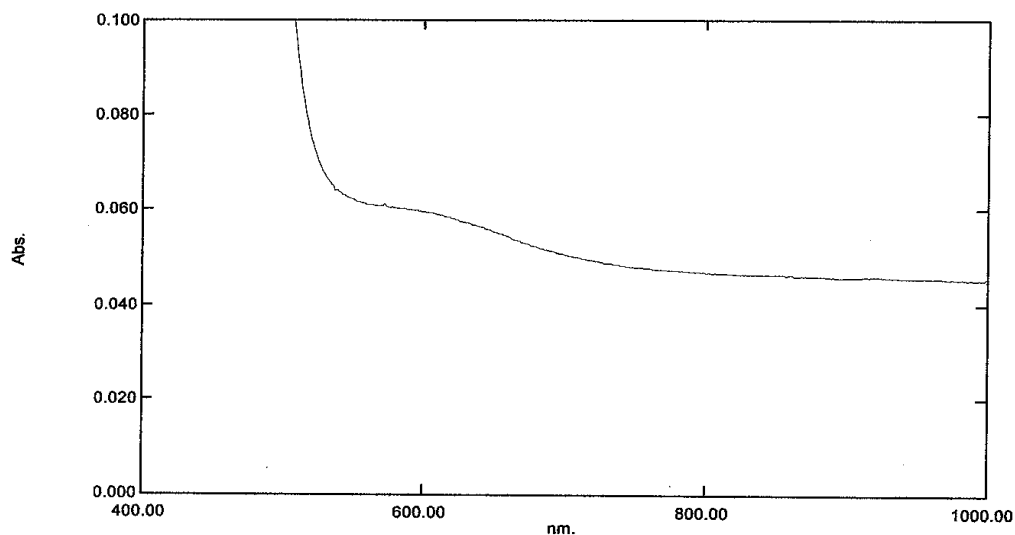


Figure 4.7 Visible spectrum of CuL1 in DMSO

Combining the results from CHN analyses, and FTIR and UV-vis spectroscopies, the structural formula proposed for CuL1 is shown in Figure 4.8.

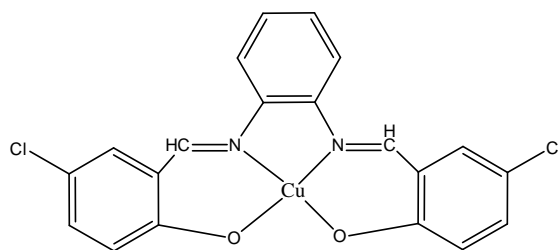


Figure 4.8 Proposed structural formula for CuL1 ($[\text{Cu}(\text{C}_{20}\text{H}_{12}\text{O}_2\text{N}_2\text{Cl}_2)]$)

The cyclic voltammogram of CuL1 in DMSO (Figure 4.9), scanned cathodically from 0 V in the voltage range -1.5 V to 1.5 V, shows two reduction peaks at -0.9 V ($I_{\text{pc}} = -1.67 \times 10^{-5}$ A) and -1.14 V ($I_{\text{pc}} = -1.73 \times 10^{-5}$ A), and an oxidation peak at -0.981 V ($I_{\text{pa}} = -2.01 \times 10^{-6}$ A). It is noted that the sharp and large peak (anodic stripping) due to the oxidation of Cu metal, expected at about 0 V, is not observed. From these results, it is suggested that the first peak at -0.9 V may

be due to the irreversible reduction of Cl in the ligand. The peaks at -1.14 V and -0.981 V are tentatively assigned as E_{pc} and E_{pa} for Cu(II) and Cu(I) respectively. From these, the calculated values are: $E_{1/2} = -1.06$ V, $\Delta E_p = 159$ mV, and $I_{pa}/I_{pc} = 0.12$, which suggest a quasireversible Cu(II)-Cu(I) redox reaction [57].

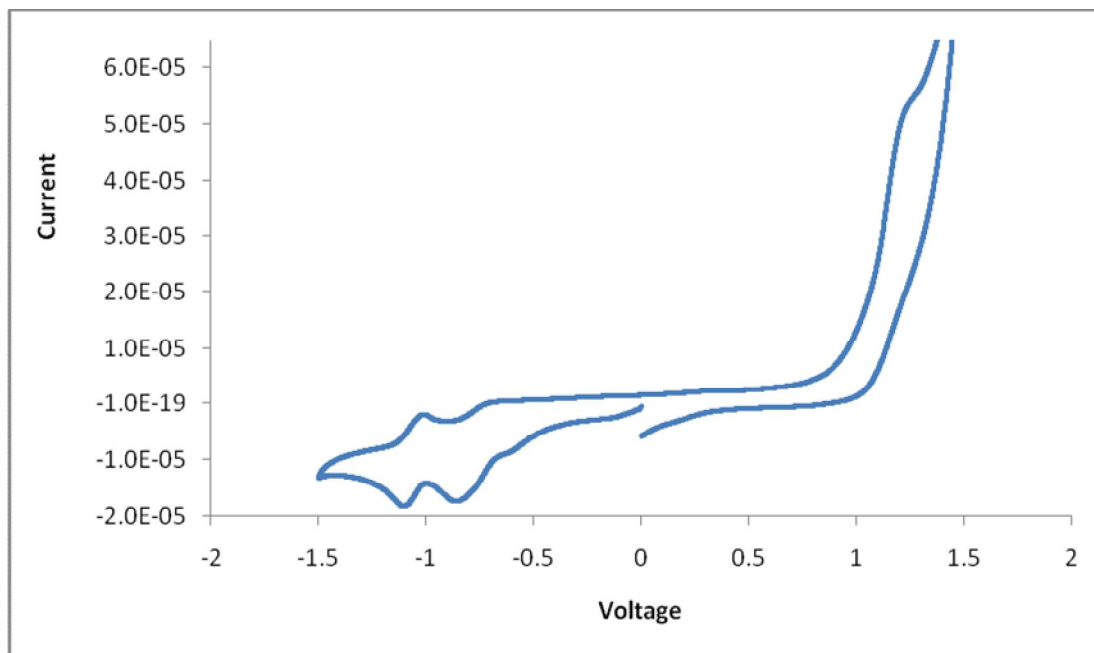


Figure 4.9 CV of CuL1 in DMSO

4.2.2 Iron(II) complex, FeL1

The iron (II) complex, FeL1, was obtained as a reddish brown powder in good yield (64%) from the reaction of iron(II) sulphate heptahydrate with H₂L1 in the presence of triethylamine. The C,H,N elemental analyses are in excellent agreement with the expected chemical formula, [Fe(C₂₀H₁₂O₂N₂Cl₂)]. Attempt to prepare Fe (III)-L1 by the same method was not successful.

The FTIR spectrum of FeL1 (Figure 4.10) shows the presence of all the expected functional groups. The wavenumbers of these functional groups are shifted as for CuL1, and may be similarly explained.

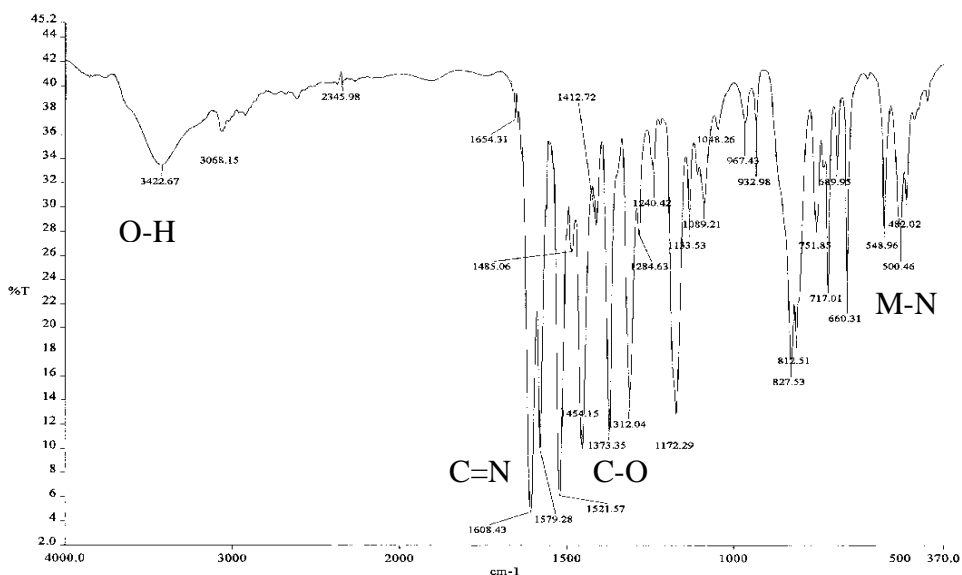


Figure 4.10 FTIR spectrum of FeL1

The FTIR data for FeL1 is compared with that of CuL1 in Table 4.1. It is of interest to note that both C=N and C-O bonds in FeL1 is stronger than in CuL1. These are supported by the weaker Fe-N and Fe-O coordinate bonds in Fe-L1 compared to the same bonds in Cu-L1. A plausible explanation is greater valence orbital contraction for Fe²⁺ ion as it has a smaller size. This results in reduced metal's orbitals overlap with the ligand's orbitals.

Table 4.1 The FTIR data (in cm^{-1}) for $\text{H}_2\text{L1}$, CuL1 , FeL1 and NiL1

Compound	ν_{OH}	$\nu_{\text{C=N}}$	$\nu_{\text{C-O}}$	$\nu_{\text{C-H}}$ (aliphatic)	$\nu_{\text{C-H}}$ (aromatic)	$\nu_{\text{M-N}}$	$\nu_{\text{M-O}}$
L1	3329	1612	1273	2923	755	-	-
CuL1	3432	1580	1168	-	759	520	558
FeL1	3422	1608	1312	3068	717	500	548
NiL1	3056	1608	1190	-	757	452	537

The UV-vis spectrum of FeL1 (Figure 4.11) shows two broad and overlapping peaks centered at 300 and 410 nm. As for CuL1 , these bands are assigned to $\pi - \pi^*$ and $n - \pi^*$ transitions of L1 . However, it is noted that the bands are significantly red shifted when compared with those of CuL1 (270 nm and 390 nm). The results are actually consistent with the weaker Fe-L1 interaction. It is further noted that the $d-d$ band is not detected, possibly because it is very weak as was also observed for CuL1 [58].

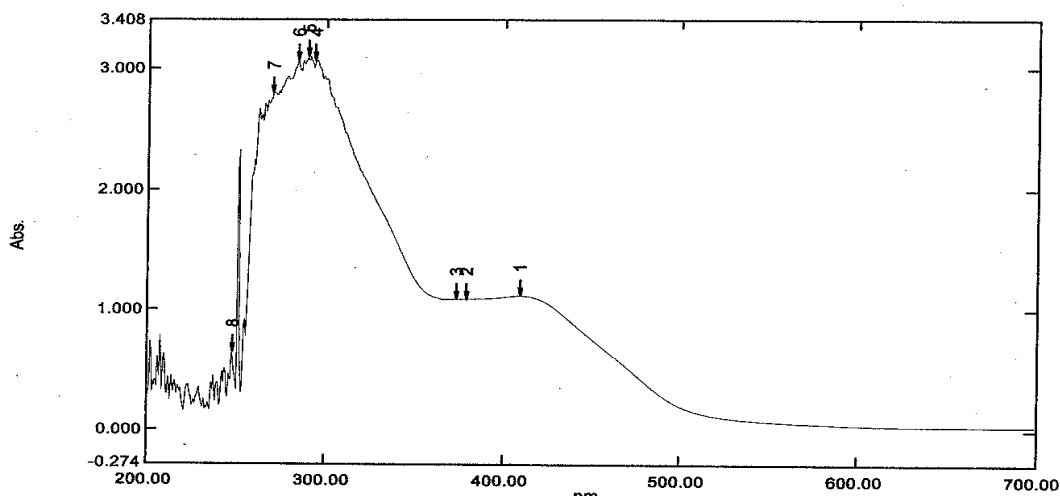


Figure 4.11 UV-vis spectrum of FeL1 in DMSO

Based on the similarity of FTIR and UV-vis spectroscopies of FeL1 with CuL1, it is proposed that the two complexes have similar structural formula.

The cyclic voltammogram of FeL1 in DMSO (Figure 4.12), similarly scanned cathodically as for CuL1, shows no reduction peaks, indicating that Fe (II) is not reduced to Fe(0). On reversing the scan, two peaks were observed at -0.57 V and -0.27 V. However, since only one peak is expected for the oxidation of Fe (II) to Fe (III), one of these peaks may correspond to the irreversible process. The other peak may be due to ligand oxidation. Thus, FeL1 is not suitable to be used as a redox catalyst.

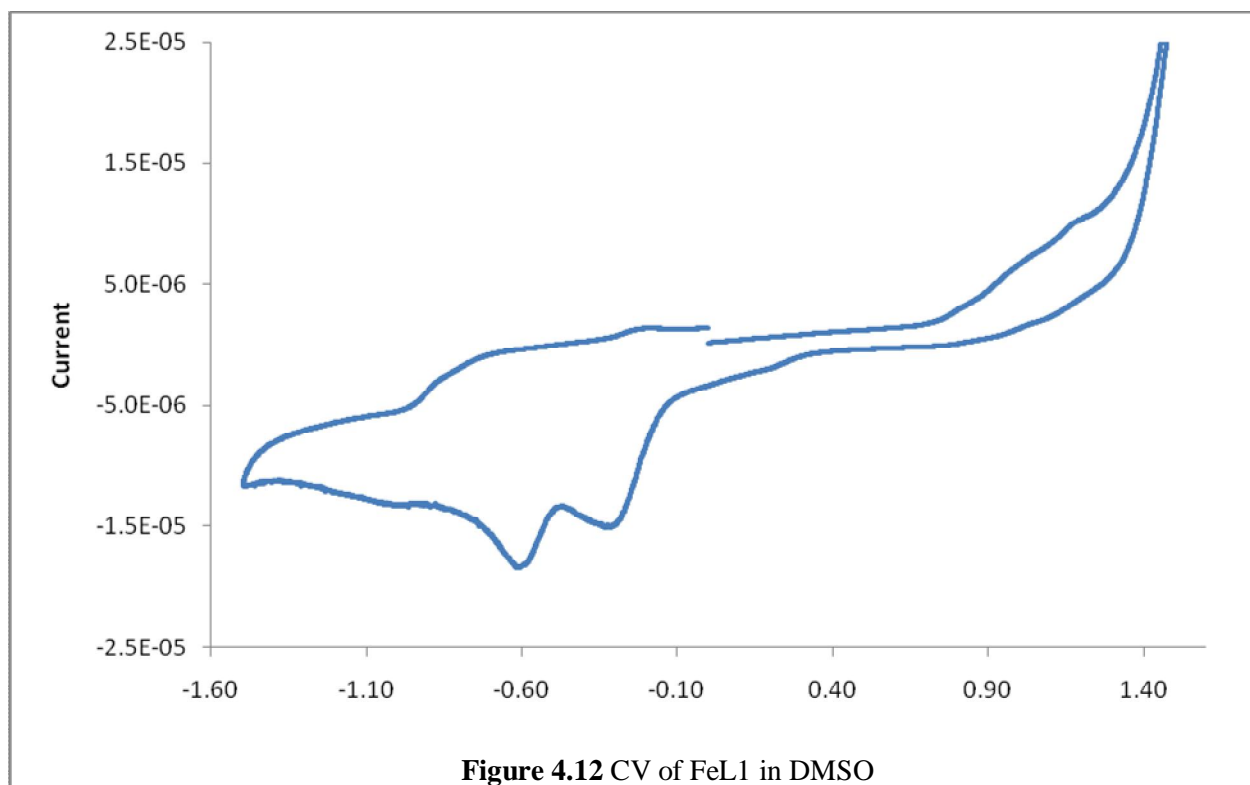


Figure 4.12 CV of FeL1 in DMSO

4.2.3 Nickel(II) complex, NiL1

Nickel(II) complex, NiL1, was obtained as a red powder in good yield (74%) from the reaction of nickel(II) acetate tetrahydrate with H₂L1 in the presence of triethylamine. The C,H,N elemental analyses are in excellent agreement with the expected chemical formula, [Ni(C₂₀H₁₂O₂N₂Cl₂)].

The FTIR spectrum of NiL1 (Figure 4.13) shows the presence of all the expected functional groups. The wavenumbers of these functional groups are shifted as for CuL1 and FeL1, and may be similarly explained.

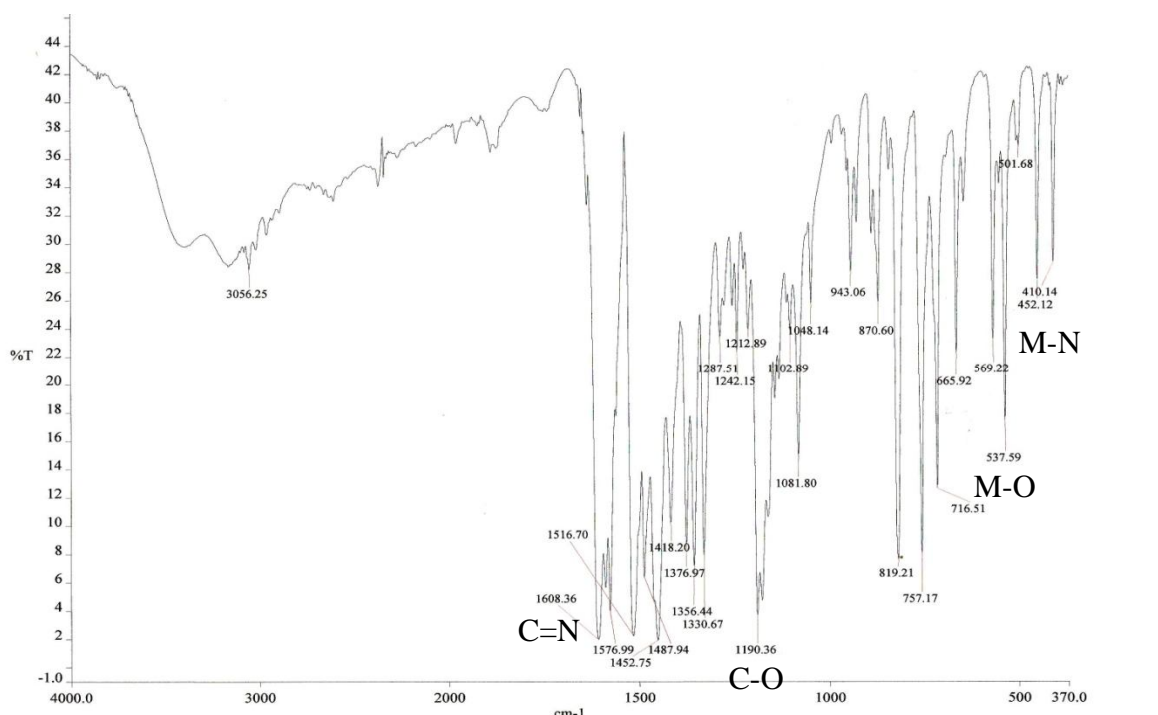


Figure 4.13 FTIR spectrum of NiL1

The FTIR data for NiL1 is compared with that of CuL1 and FeL1 in Table 4.1. It is of interest to note that the C=N bond in NiL1 is of the same strength as FeL1, but its C-O bond is significantly weaker than FeL1 but slightly stronger than CuL1. These suggest that Ni(II) formed

stronger bond with the phenolic oxygen compared with the azomethine nitrogen, which are further supported by the FTIR data for Ni-N and Ni-O.

The UV-vis spectrum of NiL1 (Figure 4.14) shows broad and overlapping peaks centered at 379 and 441 nm. As before, these bands are assigned to $\pi - \pi^*$ and $n - \pi^*$ transitions of L1. However, it is noted that the bands are significantly red shifted when compared with those of CuL1 (270 nm and 390 nm) and FeL1 (300 nm and 410 nm). The results are actually consistent with the higher charge density of Ni^{2+} ion compared with Cu^{2+} ion, and stronger Ni-L1 interaction compared to Cu-L1. It is further noted that the $d-d$ band is not detected, possibly because it is very weak as was also observed for FeL1.

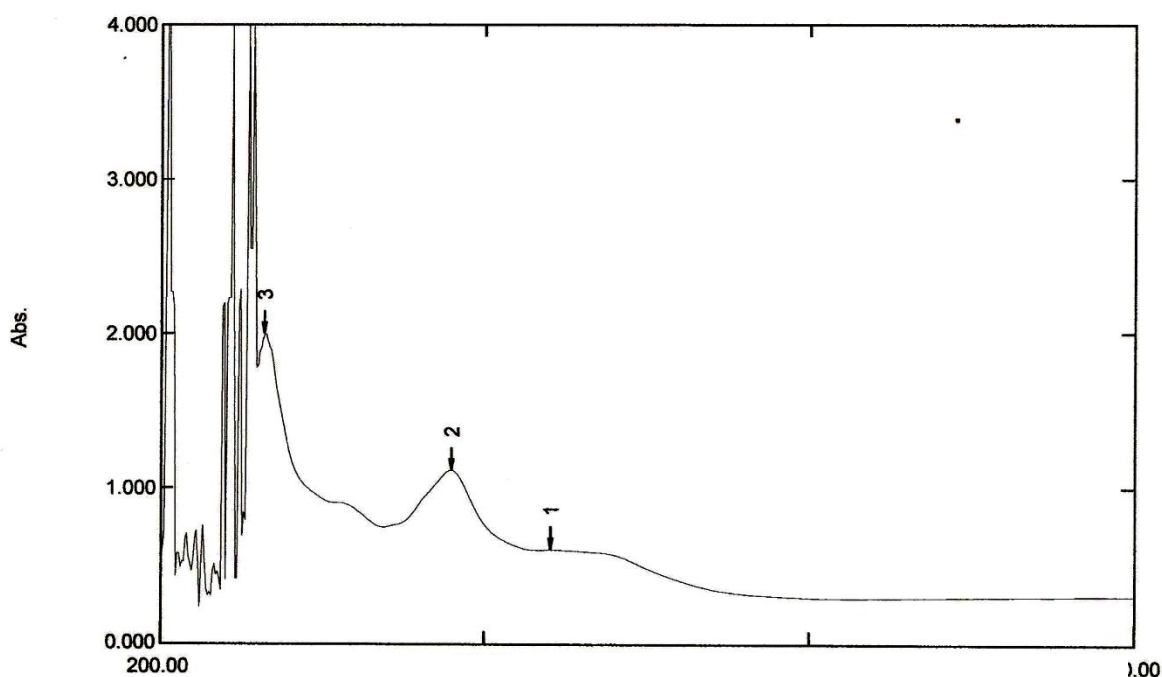


Figure 4.14 UV-vis spectrum of NiL1 in DMSO

Based on the similarity of FTIR and UV-vis spectroscopies of NiL1 with FeL1 and CuL1, it is proposed that the three complexes have similar structural formula.

The cyclic voltammogram of NiL1 in DMSO (Figure 4.15), similarly scanned cathodically as for CuL1 and FeL1, shows two irreversible reduction peaks at -0.98 V and -0.35 V. By referring to the result by Salih Ilhan et. al [62], the peak at -0.98 V is assigned to reduction of Ni(II) to Ni(I). Since this process is irreversible, NiL1 is not suitable to be used as a redox catalyst.

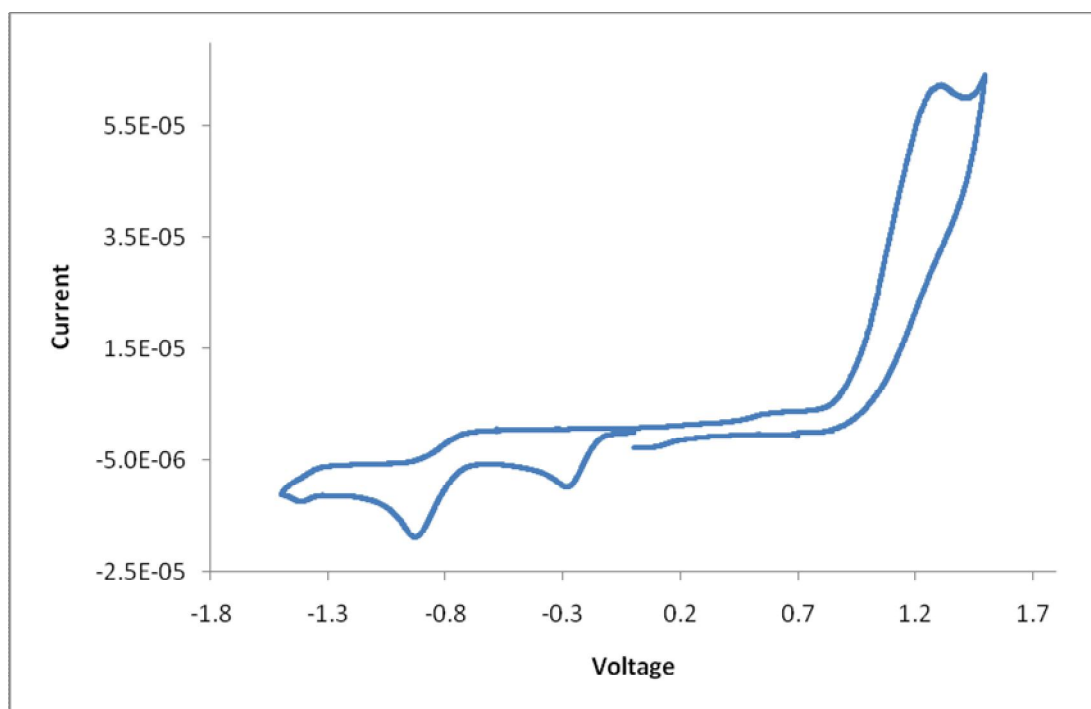


Figure 4.15 CV of NiL1 in DMSO

4.3 *N,N'*-1,2-Benzene-1,2-diyl-bis(4-bromosalicylideneimine) (H_2L2) and its copper(II), iron(II) and nickel(II) complexes

N,N'-1,2-Benzene-1,2-diyl-bis(4-bromosalicylideneimine) (H_2L2) was obtained as an orange powder in good yield (75%) from the reaction shown in Scheme 4.1 ($X = 5\text{-Br}$). The results from the C,H,N elemental analyses are in excellent agreement with the expected chemical formula, $C_{20}H_{14}O_2N_2Br_2$.

The FTIR spectrum of H_2L2 , recorded as a KBr pellet (Figure 4.16), is similar to H_2L1 , and may be similarly explained. It suggests that Br in H_2L2 has similar effect on the functional groups and bonds as Cl in H_2L1 . The important difference is that at 3423 cm^{-1} , the peak for H_2L2 is broad, while the peak for H_2L1 is sharp. The crystal structure of H_2L2 [54] showed that the molecule is not planar. Thus, the phenolic hydrogen in H_2L2 may form inter- and/or intra-molecular H-bonding. It is likely that this effect is due to the much larger size of Br compared to Cl.

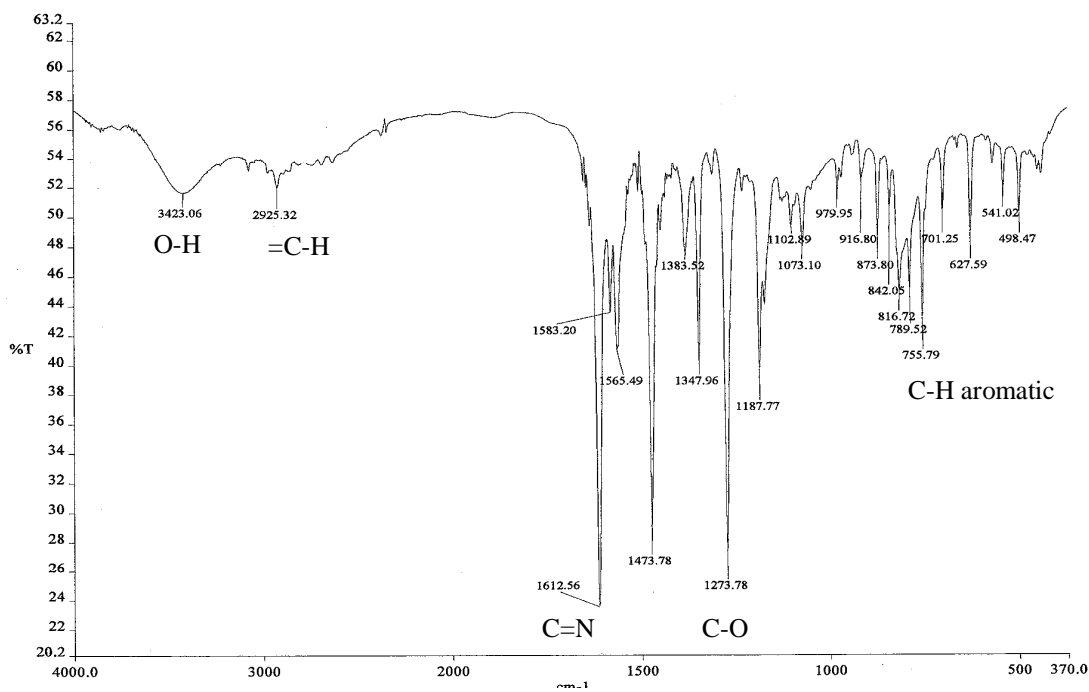


Figure 4.16 FTIR spectrum of H_2L2

The ^1H -NMR spectrum of $\text{H}_2\text{L2}$, recorded as a solution in DMSO-d_6 , is shown in Figure 4.16. The assignments of the spectrum are the same as for $\text{H}_2\text{L1}$: a singlet at 13.3 ppm is due to phenolic hydrogen; a singlet at 8.3 ppm is due to imino hydrogen; and a multiplet in the range 6.6-7.6 ppm is due to the aromatic hydrogens [63]. The integration ratio for these hydrogens is 1:1:5 respectively. Thus, $\text{H}_2\text{L2}$ is postulated to have similar structural formula as $\text{H}_2\text{L1}$, as shown in Figure 4.18.

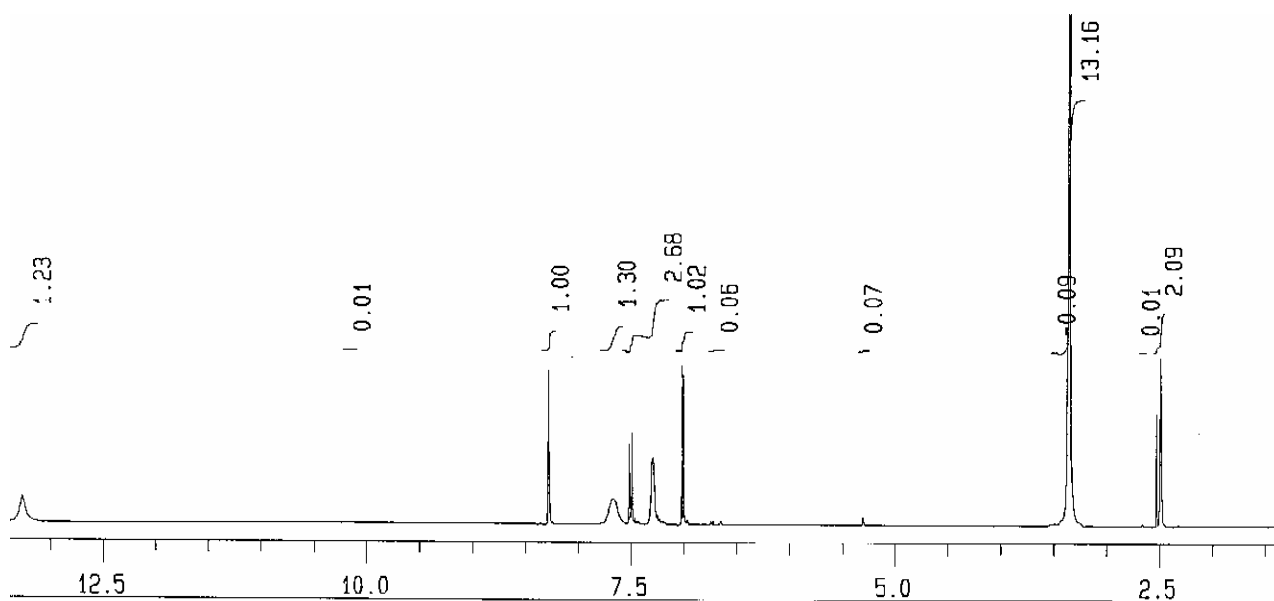


Figure 4.17 ^1H -NMR spectrum of $\text{H}_2\text{L2}$

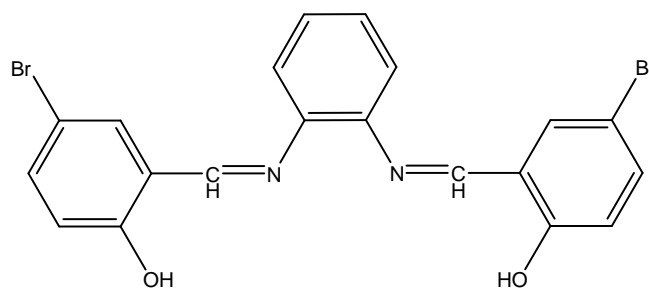


Figure 4.18 Proposed structural formula of H₂L2

The electronic spectrum of a solution of H₂L2 in DMSO (Figure 4.19) shows two moderately intense absorption bands at 260 nm ($\epsilon = 229 \text{ M}^{-1}\text{cm}^{-1}$) and 340 nm ($\epsilon = 83 \text{ M}^{-1}\text{cm}^{-1}$), and a weak shoulder at about 450 nm. These bands are at about the same wavenumbers as for H₂L1 (270 nm and 343 nm), and may be similarly assigned [64]. The results support the suggestion from FTIR that Br in H₂L2 has similar effect as Cl in H₂L1. It is probably due to the location of these halogens on the aromatic rings, specifically *meta*- to the azomethine group and *para*- to the hydroxyl group.

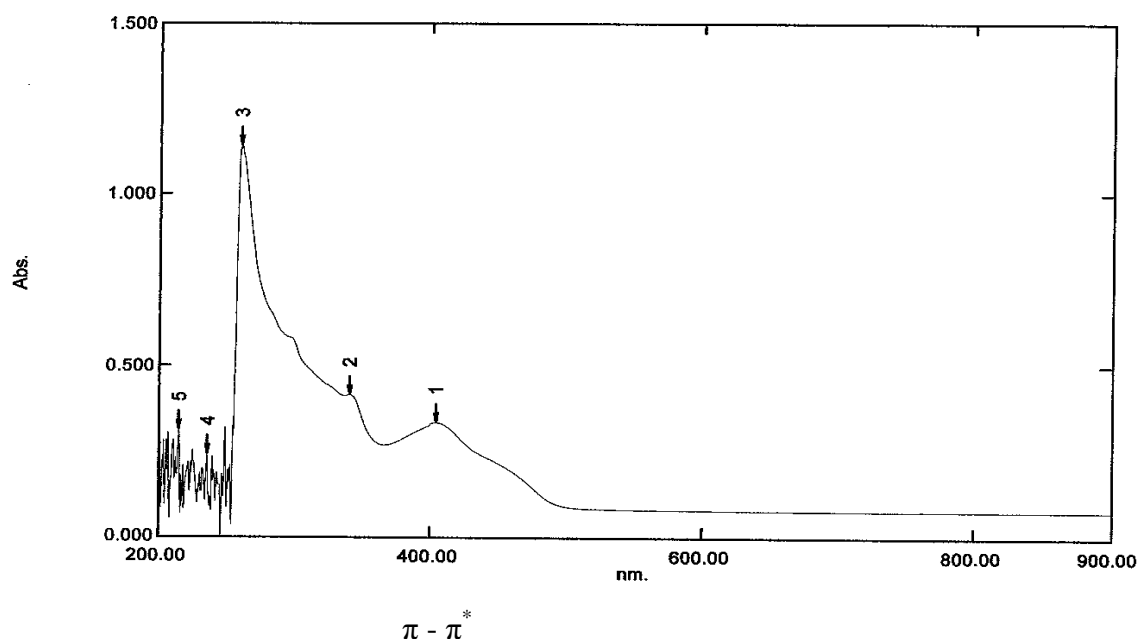


Figure 4.19 UV-vis spectrum of H₂L2 in DMSO

4.3.1 Copper(II) complex, CuL2

The copper(II) complex, CuL2, was obtained as a brown powder in good yield (71%) in the reaction between H₂L2 and copper(II) acetate monohydrate in the presence of triethylamine. The C,H,N elemental analyses are in excellent agreement with the expected chemical formula, [Cu(C₂₀H₁₂O₂N₂Br₂)].

The FTIR spectrum of CuL2 (Figure 4.20) is compared with that of H₂L2 (Figure 4.15). The spectrum of the complex shows a peak for C=N at 1606 cm⁻¹ and for C-O at 1177 cm⁻¹, while the corresponding peaks for H₂L2 are at higher wavenumbers (1612 and 1273 cm⁻¹). These suggest that the azomethine nitrogens and phenolic oxygens are coordinated to Cu(II).

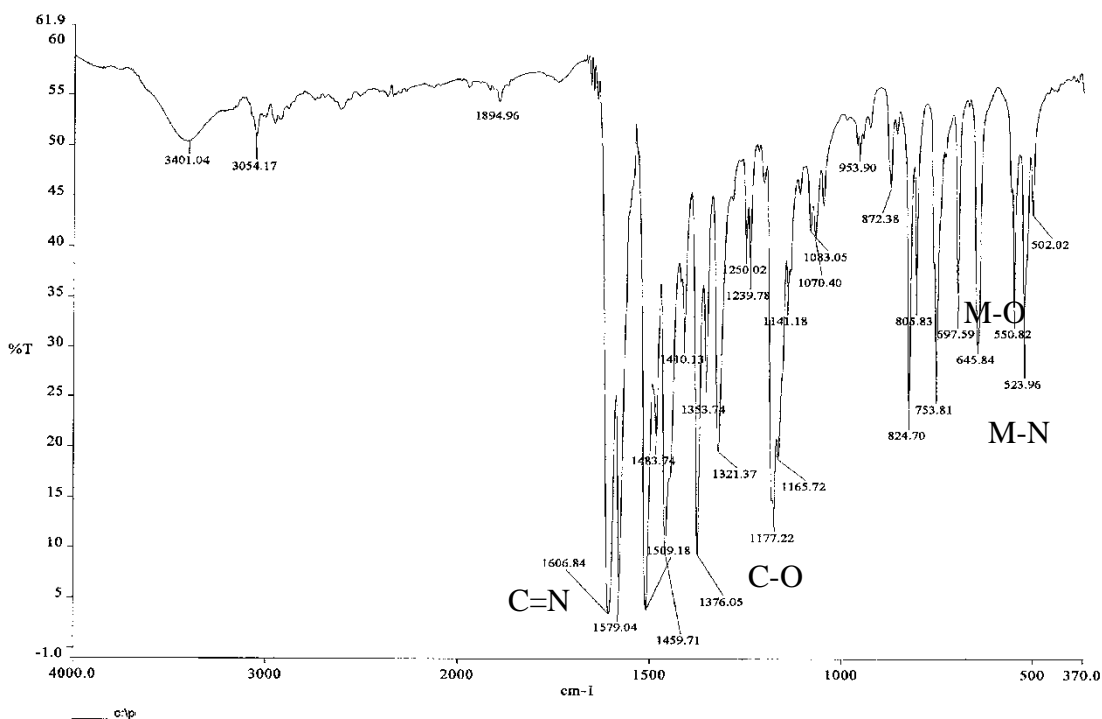


Figure 4.20 FTIR spectrum of CuL2

To compare the electronic effect of Br and Cl on the structure of the complex, the FTIR data for CuL2 (Table 4.2) is compared with that of CuL1 (Table 4.1). It is noted that the C=N and C-O energies for CuL2 (1606 and 1177 cm⁻¹) are higher than those of CuL1 (1580 and 1168 cm⁻¹). These suggests that the coordinate bonds between Cu(II) and L2 are weaker than between Cu(II) and L1. A tentative explanation, which is in line with the crystal structure of H₂L2 [54], is that the geometry of CuL2 is more distorted than CuL1 due to the larger size of Br compared with Cl.

Table 4.2 FTIR data for H₂L2 and its metal complexes

Compound	ν_{OH}	$\nu_{\text{C=N}}$	$\nu_{\text{C-O}}$	$\nu_{\text{C-H}}$ (aliphatic)	$\nu_{\text{C-H}}$ (aromatic)	$\nu_{\text{M-N}}$	$\nu_{\text{M-O}}$
H₂L2	3423	1612	1273	2925	755	-	-
CuL2	3401	1606	1177	3054	753	523	550
FeL2	3400	1605	1170	3067	750	446	546
NiL2	3398	1606	1188	2929	755	450	536

The UV-vis spectrum of CuL2 (Figure 4.21) in the UV region is almost similar to that of H₂L2 (Figure 4.4). Thus, complexation of Cu(II) to the deprotonated Schiff base has insignificant effect on the electronic transitions of the organic moiety [65,66].

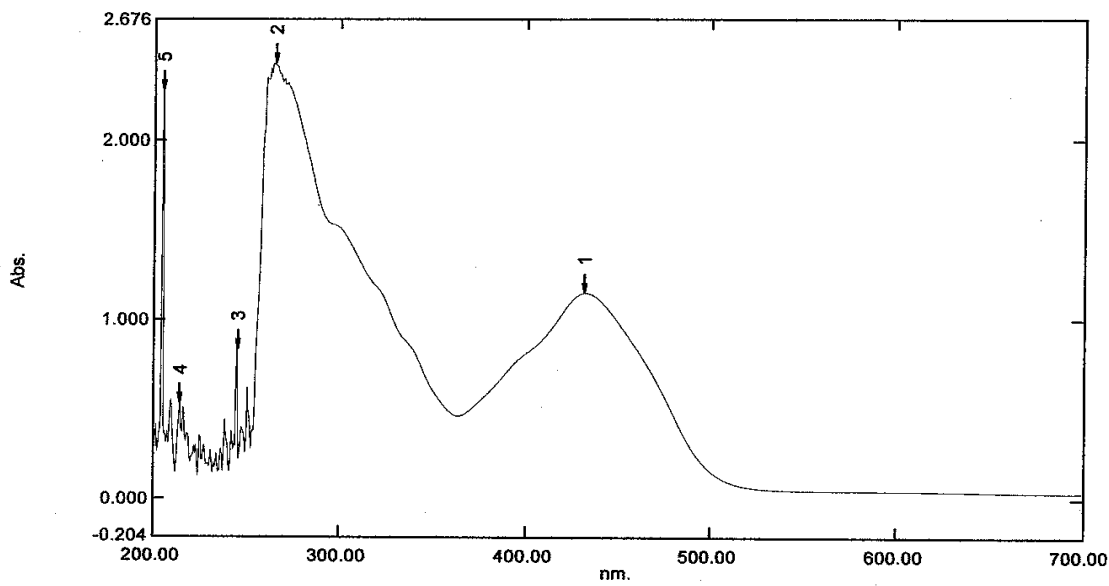


Figure 4.21 UV-vis spectrum of CuL2 in DMSO

In a separate run in the visible region (not shown), a weak and broad shoulder is observed at 591 nm ($\epsilon = 13 \text{ M}^{-1}\text{cm}^{-1}$). This *d-d* band is at almost the same wavelength as for CuL1 (588 nm), and may be similarly explained as well as consistent with the suggestion from FTIR data that Br and Cl have similar effect on the complex.

Combining the results from CHN analyses, and FTIR and UV-vis spectroscopies, the structural formula proposed for CuL2 is shown in Figure 4.22.

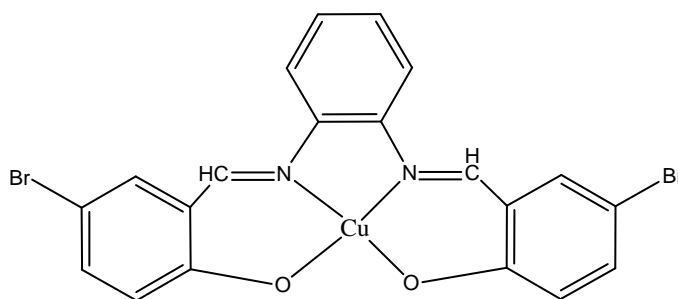


Figure 4.22 Proposed structural formula for CuL2, $[\text{Cu}(\text{C}_{20}\text{H}_{12}\text{O}_2\text{N}_2\text{Br}_2)]$

The cyclic voltammogram of CuL2 in DMSO (Figure 4.23), similarly scanned as for the other complexes, is similar to CuL1 and thus may be similarly explained. Specifically, there are reduction peaks at -0.99 V ($I_{pc} = -1.47 \times 10^{-5}$ A) and -1.22 V ($I_{pc} = -1.51 \times 10^{-5}$ A), and an oxidation peak at -1.0 V ($I_{pa} = -3.55 \times 10^{-6}$ A). From these, the calculated values are: $E_{1/2} = -1.1$ V, $\Delta E_p = 230$ mV, and $I_{pa}/I_{pc} = 0.24$. The larger peak separation for CuL2 compared to CuL1 suggests greater structural reorganization in the former complex upon reduction, which can be accounted for by the larger size of Br.

It is further noted that a new irreversible oxidation peak is observed for CuL2 at + 0.73 V, which is not observed for CuL1. This peak is tentatively assigned to the oxidation of Br.

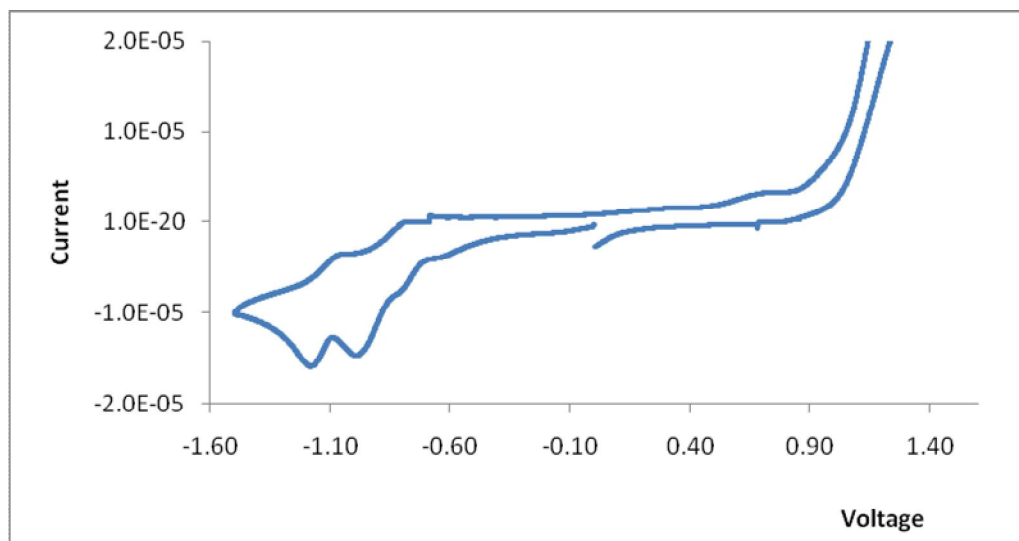


Figure 4.23 CV of CuL2 in DMSO

4.3.2 Iron(II) complex, FeL2

The iron(II) complex, FeL2, was obtained as a reddish brown powder in good yield (67%) from the reaction of iron(II) sulphate heptahydrate with H₂L2 in the presence of triethylamine. The C,H,N elemental analyses are in excellent agreement with the expected chemical formula, [Fe(C₂₀H₁₂O₂N₂Br₂)]. Attempt to prepare Fe(III)-L2 by the same method was not successful.

The FTIR spectrum of FeL2 (Figure 4.24) shows the presence of all the expected functional groups. The wavenumbers of these functional groups (Table 4.3) are shifted as for CuL2, and may be similarly explained.

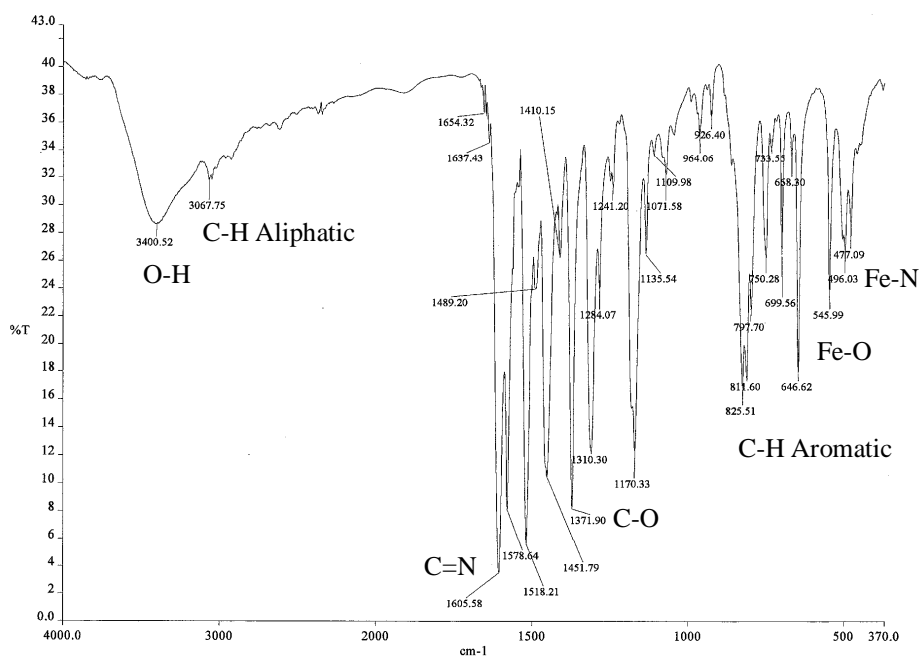


Figure 4.24 FTIR spectrum of FeL2

The FTIR data for FeL2 is also compared with that of CuL2. It is noted that the strength of both C=N and C-O bonds are almost the same in both complexes. This is supported by the similar M-N and M-O bond strengths for both complexes. An explanation that may be offered at

this stage is that both complexes adopt similar non-planar structure, as was reported for the ligand [57].

Table 4.3 The FTIR data (in cm^{-1}) for $\text{H}_2\text{L2}$, CuL2 , FeL2 and NiL2

Compound	ν_{OH}	$\nu_{\text{C=N}}$	$\nu_{\text{C-O}}$	$\nu_{\text{C-H}}$ (aliphatic)	$\nu_{\text{C-H}}$ (aromatic)	$\nu_{\text{M-N}}$	$\nu_{\text{M-O}}$
L2	3423	1612	1273	2925	755	-	-
CuL2	3401	1606	1177	3054	753	502	550
FeL2	3400	1605	1170	3067	750	496	546
NiL2	3398	1606	1188	2929	755	450	536

The UV-vis spectrum of FeL2 (Figure 4.25) shows two broad and overlapping peaks centered at 294 and 400 nm. These bands are respectively assigned to $\pi - \pi^*$ and $n - \pi^*$ transitions of L2 . Further, it is noted that both bands are at the same wavenumbers as those of CuL2 (300 nm and 410 nm). The results support the suggestion from FTIR. It is further noted that the $d-d$ band for Fe(II) is not observed, possibly because it is very weak, as was also noted for FeL1 .

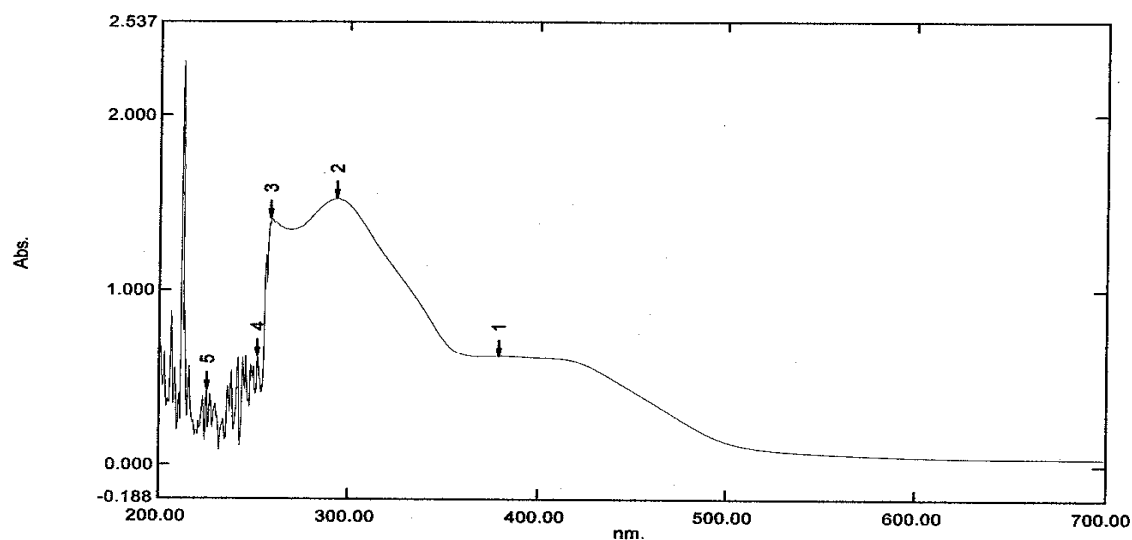


Figure 4.25 UV-vis spectrum of FeL2 in DMSO

Based on the similarity of FTIR and UV-vis spectroscopies of FeL2 with CuL2, it is proposed that the two complexes have similar structural formula (Figure 4.22).

The cyclic voltammogram of FeL2 in DMSO (Figure 4.26), is similar to FeL1 (Figure 4.12). Specifically, there was no reduction peaks, indicating that Fe(II) is not reduced to Fe(0). On reversing the scan, three oxidation peaks were observed at -0.92 V, -0.83 V and -0.29 V. Since, the small peak at -0.29 V is also found for FeL1 at -0.27 V, it may corresponds to the irreversible oxidation of Fe(II) to Fe(III). The other peaks may be due to ligand oxidation. A cathodic peak at +1.14 V, which is not found for FeL1, may corresponds to either reduction of Fe(III) to Fe(II) or to reduction of the ligand at Br. Thus, FeL2 may be suitable to be used as a redox catalyst.

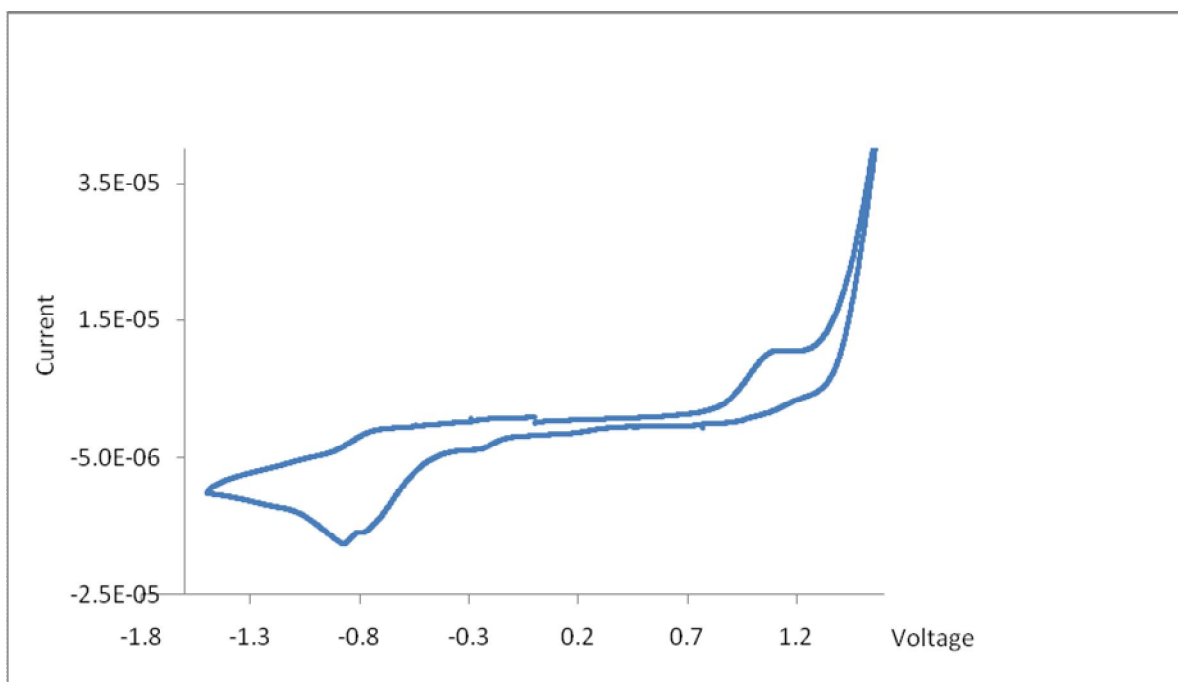


Figure 4.26 CV of FeL2 in DMSO

4.3.3 Nickel(II) complex, NiL2

Nickel(II) complex, NiL2, was obtained as a red powder in good yield (72%) from the reaction of nickel(II) acetate tetrahydrate with H₂L2 in the presence of triethylamine. The C,H,N elemental analyses are in excellent agreement with the expected chemical formula, [Ni(C₂₀H₁₂O₂N₂Br₂)].

The FTIR spectrum of NiL2 (Figure 4.27) shows the presence of all the expected functional groups. The wavenumbers of these functional groups are shifted as for CuL2 and FeL2, and may be similarly explained.

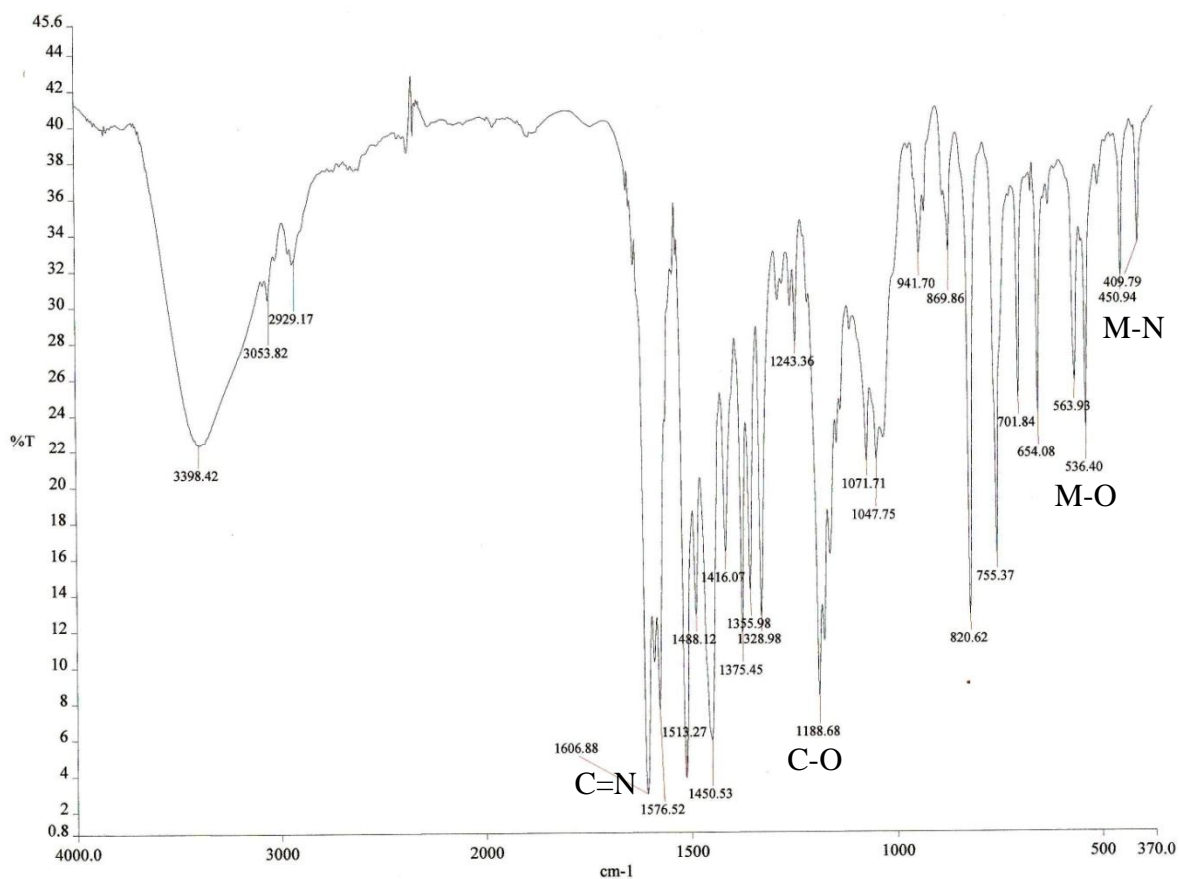


Figure 4.27 FTIR spectrum of NiL2

The FTIR data for NiL2 is compared with that of CuL2 and FeL2 in Table 4.4. It is of interest to note that the C=N bond of NiL2 is of the same strength as CuL2 and FeL2, while the C-O bond is significantly stronger. These suggest that Ni(II) formed weaker bond with the phenolic oxygen compared to Cu(II) and Fe(II), which are further supported by the FTIR data for Cu-O, Fe-O, and Ni-O.

Table 4.4 FTIR data for L2 and its metal(II) complexes

Compound	ν_{OH}	$\nu_{\text{C=N}}$	$\nu_{\text{C-O}}$	$\nu_{\text{C-H}}$ (aliphatic)	$\nu_{\text{C-H}}$ (aromatic)	$\nu_{\text{M-N}}$	$\nu_{\text{M-O}}$
L2	3423	1612	1273	2925	755	-	-
CuL2	3401	1606	1177	3054	753	502	550
FeL2	3400	1605	1170	3067	750	496	546
NiL2	3398	1606	1188	2929	755	450	536

The UV-vis spectrum of NiL2 (Figure 4.28) shows three broad peaks centered at 267, 379 and 475 nm. As before, these bands are assigned to $\pi - \pi^*$ and $n - \pi^*$ transitions of L2. However, it is noted that the $n - \pi^*$ bands are significantly red shifted when compared with those of CuL2 (300 nm and 410 nm) and FeL2 (294 nm and 400 nm). The result may be due to the weaker Ni(II)-O bond (reduced interaction) as suggested from FTIR, making the π^* antibonding orbital has less energy.

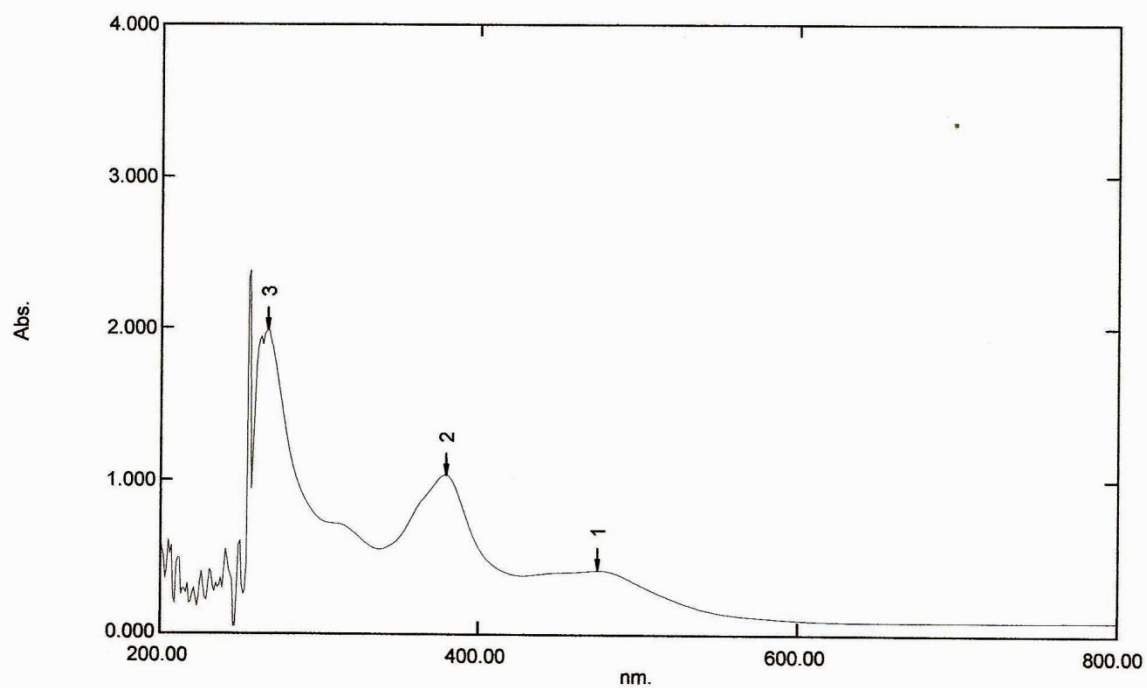


Figure 4.28 UV-vis spectrum of NiL2 in DMSO

The cyclic voltammogram of NiL2 in DMSO (Figure 4.29) is similar to NiL1 (Figure 4.15), and may be similarly explained. Since this process is irreversible, NiL2 is also not suitable to be used as a redox catalyst.

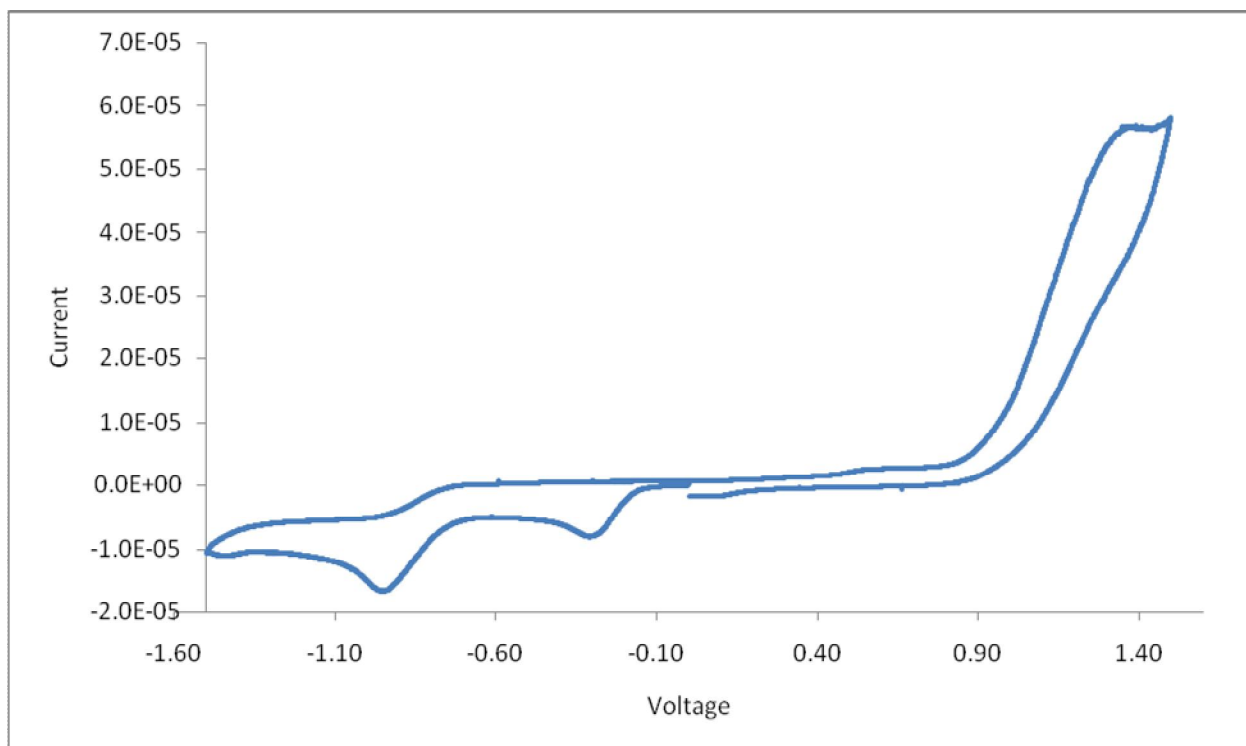


Figure 4.29 CV of NiL2 in DMSO

4.4 *N,N'*-1,2-Benzene-1,2-diyl-bis(4-hydroxysalicylideneimine) (H_2L3) and its copper(II), iron(II) and nickel(II) complexes

N,N'-1,2-Benzene-1,2-diyl-bis(4-hydroxysalicylideneimine) (H_2L3) was obtained as a yellow powder in good yield (75%) from the reaction shown in Scheme 4.1 ($X = 4\text{-OH}$). The results from the C,H,N elemental analyses are in excellent agreement with the expected chemical formula, $C_{20}H_{14}O_2N_2(OH)_2$.

The FTIR spectrum of H_2L3 (Figure 4.30) is similar to that of H_2L2 and may be similarly explained. The important difference is that its broad OH peak is at significantly lower energy (3064 cm^{-1}) compared to H_2L1 and H_2L2 (3329 and 3423 cm^{-1} respectively). Also, its C-O peak is shifted to lower energy (1249 cm^{-1}) compared to H_2L1 and H_2L2 (both at 1273 cm^{-1}).

Accordingly, the presence of two –OH groups *meta* to each other may cause more extensive intermolecular and intramolecular H-bonding compared to just one for H₂L1 and H₂L2.

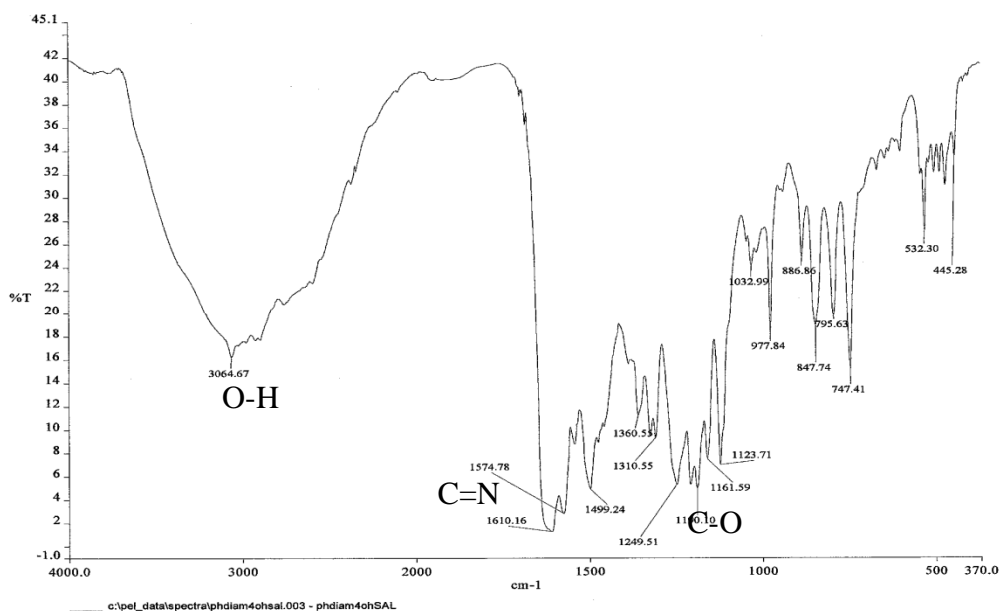


Figure 4.30 FTIR spectrum of H₂L3

The ¹H-NMR spectrum of H₂L3, recorded as a solution in DMSO-d₆, and the assignment of the peaks (H_a = 13.38 ppm, H_b = 8.76 ppm [52, 65], H_c = 10.26 ppm, and H_(aromatic) = 6.3-7.3 ppm) are shown in (Figure 4.31). The integration ratio for these hydrogens is 1:1:1:5 respectively, which agrees with the structural formula shown.

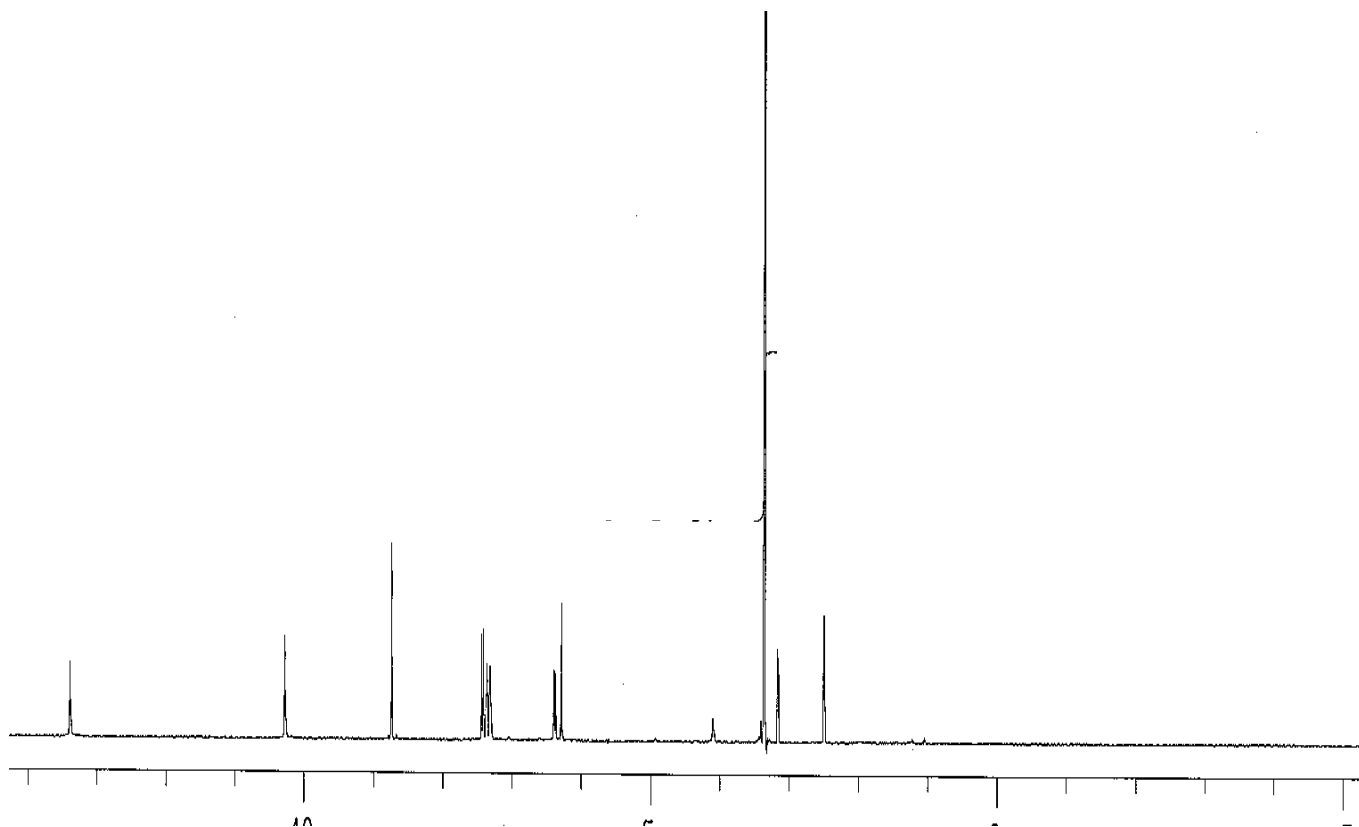


Figure 4.31 ^1H -NMR spectrum of $\text{H}_2\text{L3}$

The electronic spectrum of a solution of $\text{H}_2\text{L3}$ in DMSO (Figure 4.31) shows three broad overlapping peaks centred at 329 nm and a weak shoulder at about 450 nm. These bands are may be similarly assigned as for $\text{H}_2\text{L1}$ and $\text{H}_2\text{L2}$. However, it is noted that its $n\text{-}\pi^*$ transition is blue shifted (329 nm) compared to the former Schiff bases (~ 343 nm). This translates to increased energy of π^* molecular orbitals from the effect of additional -OH group in the aromatic ring.

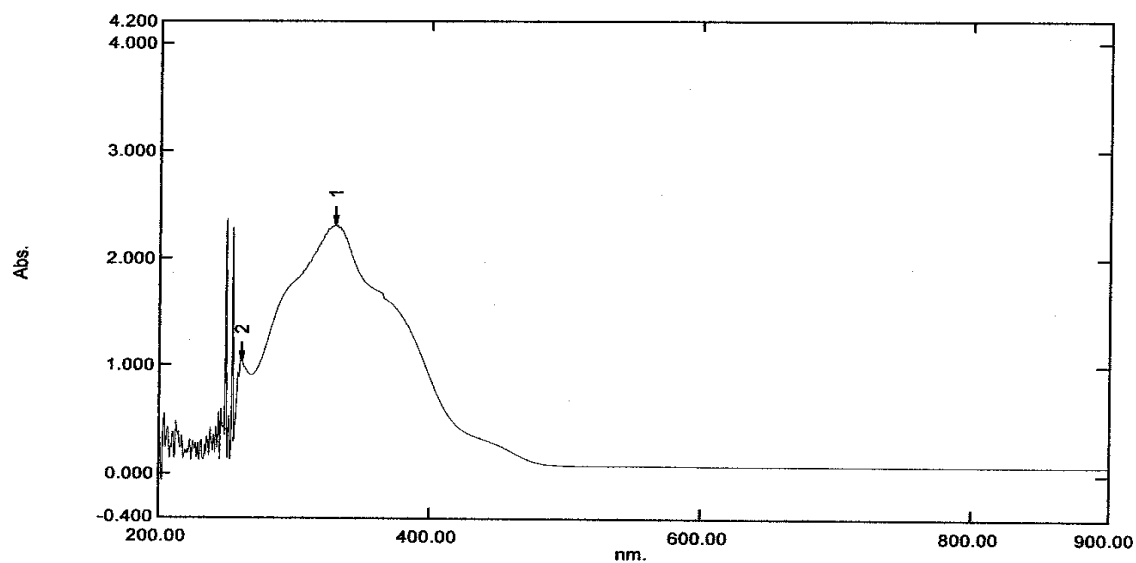


Figure 4.32 UV-vis spectrum of H₂L3 in DMSO

4.4.1 Copper(II) complex, CuL3

The copper(II) complex, CuL3, was obtained as a brown powder in good yield (78%) in the reaction between H₂L3 and copper(II) acetate monohydrate in the presence of triethylamine. The C,H,N elemental analyses are in excellent agreement with the expected chemical formula,

[Cu(C₂₀H₁₂O₂N₂(OH)₂)]. The FTIR spectrum of CuL3 (Figure 4.33) and the corresponding data (Table 4.5) shows the expected decrease in the wavenumbers for -C=N and -C-O functional groups, compared to those of H₂L3. The broad and strong peak(s) in the range 2800-3538 cm⁻¹ suggest(s) the presence of inter- and/or intra-molecular H-bonding of OH group.

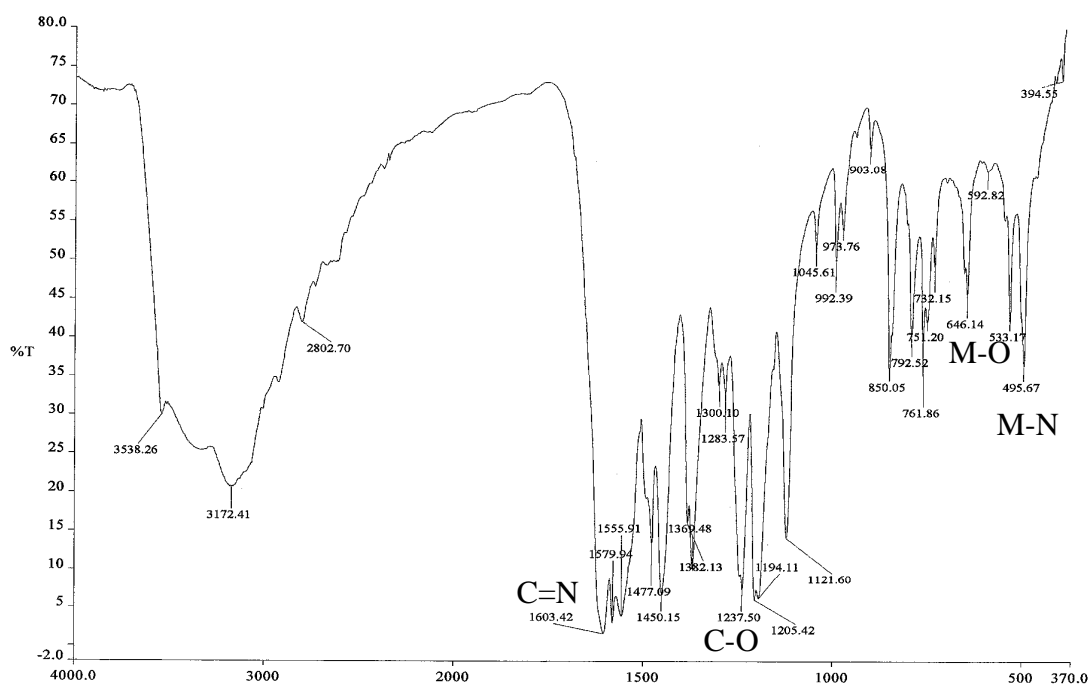


Figure 4.33 FTIR spectrum of CuL3

Table 4.5 FTIR data for H₂L3 and its metal complexes

Compound	ν_{OH}	$\nu_{\text{C=N}}$	$\nu_{\text{C-O}}$	$\nu_{\text{C-H}}$ (aliphatic)	$\nu_{\text{C-H}}$ (aromatic)	$\nu_{\text{M-N}}$	$\nu_{\text{M-O}}$
H ₂ L3	3064	1610	1249	-	747	-	-
CuL3	3172	1603	1237	-	761	495	533
FeL3	3385	1597	1203	-	756	488	559
NiL3	3331	1604	1209	-	745	504	542

To probe the electronic effect of OH on the structure of the complex, the FTIR data for CuL3 is compared with that of CuL1 and CuL2 (Table 4.6). It is noted that there is no significant

change in the strength of Cu-N bonds in all of these complexes. However, the Cu-O bond in CuL3 is weaker than the corresponding bond in CuL1 and CuL2. Two explanations may be forwarded. Firstly, the -OH group of L3 is more strongly electron-donating compared to -Cl of L1 and -Br of L2. Secondly, the -OH group has a stronger effect as it is located closer to the C-O group than the halogens.

The UV-vis spectrum of CuL3 (Figure 4.34) in the UV region shows four overlapping broad bands at 270, 322 and 345 nm assigned to previously stated electronic transitions of the ligands, and at 396 nm assigned to charge transfer.

The *d-d* electronic transition is observed as a very weak shoulder at 572 nm (not shown); the high energy of this transition indicates a square planar Cu(II) geometry. The higher energy for the transition, when compared with CuL1 (588 nm) and CuL2 (591 nm), suggests that the geometry at Cu(II) in CuL3 is more planar (or less distorted).

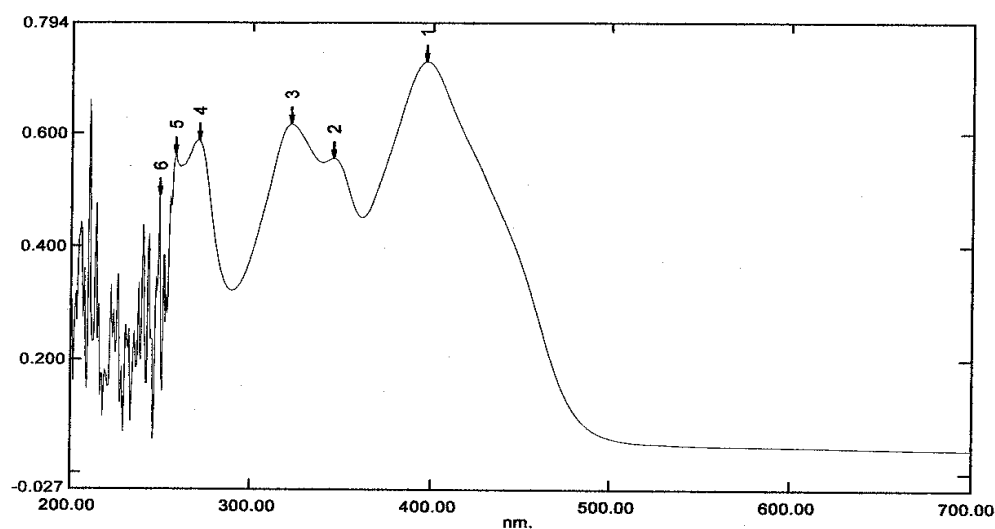


Figure 4.34 UV-vis spectrum of CuL3 in DMSO

Combining the results from CHN analyses, and FTIR and UV-vis spectroscopies, the structural formula proposed for CuL3 is shown in Figure 4.35

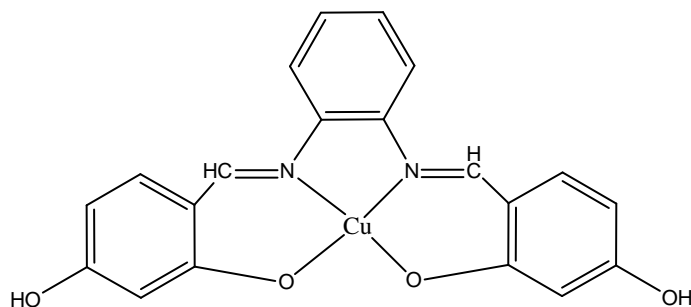


Figure 4.35 Proposed structural formula for CuL3, $[\text{Cu}(\text{C}_{20}\text{H}_{12}\text{O}_2\text{N}_2(\text{OH})_2)]$

The cyclic voltammogram of CuL3 in DMSO (Figure 4.36) is different from CuL1 and CuL2. Specifically, there is only a cathodic peak at -1.12 V ($I_{\text{pc}} = -1.9 \times 10^{-5} \text{ A}$) and a weak and broad anodic peak at about $+0.65 \text{ V}$ ($I_{\text{pa}} \sim 8.1 \times 10^{-6} \text{ A}$). The cathodic peak is assigned to irreversible reduction of Cu(II) to Cu(I). It is noted that the reduction of Cu(II) in CuL3 occurs at a higher potential compared to CuL1 and CuL2. This supports the more planar geometry of Cu(II) in CuL3, as suggested from the UV-vis spectroscopy.

The anodic peak, which is also found for CuL2 (at $+0.73 \text{ V}$) but not for CuL1, is tentatively assigned to the irreversible oxidation of $-\text{OH}$ at the ligand.

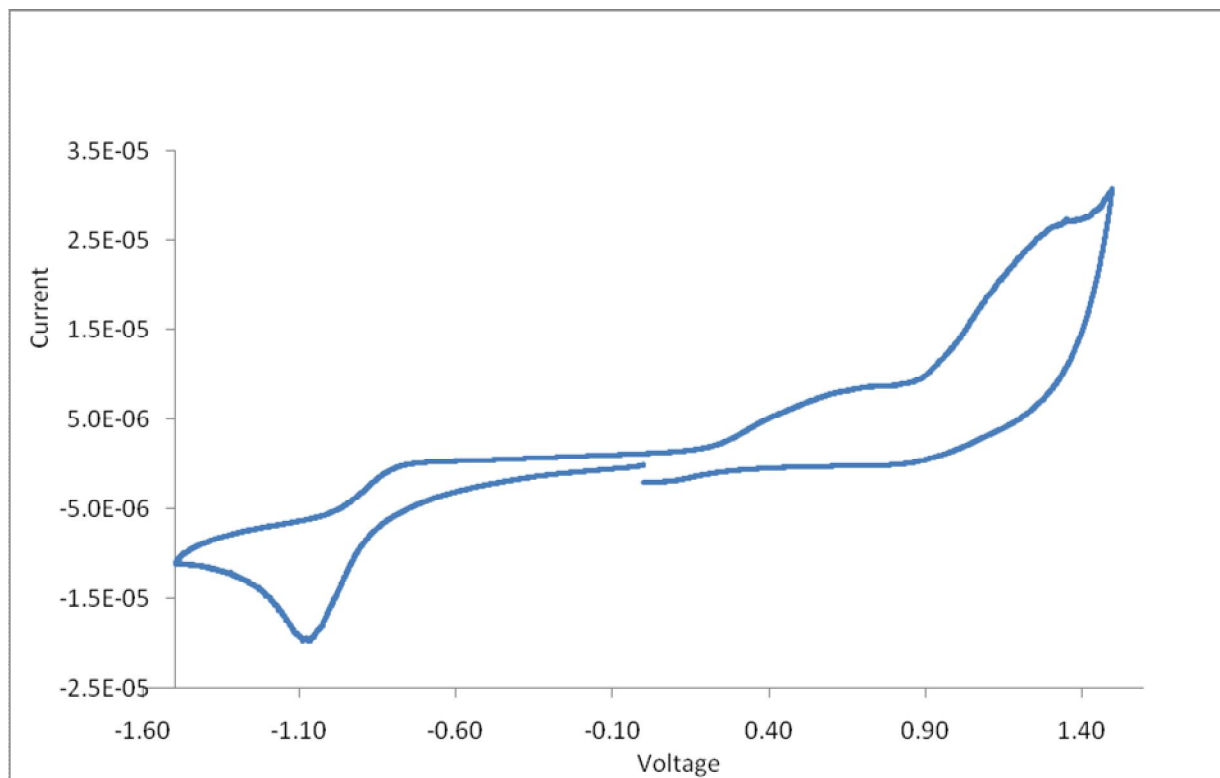


Figure 4.36 CV of CuL3 in DMSO

To summarise, CuL3 has a more planar geometry than CuL1 and CuL2, and it undergoes irreversible reduction of Cu(II) to Cu(I). Thus, it may not function as a redox catalyst.

4.4.2 Iron(II) complex, FeL3

The iron(II) complex, FeL3, was obtained as a deep brown powder in good yield (70%) from the reaction of iron(II) sulphate heptahydrate with H₂L3 in the presence of triethylamine. The C,H,N elemental analyses are in excellent agreement with the expected chemical formula, [Fe(C₂₀H₁₂O₂N₂Br₂)]. Attempt to prepare Fe(III)-L3 by the same method was not successful.

The FTIR spectrum of FeL3 (Figure 4.37) shows the presence of all the expected functional groups. The wavenumbers of these functional groups (Table 4.7) are shifted as for the other complexes, and may be similarly explained.

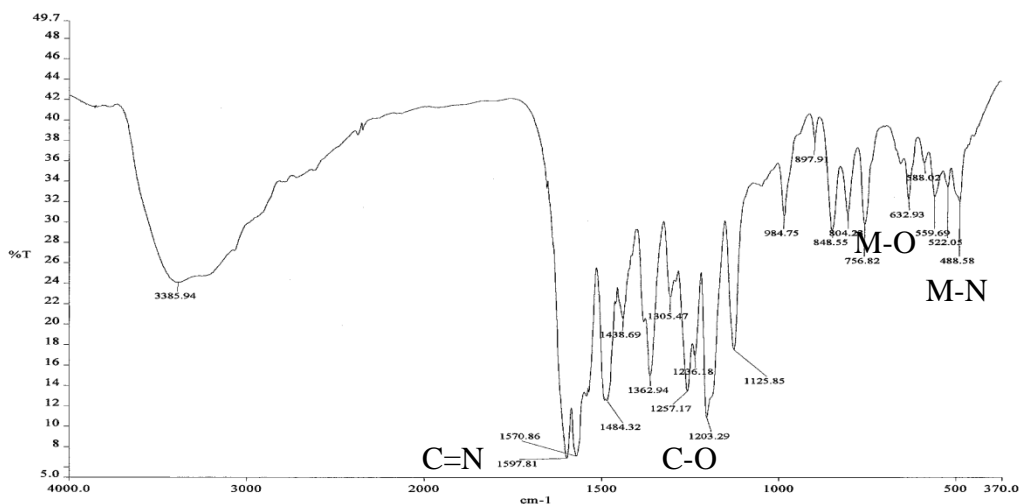


Figure 4.37 FTIR spectrum of FeL3

To probe the electronic effect of OH on the structure of the complex, the FTIR data for FeL3 is compared with that of FeL1 and FeL2 (Table 4.7). The effect is similar to CuL3, and may be similarly explained.

Table 4.7 FTIR data for FeL1, FeL2 and FeL3

Compound	$\nu_{\text{C=N}}$	$\nu_{\text{C-O}}$	$\nu_{\text{M-N}}$	$\nu_{\text{M-O}}$
FeL1	1608	1172	482	500
FeL2	1605	1170	496	545
FeL3	1604	1209	488	559

The FTIR data for FeL3 is also compared with that of CuL3. It is noted that the strength of M-N bond is almost the same in both complexes, but the M-O bond is slightly stronger for

Fe(II) complex. This may be due to the larger charge density of Fe(II) compared to Cu(II), which allow better orbital overlaps.

The UV-vis spectrum of FeL3 (Figure 4.38) in the UV region shows four overlapping broad bands at 259, 316, and 363 nm, assigned to previously stated electronic transitions of the ligands, and at 450 nm assigned to charge transfer [10]. These bands are at approximately similar wavenumbers as for CuL3. It is further noted that the *d-d* band for Fe(II) is not observed, possibly because it is very weak, as was also noted for FeL1 and FeL2.

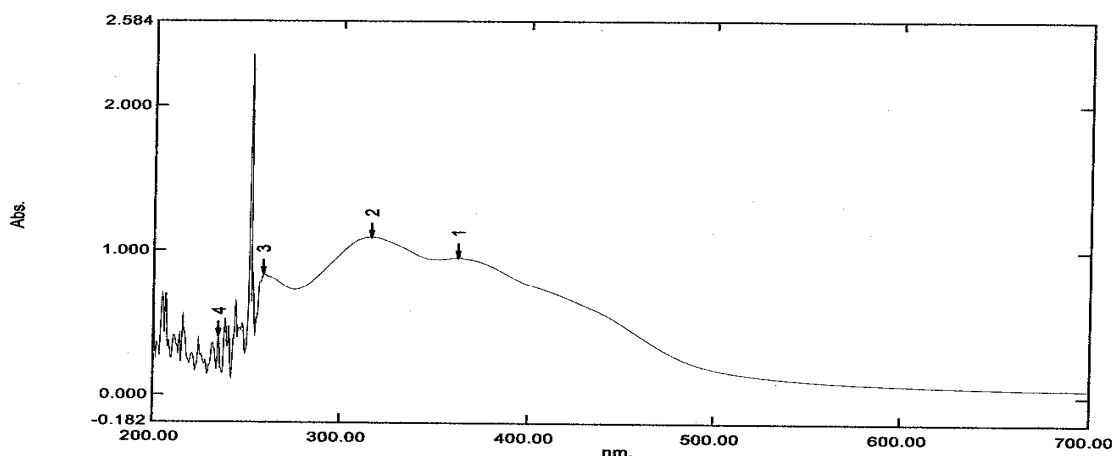


Figure 4.38 UV-vis spectrum of FeL3 in DMSO

Based on the similarity of FTIR and UV-vis spectroscopies of FeL3 and CuL3, it is proposed that the two complexes have similar structural formula (Figure 4.35).

The cyclic voltammogram of FeL3 in DMSO (Figure 4.39) shows no reduction peaks, indicating that Fe(II) is not reduced to Fe(0). On reversing the scan, two oxidation peaks were observed at -1.08 V and -0.55 V, which were previously assigned to ligand oxidation. The expected peak for irreversible oxidation of Fe(II) to Fe(III) at about -0.29 V (also found for FeL1 and FeL2) is hidden by the strong peak at -0.55 V. A cathodic peak at +0.94 V, which is also

found for FeL2 (at +1.14 V), may likely corresponds to reduction of Fe(III) to Fe(II). The peak separation for Fe(II)-Fe(III) redox is 1230 mV, which suggests a quasireversible reaction. Thus, FeL3 may be suitable to be used as a redox catalyst.

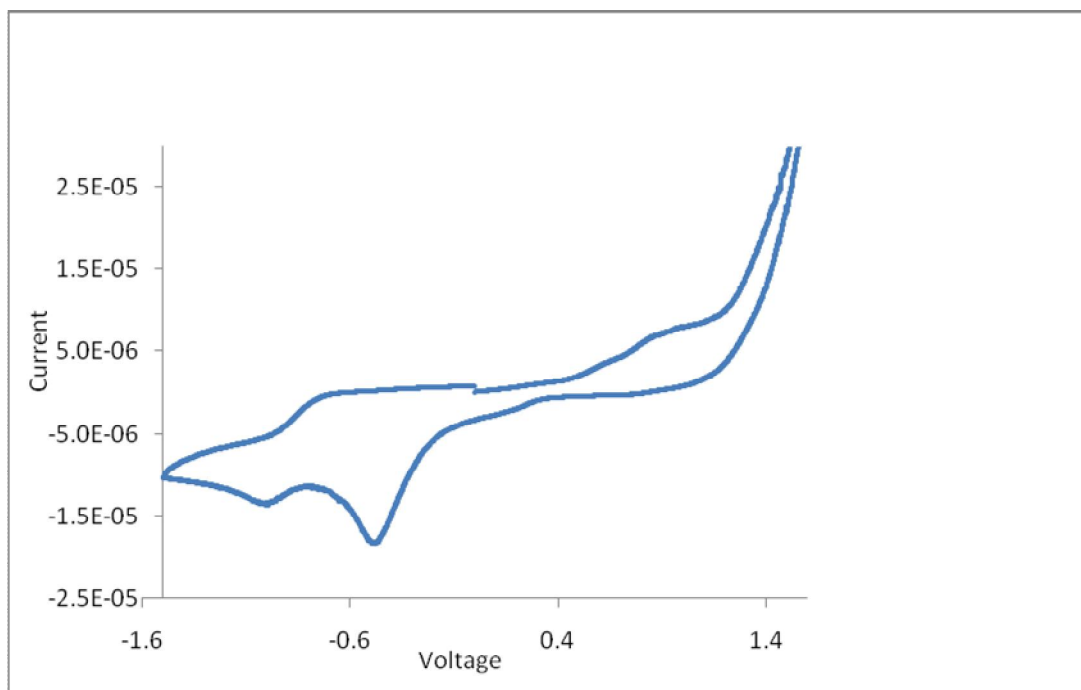


Figure 4.39 CV of FeL3 in DMSO

4.4.3 Nickel(II) complex, NiL3

Nickel(II) complex, NiL3, was obtained as a red powder in good yield (82%) from the reaction of nickel(II) acetate tetrahydrate with H₂L3 in the presence of triethylamine. The C,H,N elemental analyses are in excellent agreement with the expected chemical formula, [Ni(C₂₀H₁₂O₂N₂(OH)₂)].

The FTIR spectrum of NiL3 (Figure 4.40) shows the presence of all the expected functional groups. The wavenumbers of these functional groups are shifted as for the other complexes, and may be similarly explained.

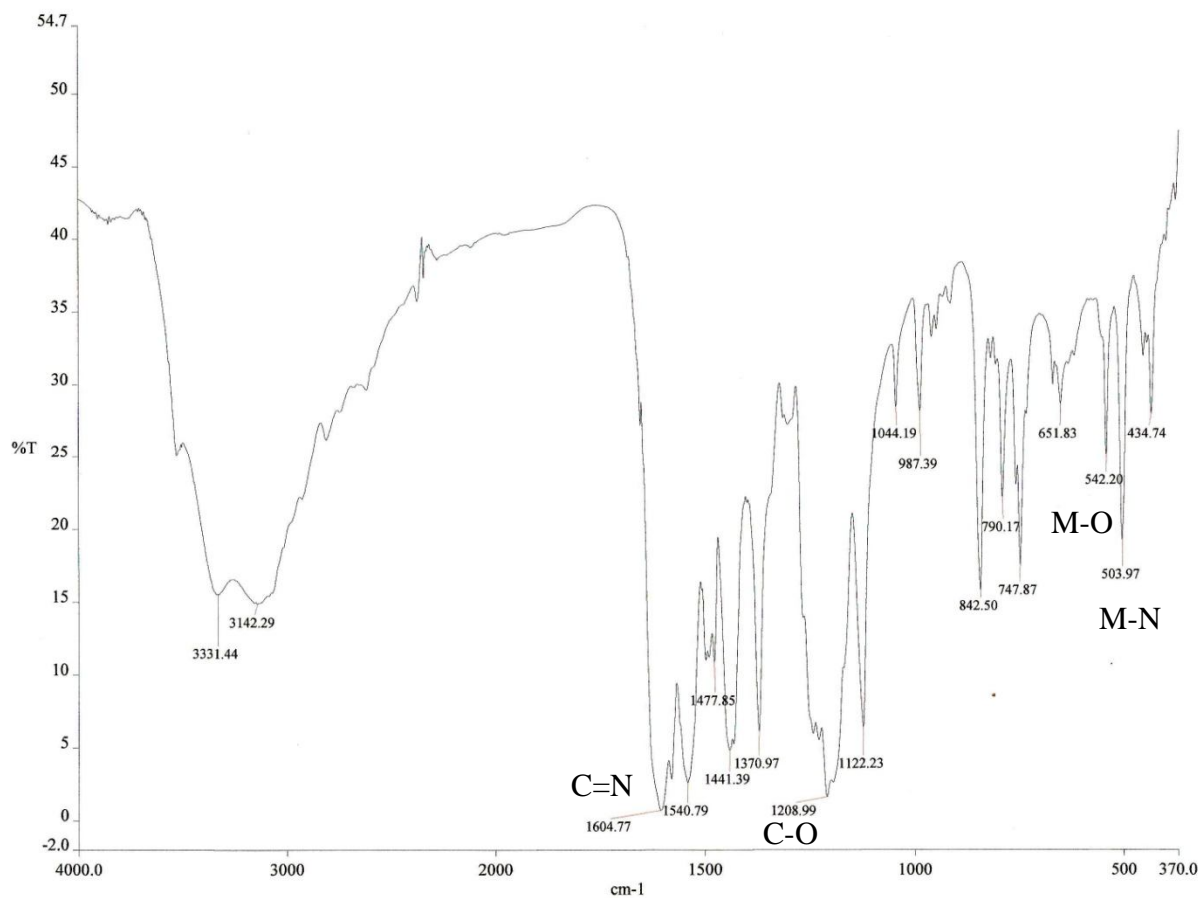


Figure 4.40 FTIR spectrum of NiL3

The FTIR data for NiL3 is compared with that of CuL3 and FeL3 in Table 4.7. It is of interest to note that the C=N and C-O bonds of NiL3 is about the same strength as CuL3 and FeL3.

The UV-vis spectrum of NiL3 (Figure 4.41) shows four broad peaks centered at 265, 313, 385, and 426 nm. As before, these bands are assigned to $\pi - \pi^*$ and $n - \pi^*$ transitions of L3, and they are at similar wavenumbers at for CuL3 and FeL3. The result is consistent with FTIR. As for the other Ni(II) and Fe(II) complexes, the $d-d$ transition is too weak to be detected.

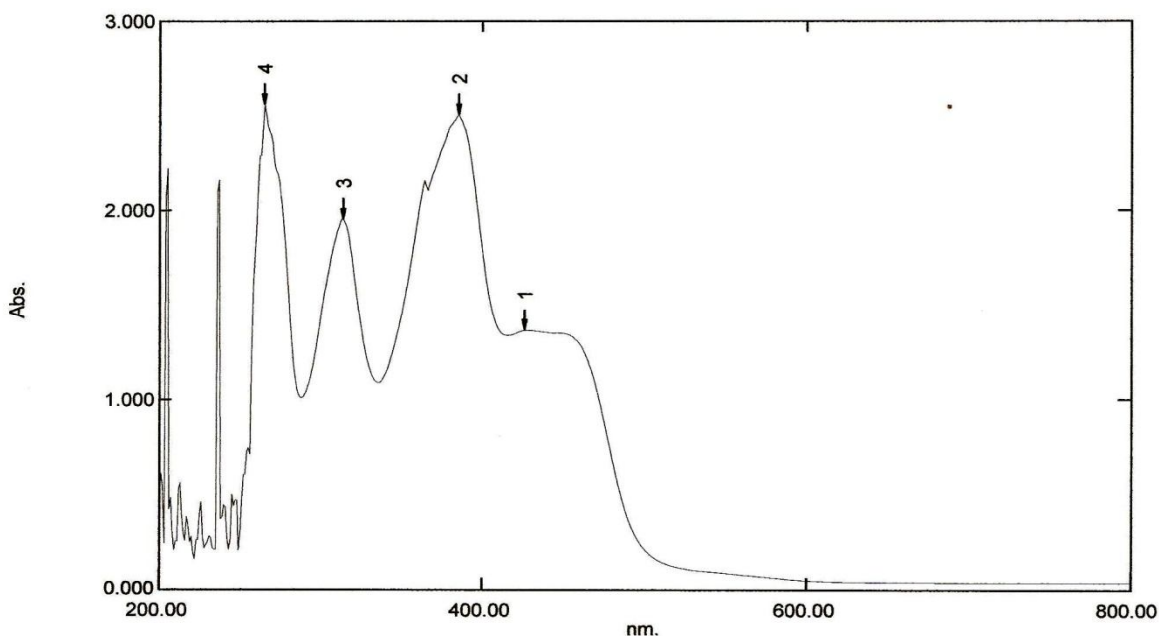


Figure 4.41 UV-vis spectrum of NiL3 in DMSO

The cyclic voltammogram of NiL3 in DMSO (Figure 4.42) shows similar reduction processes (at -0.5 and -1.0 V) as for NiL1 (Figure 4.15), and may be similarly explained. However, there were three overlapping anodic peaks at +0.37, +0.74 and +0.99 V for NiL3 but not for NiL1. The peak at +0.74 V, also found for CuL3, was assigned for the oxidation of -OH group at the ligand. The peak at +0.37 V is probably due to oxidation of Ni(I) to Ni(II). The peak separation for Ni(II)-Ni(I) redox is 870 mV, which suggests a quasireversible reaction. Thus, NiL3 may be suitable to be used as a redox catalyst.

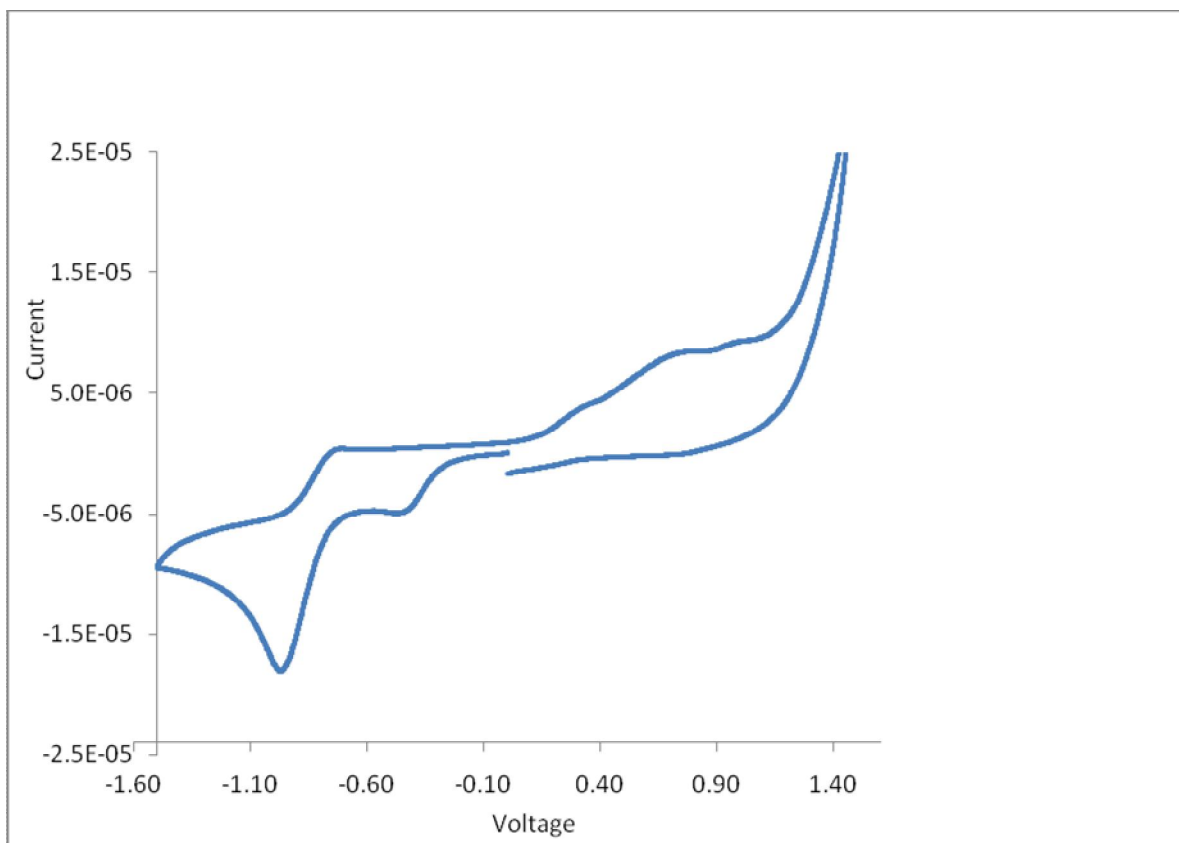


Figure 4.42 CV of NiL3 in DMSO

4.5 *N,N'*-1,2-Benzene-1,2-diyl-bis(3-bromo-5-chlorosalicylideneimine) (*H*₂L4) and its copper(II), iron(II) and nickel(II) complexes

N,N'-1,2-Benzene-1,2-diyl-bis(3-bromo-5-chlorosalicylideneimine) (*H*₂L4) was obtained as an orange powder in good yield (71%) from the reaction shown in Scheme 4.1 (X = 3-Br-5-Cl). The results from the C,H,N elemental analyses are in excellent agreement with the expected chemical formula, C₂₀H₁₂O₂N₂Br₂Cl₂.

The FTIR spectrum of *H*₂L4, recorded as a KBr pellet (Figure 4.43), is similar to the other Schiff bases studied, and may be similarly explained. The wavenumbers for C=N and C-O

bonds are about the same as H₂L1 (5-Cl) and H₂L2 (5-Br) [63,67]. Thus, the presence of two halogens (3-Br and 5-Cl) in H₂L4 has no significant effect on the strengths of these bonds.

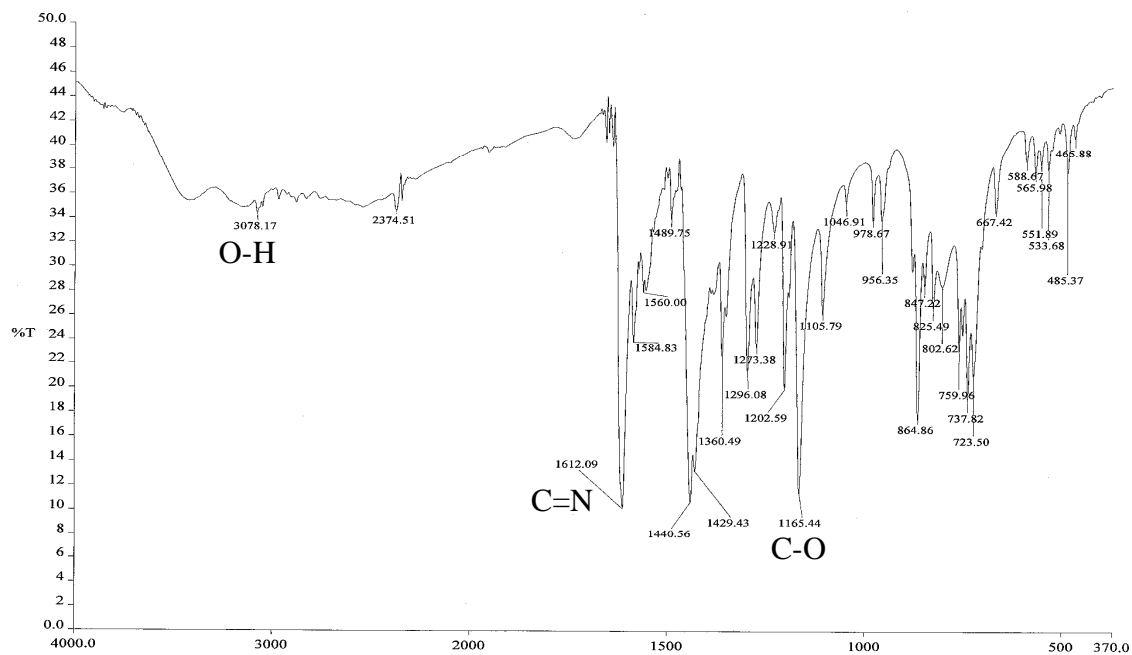


Figure 4.43 FTIR spectrum of H₂L4

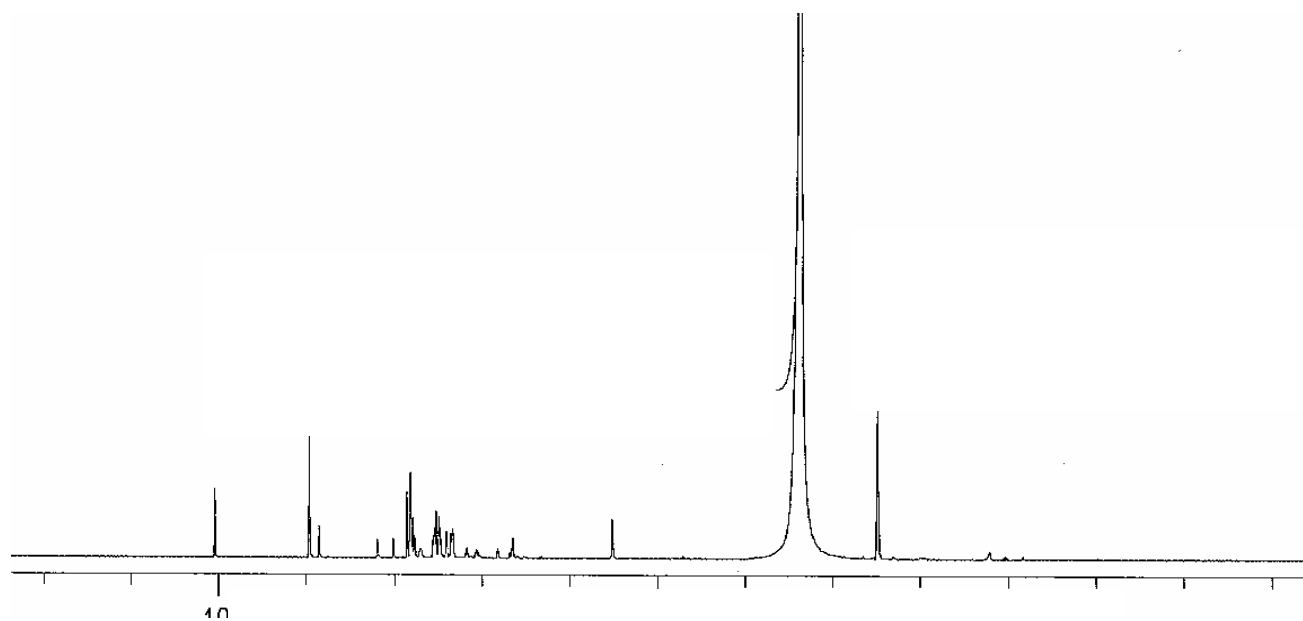


Figure 4.44 ¹H-NMR spectrum of H₂L4 in DMSO-d₆

The ^1H -NMR spectrum of $\text{H}_2\text{L4}$, recorded as a solution in DMSO-d_6 , is shown in Figure 4.44. The assignments of the spectrum are the same as for the other Schiff bases: a singlet at 10.04 ppm is due to phenolic hydrogen; a singlet at 8.85 ppm is due to imino hydrogen; and a multiplet in the range 6.80-7.85 ppm is due to the aromatic hydrogens. The integration ratio for these hydrogens is 1:1:4 respectively. Thus, $\text{H}_2\text{L4}$ is postulated to have similar structural formula as the other Schiff bases (Figure 4.45).

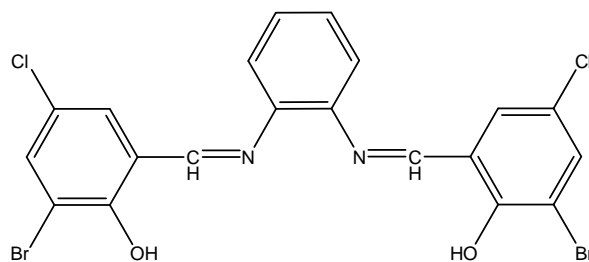


Figure 4.45 Proposed structural formula of $\text{H}_2\text{L4}$

The electronic spectrum of a solution of $\text{H}_2\text{L4}$ in DMSO (Figure 4.46) shows overlapping broad absorption bands at similar wavenumbers as for $\text{H}_2\text{L1}$ (Figure 4.4) and $\text{H}_2\text{L2}$ (Figure 4.18), and may be similarly assigned. The results support the suggestion from FTIR that the presence of two halogens (3-Br and 5-Cl) in $\text{H}_2\text{L4}$ has no significant effect on the structure of these Schiff bases.

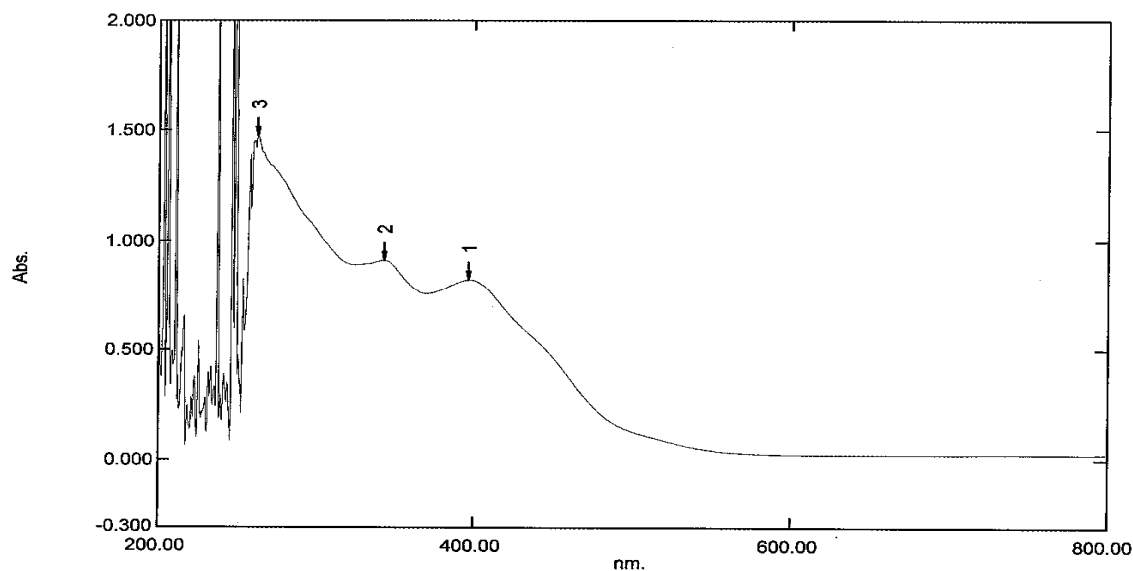


Figure 4.46 UV-vis spectrum of H₂L4 in DMSO

4.5.1 Copper(II) complex, CuL4

The copper(II) complex, CuL4, was obtained as a brown powder in good yield (63%) in the reaction between H₂L4 and copper(II) acetate monohydrate in the presence of triethylamine. The C,H,N elemental analyses are in excellent agreement with the expected chemical formula, [Cu(C₂₀H₁₀O₂N₂Br₂Cl₂)].

The FTIR spectrum of CuL4 (Figure 4.47) and the corresponding data (Table 4.8) show the expected decrease in the wavenumbers for -C=N and -C-O functional groups, compared to those of H₂L4.

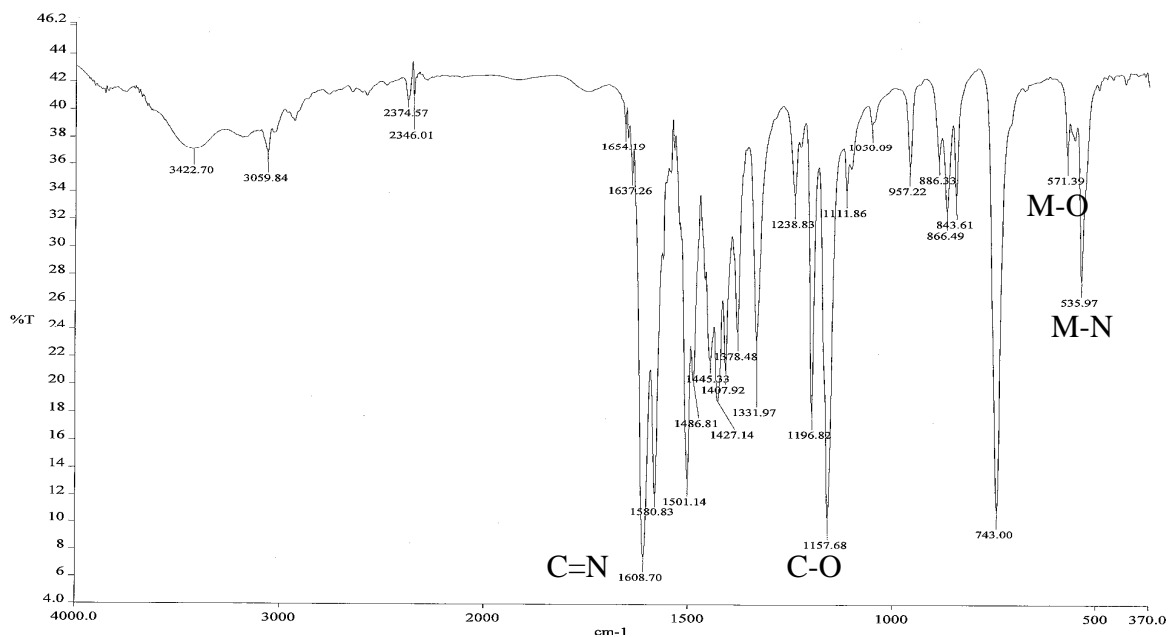


Figure 4.47 FTIR spectrum of CuL4

Table 4.8 FTIR data for H₂L4 and its metal complexes

Compound	ν_{OH}	$\nu_{\text{C=N}}$	$\nu_{\text{C-O}}$	$\nu_{\text{C-H}}$ (aliphatic)	$\nu_{\text{C-H}}$ (aromatic)	$\nu_{\text{M-N}}$	$\nu_{\text{M-O}}$
H₂L4	3078	1612	1165	-	737	-	-
CuL4	3422	1608	1157	3059	743	536	571
FeL4	3402	1604	1162	-	747	488	516
NiL4	3423	1606	1173	3167	747	406	547

To see the electronic effect of two halogens (Br and Cl) on the strengths of C=N, C-O, M-N and M-O bonds, the FTIR data for CuL4 is compared with that of CuL1 and CuL2 (Table 4.9). It is noted that there is no significant change in the wavelengths of these bonds. Thus, the presence of additional halogen in the CuL4 does not affect their strengths.

Table 4.9 FTIR data for CuL1, CuL2 and CuL4

Compound	$\nu_{\text{C=N}}$	$\nu_{\text{C-O}}$	$\nu_{\text{M-N}}$	$\nu_{\text{M-O}}$
CuL1	1580	1168	520	558
CuL2	1579	1177	524	550
CuL4	1580	1157	536	571

The UV-vis spectrum of CuL4 (Figure 4.48) in the UV region is almost similar to that of CuL1 (Figure 4.6) and CuL2 (Figure 4.21). Thus, the presence of additional halogen in the CuL4 has insignificant effect on the electronic transitions of the organic moiety.

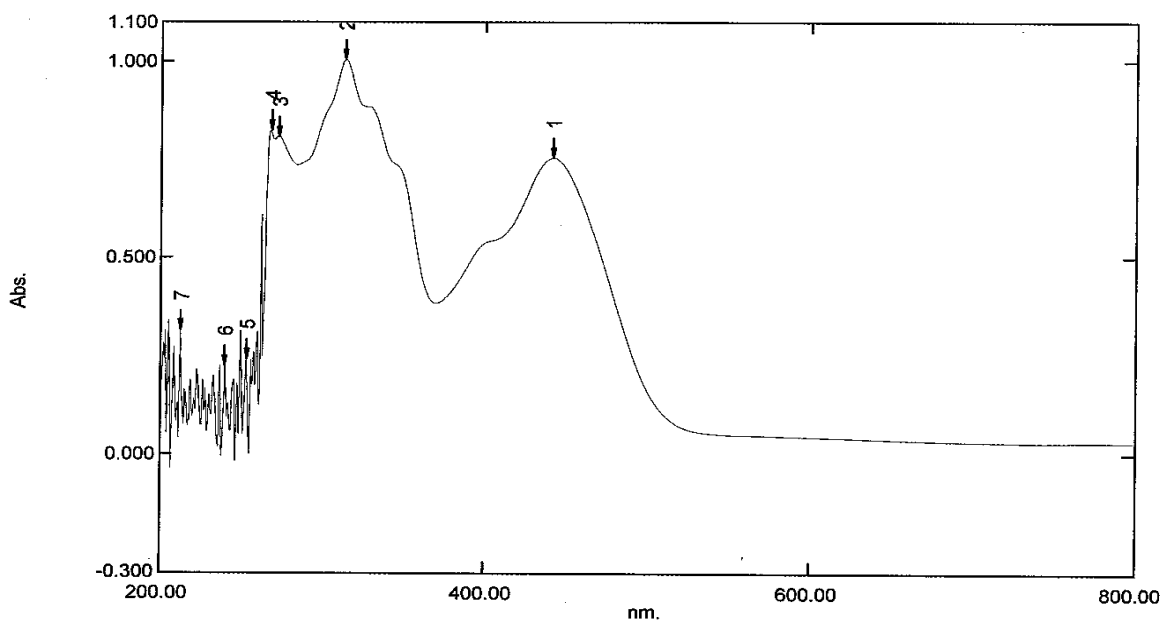


Figure 4.48 UV-vis spectrum of CuL4 in DMSO

In a separate run in the visible region (not shown), a weak and broad band is observed at 590 nm ($\epsilon = 46.3 \text{ M}^{-1}\text{cm}^{-1}$). This *d-d* band is at almost the same wavelength as for CuL1 (588 nm) and CuL2 (591 nm), and may be similarly explained, as well as consistent with the suggestion from FTIR data.

Combining the results from CHN analyses, and FTIR and UV-vis spectroscopies, the structural formula proposed for CuL4 is shown in (Figure 4.49).

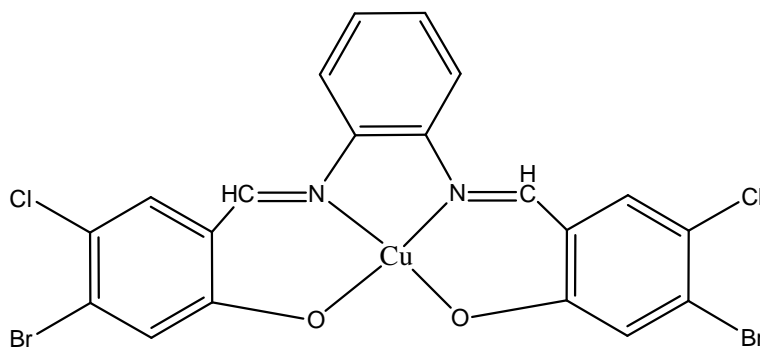


Figure 4.49 Proposed structural formula for CuL4, $[\text{Cu}(\text{C}_{20}\text{H}_{10}\text{O}_2\text{N}_2\text{Br}_2\text{Cl}_2)]$

The cyclic voltammogram of CuL4 in DMSO (Figure 4.50), scanned anodically in the same range as before, shows an initial anodic peak at +0.5 V (9.6×10^{-6} A) assigned to ligand oxidation. On reversing the scan at +1.5 V, a cathodic peak is observed at -1.0 V (2.5×10^{-5} A) assigned for Cu(II)-Cu(I) process. This is followed by two anodic peaks at -0.76 V (2×10^{-6} A) assigned as Cu(I)-Cu(II) process, and at -0.04 V (1.6×10^{-6} A). From these, the calculated values are: $E_{1/2} = -0.88$ V, $\Delta E_p = 240$ mV, and $I_{pa}/I_{pc} = 0.08$. These values are comparable with CuL1 ($E_{1/2} = -1.06$ V) and CuL2 ($E_{1/2} = -1.1$ V), and may be similarly explained. However, the lower reduction potential for CuL4 indicates that the complex is easier to be reduced, probably due to the presence of two halogens in its ligand.

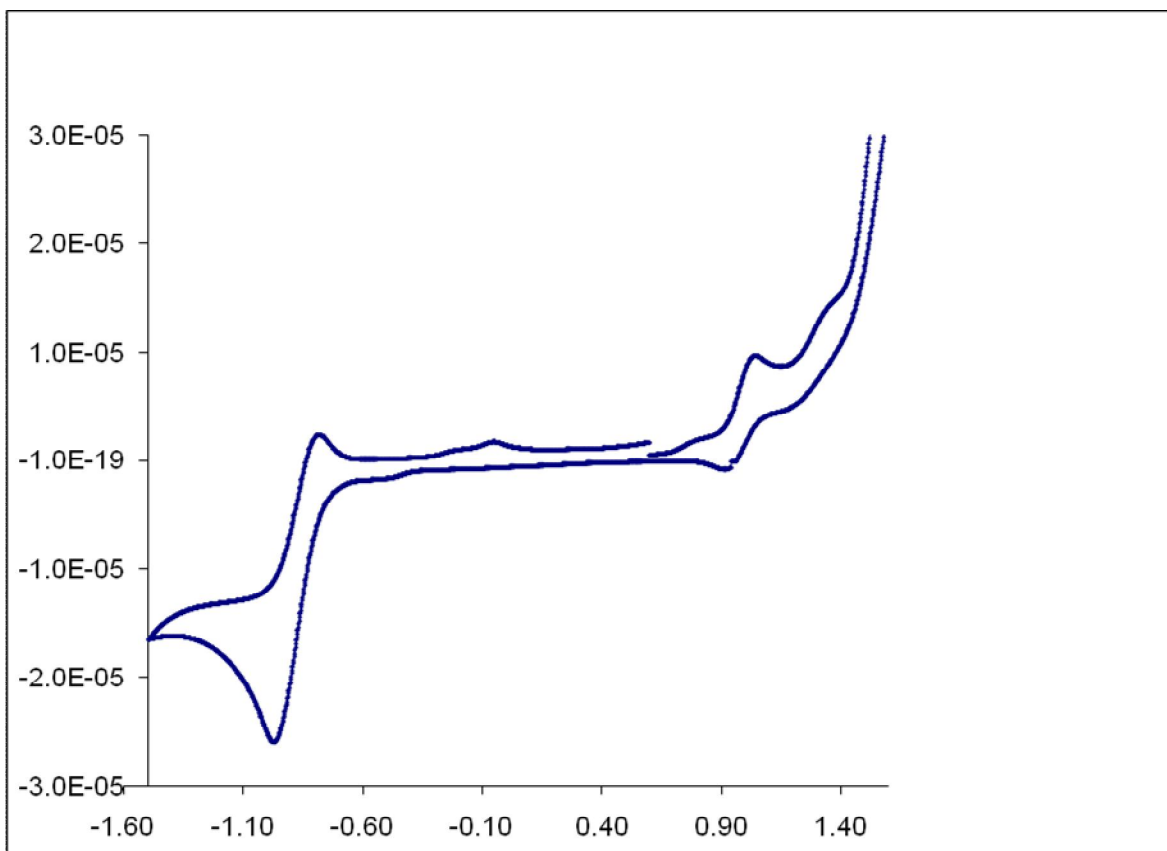


Figure 4.50 CV of CuL4 in DMSO

4.5.2 Iron(II) complex, FeL4

The iron(II) complex, FeL4, was obtained as a light brown powder in good yield (70%) from the reaction of iron(II) sulphate heptahydrate with H₂L4 in the presence of triethylamine. The C,H,N elemental analyses are in excellent agreement with the expected chemical formula, [Fe(C₂₀H₁₀O₂N₂Br₂Cl₂)]. Attempt to prepare Fe(III)-L4 by the same method was not successful.

The FTIR spectrum of FeL4 (Figure 4.51) shows the presence of all the expected functional groups. The wavenumbers of these functional groups (Table 4.10) are shifted as for the other complexes, and may be similarly explained.

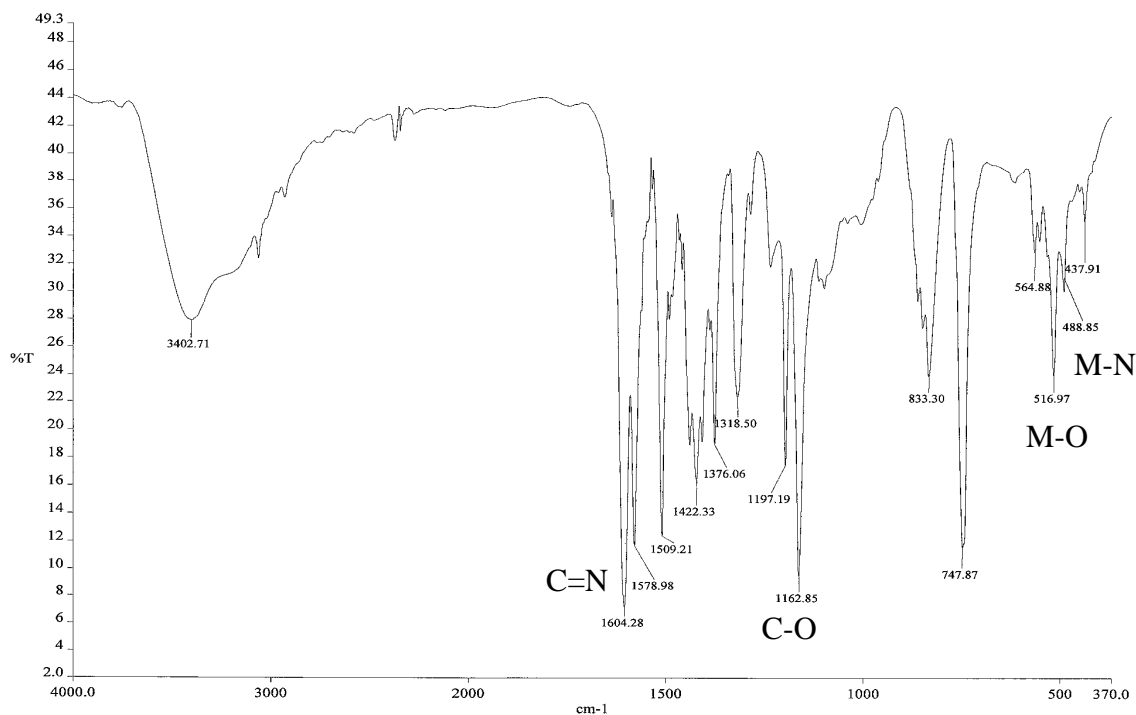


Figure 4.51 FTIR spectrum of FeL4

As was done for CuL4, the FTIR data for FeL4 (3-Br, 5-Cl) is also compared with that of FeL1 (5-Cl) and FeL2 (5-Br). It is noted that the M-O bond is significantly weaker for FeL4 compared to FeL1 and FeL2. Thus, the presence of additional halogen in the FeL4 does affect their strengths.

Table 4.10 FTIR data for FeL1, FeL2 and FeL4

Compound	$\nu_{\text{C=N}}$	$\nu_{\text{C-O}}$	$\nu_{\text{M-N}}$	$\nu_{\text{M-O}}$
FeL1	1608	1172	500	548
FeL2	1605	1170	496	546
FeL4	1604	1197	488	516

The UV-vis spectrum of FeL4 (Figure 4.52) shows two broad and overlapping peaks centered at 293 and 404 nm. These wavenumbers are similar to those of FeL1 (300 and 410 nm) and FeL2 (294 and 400 nm). Thus, the presence of two halogens on the ligand of FeL4 does not affect the electronic transitions of the organic moiety. The same finding was noted for CuL4.

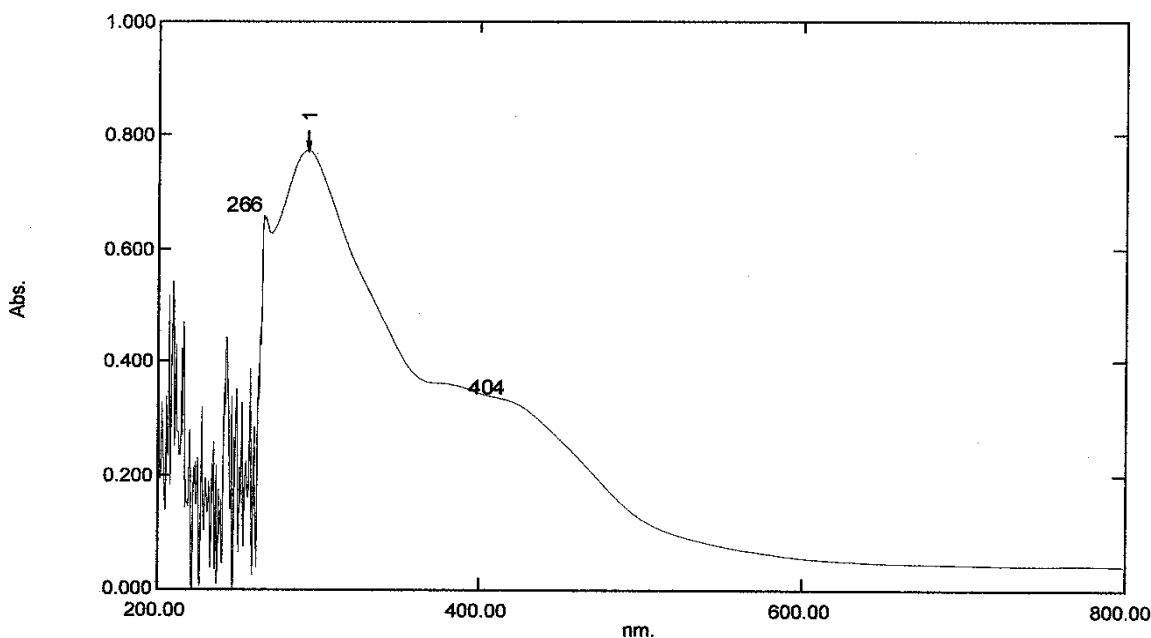


Figure 4.52 UV-vis spectrum of FeL4 in DMSO

Based on the similarity of FTIR and UV-vis spectroscopies of FeL4 with FeL1 and FeL2, it is proposed that these complexes have similar structural formula.

The cyclic voltammogram of FeL4 in DMSO (Figure 4.53), is similar to FeL1 (Figure 4.12) and FeL2 (Figure 4.26), and may be similarly explained. The result is in agreement with FTIR and UV-vis above. Thus, FeL4 may also be suitable to be used as a redox catalyst.

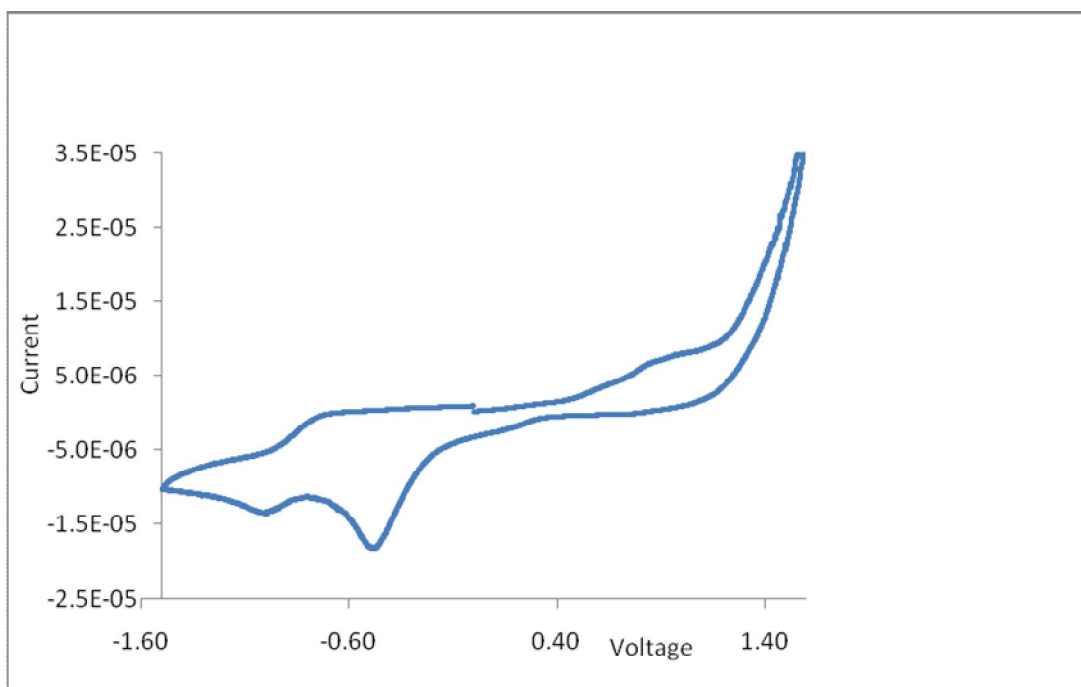


Figure 4.53 CV of FeL4 in DMSO

4.5.3 Nickel(II) complex, NiL4

Nickel(II) complex, NiL4, was obtained as a red powder in good yield (74%) from the reaction of nickel(II) acetate tetrahydrate with H₂L4 in the presence of triethylamine. The C,H,N elemental analyses are in excellent agreement with the expected chemical formula, [Ni(C₂₀H₁₀O₂N₂Br₂Cl₂)].

The X-ray crystal structure of NiL4 is shown in Figure 4.54, and the crystallographic data is shown in Appendix 2. In the crystal structure, the nickel atom is coordinated to two phenoxy oxygen atoms and two imino nitrogen atoms in a square-planar geometry. The molecule is virtually planar with a rms deviation of 0.034(1) Å from the least-squares plane defined by the two nitrogen, two oxygen and the nickel atoms. The nickel atom is situated 0.003(1) Å away from this plane. The Ni-O bond distances [1.836(2), 1.838(2) Å] and Ni-N bond distances

[1.853 (3), 1.858 (3) Å]. The bond angles in NiL4 complex O2–Ni1–O1, O1–Ni1–N2, N2–Ni1–N1, O2–Ni1–N1, O2–Ni1–N2 and O1–Ni1–N1 are 83.74°, 94.91°, 86.31°, 95.14°, 176.99° and 177.58°, respectively. The bond angles and the bond lengths indicate that nickel centre in the complex [Ni(L4)2] lies in a slightly distorted square planar coordination environment.

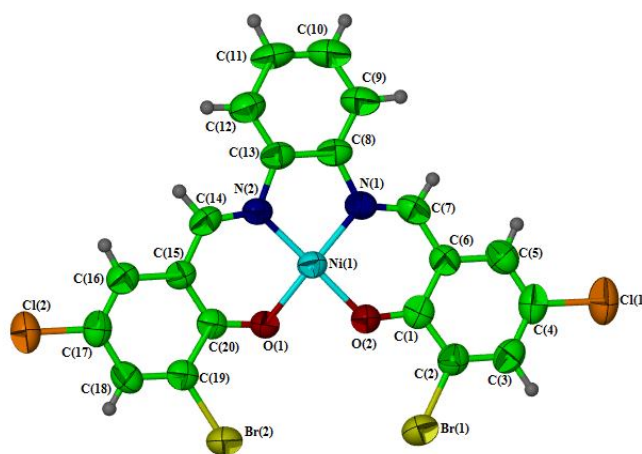


Figure 4.54 Molecular structure of NiL4

The FTIR spectrum of NiL4 (Figure 4.55) shows the presence of all the expected functional groups. The wavenumbers of these functional groups are shifted as for the other complexes, and may be similarly explained.

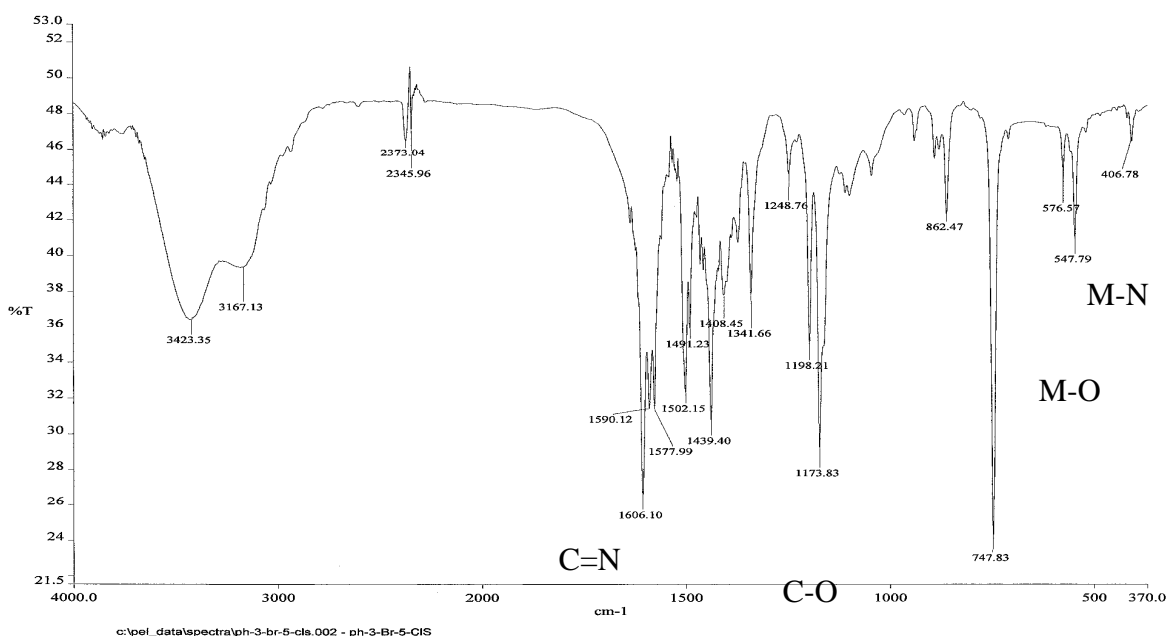


Figure 4.55 FTIR spectrum of NiL4

As was done for CuL4 and FeL4, The FTIR data for NiL4 (3-Br, 5-Cl) is also compared with that of NiL1 (5-Cl) and NiL2 (5-Br). In contrast to CuL4 and FeL4, the M-O bond is significantly stronger for NiL4 compared to NiL1 and NiL2. This may result from the planar structure of the crystal (Figure 4.54).

Table 4.11 FTIR data for NiL1, NiL2 and NiL4

Compound	$\nu_{\text{C=N}}$	$\nu_{\text{C-O}}$	$\nu_{\text{M-N}}$	$\nu_{\text{M-O}}$
NiL1	1608	1190	452	537
NiL2	1606	1188	450	536
NiL4	1606	1173	406	547

The UV-vis spectrum of NiL4 (Figure 4.56) shows two broad and overlapping peaks centered at 293 and 404 nm. These wavenumbers are similar to those of FeL1 (300 and 410 nm) and FeL2 (294 and 400 nm). Thus, the presence of two halogens on the ligand of FeL4 does not affect the electronic transitions of the organic moiety. The same finding was noted for CuL4.

The UV-vis spectrum of NiL4 (Figure 4.56) is similar to that of NiL1 (Figure 4.14) and NiL2 (Figure 4.28), and may be similarly explained. This supports the above suggestions for CuL4 and FeL4 that the presence of additional halogen on the aromatic ring has insignificant effect on the electronic transitions of the organic moiety.

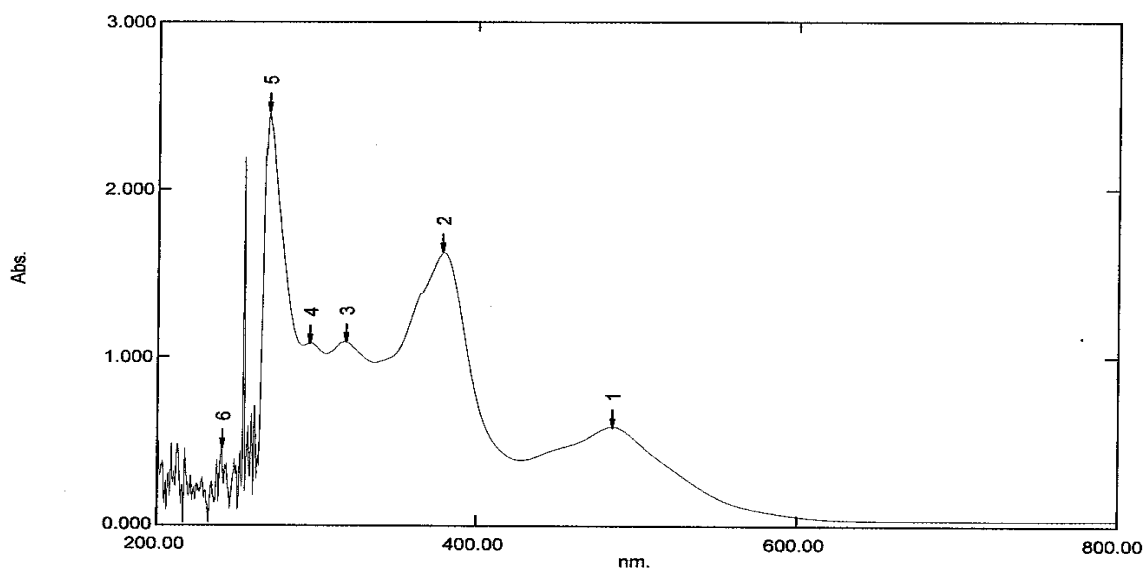


Figure 4.56 UV-vis spectrum of NiL4 in DMSO

The cyclic voltammogram of NiL4 in DMSO (Figure 4.57) is similar to NiL1 (Figure 4.15), and may be similarly explained. Since this process is irreversible, NiL4 is also not suitable to be used as a redox catalyst.

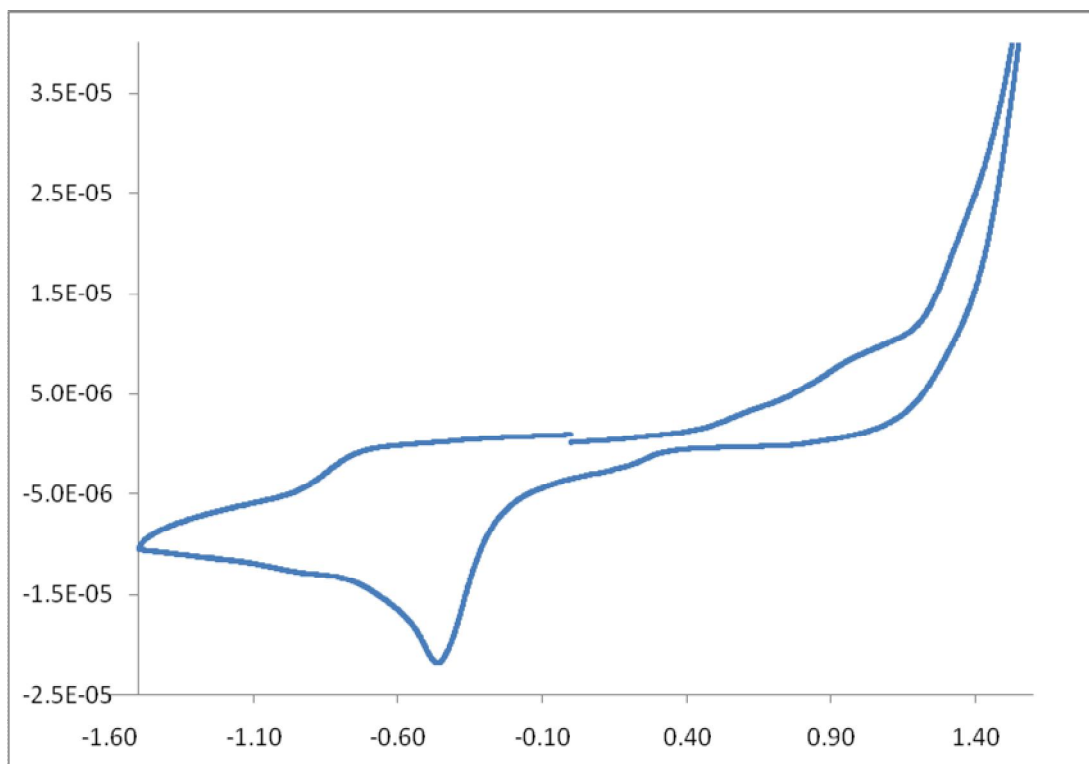


Figure 4.57 CV of NiL4 in DMSO

CHAPTER 5

CONCLUSIONS AND SUGGESTIONS FOR FUTURE WORK

CHAPTER 5: CONCLUSIONS AND SUGGESTIONS FOR FUTURE WORK

5.1 Conclusions

Four Schiff bases, N,N'-1,2-benzene-1,2-diyl-bis(5-chlorosalicylideneimine) (H₂L1), N,N'-1,2-benzene-1,2-diyl-bis(4-bromosalicylideneimine) (H₂L2), N,N'-1,2-benzene-1,2-diyl-bis(4-hydroxysalicylideneimine) (H₂L3), and N,N'-1,2-benzene-1,2-diyl-bis(3-bromo-5-chlorosalicylideneimine) (H₂L4), may be obtained in good yields from the condensation reaction of *o*-phenylenediamine with 5-chlorosalicylaldehyde, 5-bromosalicylaldehyde, 4-hydroxysalicylaldehyde and 3-bromo-5-chlorosalicylaldehyde respectively.

These Schiff bases formed complexes with copper(II), iron(II) and nickel(II) ions in good yields. The structures of these complexes are mainly square planar, which is confirmed by the crystal structure of nickel(II) complex of N,N'-1,2-benzene-1,2-diyl-bis(3-bromo-5-chlorosalicylideneimine). Attempts to prepare the corresponding iron(III) complexes were unsuccessful.

The different substituents (Cl, Br, OH) on the ligands, and different metal(II) ions, did not significantly affect the structure of these complexes, but do affect their electrochemical properties.

For the metal(II) complexes of H₂L1, the strengths of the metal-ligand bonds are in the following order: Ni-L1 > Cu-L1 > Fe-L1. The Cu(II) complex undergoes a quasireversible redox reaction, while the Fe(II) and Ni(II) complexes undergo irreversible redox reactions.

For the metal(II) complexes of H₂L₂, the bigger Br in the ligand results in a more distorted geometry. The strengths of the metal-ligand bonds are in the following order: Ni-L₂ < Cu-L₂ ~ Fe-L₂. The Cu(II) and Fe(II) complexes undergo quasireversible redox reactions, while the Ni(II) complex undergoes irreversible redox reaction.

For the metal(II) complexes of H₂L₃, the strengths of the metal-ligand bonds are in the following order: Fe-L₃ > Cu-L₃ ~ Ni-L₃. The Cu(II) and Fe(II) complexes undergo irreversible redox reactions, while the Ni(II) complex undergoes quasireversible redox reaction.

For the metal(II) complexes of H₂L₄, the presence of additional halogens on the ligand has the following effect on the metal-ligand bonds: none for Cu(II), weaker for Fe(II) and stronger for Ni(II), when compared with monohalogenated ligand. For the electrochemical properties, CuL₄ is easier to be reduced compared to CuL₁ and CuL₂, while the electrochemical properties of FeL₄ and NiL₄ are the same as their monohalogenated analogs.

Based on cyclic voltammetry, only CuL₁, CuL₂, FeL₂, and NiL₃ are potential redox catalysts.

5.2 Suggestions for future work

For future work, the catalytic properties of these complexes for polymerization and oxidation reactions should be studied.

Also, the effect of other substituents, such as strongly deactivating groups (NO₂, CN, COOH) and strongly activating group (NH₂), suitably located on the ring for strong

interaction with the metal(II) ions, and complexes with other first-row transition metal ions, such as Mn(II) and Co(II), also should be systematically studied.

It is of interest to study a more geometrically flexible Schiff bases, such as those obtain from diaminocyclohexanes and substituted salicyaldehydes, as these are expected to lead to reversible redox properties.

Other than as catalysts, other potential use of these materials should be studied. Examples are as spintronic, electronic and photonic materials, by studying their magnetic susceptibilities, electronic conductivities and electronic transitions (fluorescence and phosphorescence), respectively.

APPENDIXES

MPIC 2009
21-22 Oct 2009
Palm Garden Hotel, IOI Resort, Putrajaya.

PSM

23

SPECTROSCOPIC STUDIES OF O-PHENYLENE DIAMINE SCHIFF BASES AND THEIR METAL COMPLEXES

Alomari Abdulaziz, Ali M, Assoc. Prof. Dr. Norbani Abdullah, Prof. Dato' Dr.
Mohd. Jamil Maah

Abstract

o-phenylene diamine Schiff bases were prepared by the condensation reaction of ethanolic solution of *o*-phenylene diamine with 5-chlorosalicylaldehyde, 5-bromosalicylaldehyde and 4-hydroxysalicylaldehyde. The ligands were coordinated to Cu(II), Fe(II) and Fe(III). All prepared compounds have been characterized by IR, ¹H NMR and UV-Vis. Spectroscopy as well as elemental CHN analysis. Cyclic voltametry study was carried out in order to evaluate the redox properties of the complexes, and to test their catalytic activity.

Spectroscopic data revealed that, the ligands were coordinated to the metal ions via the azomethine nitrogen atom and phenolate oxygen atom in a square planar geometry.

Keywords: *o*-phenylene diamine, transition metal complexes, cyclic voltametry.

{6,6'-dibromo-4,4'-dichloro-2,2'-[*o*-phenylenebis(nitrilomethylidyne)]-diphenolato}nickel(II)

Abdulaziz Ali, Norbani Abdullah, Mohd Jamil Maah and Kong Mun Lo

Department of Chemistry, University of Malaya, 50603 Kuala Lumpur, Malaysia

Correspondence e-mail: kmlo@um.edu.my

Abstract

In the title nickel(II) Schiff base complex, the Ni atom is coordinated to two phenoxyl oxygen atoms and two imino nitrogen atoms in the *cis* configuration. The local coordination geometry around the nickel atom is a square planar configuration, with a rms deviation of 0.034 (1) Å from a least-squares plane defined by the two nitrogen, two oxygen and the nickel atoms in the molecule. The nickel atom is situated 0.003 (1) Å away from this plane.

Comment

Many low-spin square-planar nickel(II) complexes and high-spin octahedral nickel(II) complexes containing nitrogen and oxygen donor ligands have been reported due to their potential industrial applications [Wang *et al.*, 2003; Li *et al.*, 1993]. In continuation of our study on the optical properties of nickel(II) Schiff base complexes, we report here the molecular structure of the title nickel(II) complex, in which the nickel atom is coordinated to two phenoxyl oxygen atoms and two imino nitrogen atoms in a square-planar geometry. The molecule is virtually planar with a rms deviation of 0.034 (1) Å from the least-squares plane defined by the two nitrogen, two oxygen and the nickel atoms. The nickel atom is situated 0.003 (1) Å away from this plane. The Ni-O bond distances [1.836 (2), 1.838 (2) Å] and Ni-N bond distances [1.853 (3), 1.858 (3) Å] are very close to those reported for similar structure (1.841 (5), 1.847 (5) Å and 1.859 (6), 1.856 (6) Å, respectively, Azevedo *et al.*, 1994).

Related literature

For related structures, see Wang *et al.* (2003); Niu *et al.* (2009); Azevedo *et al.* (1994).

Experimental

The Schiff base, *o*-phenylenebis(3-bromo-5-chlorosalicylidenaminato) was prepared by the condensation reaction between *o*-phenylenediamine and 3-bromo-5-chlorosalicylaldehyde in ethanol. 0.1 g (0.183 mmol) of the Schiff base ligand and 0.04 g (0.183 mmol) of nickel(II) acetate tetrahydrate were dissolved in 100 mL of absolute ethanol. A few drops of triethylamine were added and the mixture was refluxed for 3 hours. After filtering, a red colored solid was obtained upon slow evaporation of the filtrate. It was recrystallised from DMF to obtain the red crystals suitable for X-ray analysis.

Crystal Data and Structure Refinement:

<u>C₂₀H₁₀Br₂Cl₂N₂NiO₂</u>	$D_x = \underline{2.038} \text{ Mg m}^{-3}$
$M_r = \underline{599.73}$	Melting point: ? K
<u>Monoclinic, $P2_1/c$</u>	<u>Mo $K\alpha$ radiation</u> $\lambda = \underline{0.71073} \text{ \AA}$
Hall symbol: <u>-P 2ybc</u>	Cell parameters from <u>2542</u> reflections
$a = \underline{10.4289} (2) \text{ \AA}$	$\theta = \underline{2.5-22.8}^\circ$
$b = \underline{9.2712} (2) \text{ \AA}$	$\mu = \underline{5.38} \text{ mm}^{-1}$
$c = \underline{20.6731} (4) \text{ \AA}$	$T = \underline{296} (2) \text{ K}$
$\beta = \underline{102.101} (1)^\circ$	Cell measurement pressure: ? kPa
$V = \underline{1954.43} (7) \text{ \AA}^3$	<u>Tube, red</u>
$Z = \underline{4}$	<u>0.40</u> \times <u>0.10</u> \times <u>0.10</u> mm
$F_{000} = \underline{1168}$	

<u>Bruker APEX-II CCD area-detector diffractometer</u>	<u>18381</u> measured reflections
Radiation source: <u>fine-focus sealed tube</u>	<u>4487</u> independent reflections
Monochromator: <u>graphite</u>	<u>2921</u> reflections with $I > 2\sigma(I)$
Detector resolution: ? pixels mm ⁻¹	$R_{\text{int}} = \underline{0.060}$
$T = \underline{296(2)} \text{ K}$	$\theta_{\text{max}} = \underline{27.5}^\circ$
$P = ? \text{ kPa}$	$\theta_{\text{min}} = \underline{2.0}^\circ$
<u>ω scans</u>	$h = \underline{-13} \quad \underline{13}$
Absorption correction: <u>Multi-scan (SADABS; Sheldrick, 1996)</u>	$k = \underline{-12} \quad \underline{12}$
$T_{\text{min}} = \underline{0.222}$, $T_{\text{max}} = \underline{0.616}$	$l = \underline{-26} \quad \underline{25}$

Refinement on F^2	Secondary atom site location: <u>difference Fourier map</u>
Least-squares matrix: <u>full</u>	Hydrogen site location: <u>inferred from neighbouring sites</u>
$R[F^2 > 2\sigma(F^2)] = 0.038$	<u>H atoms treated by a mixture of independent and constrained refinement</u>
$wR(F^2) = 0.085$	<u>$w = 1/[\sigma^2(F_o^2) + (0.0337P)^2]$ where $P = (F_o^2 + 2F_c^2)/3$</u>
$S = 0.99$	$(\Delta/\sigma)_{\max} \leq 0.001$
4487 reflections	$\Delta\rho_{\max} = 0.62 \text{ e } \text{\AA}^{-3}$
302 parameters	$\Delta\rho_{\min} = -0.46 \text{ e } \text{\AA}^{-3}$
2 constraints	Extinction correction: <u>none</u>
Primary atom site location: <u>structure-invariant direct methods</u>	

Geometrical parameters including bond lengths and bond angles:

Ni1—O2	1.836 (2)	C1—C2	1.411 (5)
Ni1—O1	1.838 (2)	N2—C13	1.424 (4)
Ni1—N2	1.853 (3)	C5—C4	1.349 (6)
Ni1—N1	1.858 (3)	C5—C6	1.407 (5)
Br2—C19	1.895 (4)	C5—H5	0.87 (3)
Br1—C2	1.888 (4)	C19—C18	1.362 (5)
Cl2—C17	1.752 (4)	C2—C3	1.367 (5)
Cl1—C4	1.744 (4)	C13—C12	1.381 (5)
C15—C20	1.410 (5)	C13—C8	1.394 (5)
C15—C16	1.420 (5)	C11—C12	1.379 (6)
C15—C14	1.424 (5)	C11—C10	1.388 (7)
O2—C1	1.297 (4)	C11—H11	0.95 (5)
C16—C17	1.356 (5)	C9—C10	1.372 (6)
C16—H16	0.92 (4)	C9—C8	1.389 (5)

N1—C7	1.297 (5)	C9—H9	0.99 (4)
N1—C8	1.422 (5)	C10—H10	0.89 (4)
C14—N2	1.298 (5)	C18—H18	0.87 (4)
C14—H14	0.97 (3)	C7—C6	1.426 (5)
C20—O1	1.294 (4)	C7—H7	0.87 (3)
C20—C19	1.416 (5)	C3—C4	1.393 (6)
C17—C18	1.379 (5)	C3—H3	0.97 (4)
C1—C6	1.411 (5)	C12—H12	0.99 (4)

O2—Ni1—O1	83.74 (11)	C20—C19—Br2	116.8 (3)
O2—Ni1—N2	176.99 (12)	C3—C2—C1	122.4 (4)
O1—Ni1—N2	94.91 (12)	C3—C2—Br1	119.5 (3)
O2—Ni1—N1	95.14 (12)	C1—C2—Br1	118.0 (3)
O1—Ni1—N1	177.58 (12)	C12—C13—C8	119.5 (4)
N2—Ni1—N1	86.31 (13)	C12—C13—N2	126.9 (4)
C20—C15—C16	120.1 (3)	C8—C13—N2	113.6 (3)
C20—C15—C14	121.4 (3)	C12—C11—C10	119.7 (4)
C16—C15—C14	118.4 (3)	C12—C11—H11	125 (3)
C1—O2—Ni1	127.7 (2)	C10—C11—H11	115 (3)
C17—C16—C15	119.9 (4)	C10—C9—C8	118.8 (4)
C17—C16—H16	123 (2)	C10—C9—H9	118 (3)
C15—C16—H16	117 (2)	C8—C9—H9	123 (3)
C7—N1—C8	121.6 (3)	C9—C10—C11	121.1 (5)
C7—N1—Ni1	125.3 (3)	C9—C10—H10	118 (3)
C8—N1—Ni1	113.1 (2)	C11—C10—H10	120 (3)
N2—C14—C15	125.2 (4)	C9—C8—C13	120.6 (4)
N2—C14—H14	122.3 (18)	C9—C8—N1	125.6 (4)
C15—C14—H14	112.5 (18)	C13—C8—N1	113.7 (3)

O1—C20—C15	124.2 (3)	C19—C18—C17	119.7 (4)
O1—C20—C19	119.2 (3)	C19—C18—H18	122 (3)
C15—C20—C19	116.6 (3)	C17—C18—H18	118 (3)
C16—C17—C18	121.2 (4)	N1—C7—C6	126.4 (4)
C16—C17—Cl2	119.4 (3)	N1—C7—H7	118 (2)
C18—C17—Cl2	119.4 (3)	C6—C7—H7	115 (2)
O2—C1—C6	124.9 (4)	C2—C3—C4	119.4 (4)
O2—C1—C2	118.8 (3)	C2—C3—H3	120 (2)
C6—C1—C2	116.3 (3)	C4—C3—H3	120 (2)
C20—O1—Ni1	127.9 (2)	C5—C4—C3	120.9 (4)
C14—N2—C13	120.6 (3)	C5—C4—Cl1	120.5 (3)
C14—N2—Ni1	126.1 (3)	C3—C4—Cl1	118.6 (3)
C13—N2—Ni1	113.2 (2)	C5—C6—C1	120.7 (4)
C4—C5—C6	120.2 (4)	C5—C6—C7	118.9 (4)
C4—C5—H5	122 (2)	C1—C6—C7	120.3 (3)
C6—C5—H5	118 (2)	C11—C12—C13	120.2 (4)
C18—C19—C20	122.4 (4)	C11—C12—H12	118 (3)
C18—C19—Br2	120.7 (3)	C13—C12—H12	122 (3)

REFERENCES

- [1] S. Akmal, Gaballa, S. Mohsen, Asker, S. Atiat, Barakat, M. Said Teleb, *Spectrochimica Acta Part A*, 67 (2007) 114.
- [2] S. M. El-Medani, *J. Coord. Chem.* 57/2 (2004) 115.
- [3] S. M. El-Medani, *J. Coord. Chem.*, 57/6 15 (2004) 497.
- [4] L. Sacconi; *Coord. Chem. Rev*, 1 (1966) 126.
- [5] L.F. Lindoy; *Quart Chem. Rev*, 1 (1971) 379.
- [6] S. Yamanda and A. Takeuchi; *Coord. Chem. Rev*, 43 (1982)187.
- [7] R. Hernandez-Molina, J. A. McCleverty in: T.J Meyer (Eds), *Comprehensive Coordination Chemistry II*, Vol.1, Elsevier, Amsterdam, 2004.
- [8] M. Andruh, F. Tuna, in: M.A. Cato (Eds.), *Organometallic Chemistry Research*, Nova Publisher, Hauppauge, 2005 p. 411.
- [9] S. Akmal, Gaballa, S. Mohsen, Asker, S. Atiat, Barakat, M. Said Teleb, *Spectrochimica Acta Part A*, 67 (2007) 916.
- [10] R. Kannappan, S. Tanase, M. Duncan, T. Anthony L. Spek lipo Mutikainen, U. Turpeinen, J. Reedijk, *Polyhedron* 23(2004) 2285.
- [11] C. Maxim, D. Trania, Pasatoiu, V. Kravtsov, SergiuShova, A. Christopher, M. Richard, E.P. Winpenny, F. Tuna, M. Andruh, *Inorganica Chimica Acta* 361 (2008) 3903.
- [12] Y. Muto, T.Tokii, *Bull Chem Soc Jpn*, 51(1978)139.
- [13] T. Tokii, M. Kamekoo, Y. Yamanaka, Y. Muto, M. Kato, *Bull Chem Soc Jpn*, 52 (1979) 3651.
- [14] J. P. Costers, F. Dehan, A. Dupuis, J. P. Laurent, *Inorg Chem.* 35 (1996) 2401.
- [15] J. P. Costers, F. Dehan, A. Dupuis, J. P. Laurent, *Inorg Chem.* 36 (1996) 3429.
- [16] E.G. Samsel, K. Srinivasan and J. K. Kochi, *J. Am. Chem. Soc.* 107 (1985) 7606.
- [17] K. Srinivasan, P. Michaud and J. K. Kochi, *J. Am. Chem. Soc.* 108 (1986) 2309.
- [18] C.P. Horwitz, S. E. Creager and R.W. Murray, *Inorg Chem.* 29 (1990)1006.
- [19] S. S. Djebbar, B.O Benali, and J. P. Deloume, *Trans. Metal Chem.* 23 (1998) 443.
- [20] Y. Xishi Tai Xianhong, C. Qiang and T. Minya, *Molecules* 8 (2003) 49.
- [21] A. M. Mahindra, J. M. Fisher, Rabinovitz, *Nature*, 303 (1983) 64.
- [22] P. R. Planet, B.T. Thanker, S. Zele, *Indian J. Chem A* 38 (1999) 563.

- [23] R. E. Hester, E. M. Nour, R. J. Raman Spectrosc, 11 (1981) 49.
- [24] E. M Nour, A. A. Taha, I.S. Alnaimi, Inorg Chim Acta 141 (1988) 139.
- [25] W. Wang, F. L. Zeng, X. Wang, M, Y. Tan, Polyhedron 15 (1996) 1699.
- [26] B. Rosenburg, L. Van Camp, J. E. Trosko, V. H. Mansour, Nature 222 (1996) 358.
- [27] J. J. R. Frausto, D. Silva and R. J. P. Williams, The Biological Chemistry of the Elements, Clarendon, Oxford, 1991.
- [28] W. Kaim and B. Schwederski, Bioinorganic Chemistry: Inorganic Elements in the Chemistry of Life, John Wiley & Sons, New York, 1996.
- [29] A. Panja, N. Shaikh, M. Ali, P. Vojtisek and P. Banerjee, Polyhedron 22 (2003) 1191.
- [30] H. Yoon and C. J. Burrows, J. Am. Chem. Soc. 110 (1988) 4087.
- [31] M. M. Taqui Khan, N. M. Khan, R. I. Kureshy and A. B. Boricha, J. Coord. Chem. 43 (1998) 31.
- [32] D.Y. Sabry, T. A. Youssef, S. M. El-Medani and R.M. Ramadan, J. Coord. Chem. 56 (2003) 1375.
- [33] R. M. Ramadan, M. S. A. Hamza and S. A. Ali, J. Coord. Chem. 43 (1998) 31.
- [34] S. A. Ali, A. A. Soliman, M. M. Abo-Aly and R.M. Ramadan, J. Coord. Chem. 55 (2002) 1161.
- [35] H. C. Rai, and R. Kumar, Ind J. Chem, 29A (1990) 796.
- [36] C. Natarajan, C.D. Sheela, and P.R. Athappan, Ind. J. Chem. 30A (2001) 357.
- [37] S. J. Lippard, Angew Chem Int. Ed. Engl, 27 (1988) 344.
- [38] D. E. Fenton and P. C. Hellier, Inorganica Chimica Acta 198-200 (1992) 577.
- [39] M. J. Alcón, Marta Iglesias, F. Sánchez, Inorganica Chimica Acta, 333/1 (2002) 83.
- [40] G. Cerchiaro, A. Gustavo, Micke, M. Franco, M. Tavares, A. M. Costa Ferreira, J. Molecular Catal. A, 221/1 (2004) 29.
- [41] M. Tümer, D. Ekinici, F. Tümer, A. Bulut, Spectrochimica Acta Part A, 67/3 (2007) 916.
- [42] K. Wang, K. Wedeking, W. Zuo, D. Zhang, Wen-Hua Sun, J. Organomet Chem, 693/6 (2008) 1073.
- [43] Z. Long, B. Wu, P. Yang, Gang Li, Y. Liu, Y. Xiao-Juan, J. Organomet. Chem, 694/32 (2009) 3793.
- [44] J. Luybaert, M. H. Zhang, D. L. Massart, Anal Chim Acta, 478/2 (2003) 303.
- [45] W.S Lau, Infrared characterization for microelectronics, World Scientific, 1999.

- [46] P. Hamm, M. H. Lim, R. M. Hochstrasser, *J. Phys. Chem. B* 102 (1998) 6123.
- [47] S. Mukamel, *Annual Review of Physics and Chemistry* 51 (2000) 691.
- [48] N. Demirdöven, C. M. Cheatum, H. S. Chung, M. Khalil, J. Knoester, A. Tokmakoff. *J. Am. Chem Soc* 126 (2004) 7981.
- [49] James Keeler, *Understanding NMR Spectroscopy*, Cambridge University Press, 2007.
- [50] G. E. Martin, A. S. Zekter, *Two-Dimensional NMR Methods for Establishing Molecular Connectivity*, VCH Publishers, New York, 1988, pp.59.
- [51] Skoog, et al., *Principles of Instrumental Analysis*. 6th ed. Thomson, New York, 2007, pp169-173.
- [52] D. L. Pavia, G. M. Lampman, G. S. Kriz, *Introduction to Spectroscopy*, Thomson, New York, 2001.
- [53] P.T. Kissinger, W. R. J. Heineman, *J. Chem. Educ*, 60 (1983) 702
- [54] M. Kabak, A. Elmali, T. Elerman, T. N.Durlu, *J. Molecular Struc.* 553 (2000) 187.
- [55] Z. L. Yuan, Q. Long, Z. XueZiang, B. XueZhu, F. Lindoy, G. Wei, *Polyhedron* 27 (2008) 344.
- [56] E. Suresh, M. M. Bhad, and D. Srinivas, *Polyhedron* 15/23 (1996) 4133.
- [57] M. Tumer, D. Ekinici, F. Tumer, A. Bulut, *Spectrochimica Acta Part A* 67(2007) 916.
- [58] A. Ray, D. Sadhukhan, M. Rosair, J. Carlos, G. Garcia, S. Mitra, *Polyhedron* 28 (2009) 3542.
- [59] L. J. Bellamg, *The Infrared Spectra of Complex molecules*, Champan and Hall, London, 1975.
- [60] S. G. Gruber, C. M. Harris and E. Sinn, *J. Inorg. Nucl. Chem*, 30 (1968) 1805.
- [61] C. Alaaddin, Y. Ibrahim, O. Habibe and A. Misir, *Transition Met. Chem.* 27 (2002) 171
- [62] I. Salih, H. Temel, I. Yilmaz, M. Sekerci, *J. Organomet. Chem.* 692 (2007) 3855.
- [63] T. Veli, T. Kasumov, E. Tas, F. Koksall, S. Ozalp, *Polyhedron* 24 (2005) 319
- [64] S. Zolezzi, A. Decinti, E. Spodine, *Polyhedron* 18(1999) 897.
- [65] A. Pagini, M. Gullotti, R. Vgo. *J. Chem Soc. Dalton Trans* 4 (1977) 346.
- [66] R. S. Downing, F. L. Urbach, *J. Am. Chem Soc*, 91/22 (1969) 5977.
- [67] B. S. Garg, D. Nandan Kumar, *Spectrochimica Acta Part A* 59 (2003) 229.
- [68] D. Santo, D. Bella, I. Fragala, N. Leonardi, S. Sortino, *Inorganica Chimica Acta* 357(2004) 3865.